UNIVERSITÀ DEGLI STUDI DI PADOVA

DIPARTIMENTO DI INGEGNERIA INDUSTRIALE

CORSO DI LAUREA MAGISTRALE IN INGEGNERIA CHIMICA E DEI PROCESSI INDUSTRIALI

Tesi di Laurea Magistrale in
Ingegneria Chimica e dei Processi Industriali

DIRECT SYNTHESIS H_2O_2 OVER PALLADIUM SUPPORTED ON RARE EARTHS PROMOTED ZIRCONIA

Relatore: Prof. Paolo Canu
Correlatore: Academic Prof. Tapio Salmi

Laureando: ANDREA BERNARDINI

ANNO ACCADEMICO 2014–2015

Abstract

The present work is focused on the direct synthesis of hydrogen peroxide. The direct synthesis is one of the most promising alternatives to the actual process for the production of hydrogen peroxide. In the last two decades several research groups have been interested on this topic and a wide literature has been provided. The major aspects of investigation for researchers are the synthesis of new materials and the definition of kinetics of reaction. Anyway, so far, it hasn't been found a solution to promote the direct synthesis to compete with the diffuse anthraquinone auto-oxidation process on industrial level.

In this view the aim of the thesis was testing novel catalysts based on palladium supported on zirconia and ceria doped with rare earths. No studies have been reported using these solid mixtures for hydrogen peroxide direct synthesis; nevertheless their features inspired their application. The catalysts evaluation was supported by a wide and depth characterization of the materials. The experimental activity permitted to deduce valuable indications on the catalyst properties promoting/favoring the hydrogen peroxide production. The homogeneity of the solid solution and the reducibility of the support-metal system emerged as influencing factors. The supports that allowed the formation of larger, thus less energetic, metal particles resulted more selective towards H_2O_2.

Further treatments of reduction and oxidation were performed on the catalysts. The samples were tested, evaluating the different effects of the processing on the catalysts.

A preliminary study for the definition of the gas to liquid mass transfer was reported in view of a subsequent numerical modeling of the experimental apparatus.

Riassunto

Questa tesi tratta la sintesi diretta di perossido di idrogeno (H_2O_2) con catalizzatori a base di palladio. Il perossido di idrogeno, noto come acqua ossigenata, è un efficiente e ecosostenibile reagente. La recente tendenza a privilegiare processi e prodotti chimici più rispettosi dell'ambiente ha incrementato l'impiego di H_2O_2 come agente ossidante in molteplici applicazioni. Attualmente il processo industrialmente più usato per la produzione di acqua ossigenata prevede l'auto-ossidazione dell'antrachinone in una soluzione organico. La tecnica presenta un'elevata selettività, ma richiede un complesso sistema impiantistico e di purificazione. La sintesi diretta si propone come una valida alternativa, considerando la produzione di acqua ossigenata in un processo monostadio a partire dai componenti elementari, H_2 e O_2. Nonostante la reazione appaia come la più semplice possibile, il meccanismo è interessato da reazioni consecutive e competitive con formazione di acqua. Le variabili che influiscono sulla selettività della reazione sono sia legate alle condizioni operative di processo (temperatura e pressione) che concernenti lo stato del catalizzatore (caratteristiche del supporto e interazione supporto-metallo). La composizione di nuovi catalizzatori e la definizione delle più migliori condizioni di lavoro sono i temi di maggiore investigazione da parte dei numerosi gruppi di ricerca implicati nella sintesi diretta di H_2O_2.

Sulle basi di queste considerazioni la Tesi si propone di valutare le prestazioni di 7 catalizzatori preparati supportando palladio (0.3 o 0.6 wt.%) su ossidi misti (ZrO_2 e CeO_2) promossi da terre rare (La_2O_3 e Y_2O_3). Questi materiali sono stati scelti per le loro singolari caratteristiche, in particolare si considera che le capacità di aumentare la dispersione del metallo e la mobilità dell'ossigeno possano promuovere la selettiva formazione di H_2O_2.

I test catalitici sono stati condotti in un reattore *semi-batch* agitato e mantenuto a temperatura costante di 10°C e pressione di 50 bar. La miscela di gas reagenti (H_2-O_2-N_2) viene fatta gorgogliare per tutta la durata dell'esperimento in una sospensione di metanolo e catalizzatore. Nelle prove non si sono utilizzati promotori di selettività, al fine di isolare e valutare le prestazioni catalitiche. La composizione della fase gassosa all'uscita dall'impianto è valutata con analisi gascromatografiche. La concentrazione di H_2O_2 e H_2O nella fase liquida sono quantificate con titolazione iodometrica e *Karl Fischer*, rispettivamente. I valori di concentrazione di perossido di idrogeno ottenuti sono superiori rispetto a quelli riportati in letteratura con apparati simili.

Le tecniche di caratterizzazione utilizzate per definire le proprietà dei catalizzatori sono *Temperature Programmed Reduction* (TPR), *CO chemisorption*, *X-Ray Diffraction* (XRD) e *Atomic Adsorption Spectroscopy* (AAS). Le analisi hanno dimostrato che le proprietà del

supporto influenzano l'interazione e la riducibilità del sistema metallo-supporto, risultando in differenti prestazioni catalitiche. I campioni che formano una soluzione solida omogenea e sono più riducibili esibiscono *performance* migliori, probabilmente come conseguenza della più facile riduzione della fase metallica attiva. Inoltre i supporti che presentano particelle di palladio larghe (> 2 nm) risultano più selettivi verso il perossido di idrogeno; confermando la teoria, già proposta in letteratura, che i siti energetici e difettosi presenti sulle particelle piccole rompano il legame O-O della molecola di O_2, favorendo la formazione di acqua. Queste osservazioni portano a concludere che supporti facilmente riducibili e che formino particelle di metallo più larghe sono più desiderabili nella preparazione di catalizzatori per la sintesi diretta di H_2O_2.
L'attività sperimentale è proseguita con lo studio degli stessi catalizzatori, dopo che questi sono stati trattati con dei cicli di riduzione e ossidazione. I campioni sono stati testati nello stesso impianto e stesse condizioni operative precedentemente descritti. La varietà dei risultati sperimentali raccolti dimostrano come i diversi catalizzatori abbiano reagito diversamente ai processi *redox*. Solo un'analisi critica dei risultati ottenuti dalla caratterizzazione dei materiali permetterà di giungere a conclusioni definitive sull'effetto dei trattamenti.
Test sulla solubilità dell'idrogeno in metanolo in presenza di azoto e ossigeno sono stati condotti al fine di ricavare informazioni sul *mass transfer* tra fase liquida e gassosa. Lo studio è un'attività preliminare ad un più ampio progetto che si propone di presentare un modello numerico dell'apparato sperimentale.
Questa Tesi è il risultato di una produttiva collaborazione tra il Dipartimento di Ingegneria Industriale dell'Università di Padova e il *Teknisk kemi* dell'Åbo Akademi (*Turku*). Roberto Lanza, professore del *KTH Royal Institute of Technology* di Stoccolma, ha sintetizzato i catalizzatori e realizzato le analisi di caratterizzazione. Il lavoro sperimentale è stato svolto presso il laboratorio del Dipartimento di Ingegneria Chimica di *Turku* sotto la supervisione del Prof. Tapio Salmi e del Prof. Canu.

L'attività di ricerca ha permesso la pubblicazione di un articolo scientifico:
Bernardini, a., Gemo, N., Biasi, P., Canu, P., Mikkola, J. P., Salmi, T., & Lanza, R. (2015). Direct synthesis of H_2O_2 over Pd supported on rare earths promoted zirconia. *Catalysis Today*. http://doi.org/10.1016/j.cattod.2014.12.033
Un ulteriore articolo è in corso di sottomissione.

Table of content

Introduction

Hydrogen peroxide is one of the most efficient and green chemical oxidant. In the last decades, the increased environmental interest and controls favored the replacement of polluting reagents by hydrogen peroxide in numerous industrial applications. This Thesis is focused on the production of H_2O_2 by direct synthesis. Direct synthesis is a cleaner and simpler alternative to the diffuse anthraquinone autoxidation process (AO), but selectivity and safety of the process are still issues that limit its industrial application. Several research groups are focused on the synthesis of new catalysts and the identification of the reaction mechanism.

The core of the Thesis is the critical evaluation of the performances of 7 novel catalysts for the direct synthesis of hydrogen peroxide.

The first Chapter gives an overview of the hydrogen peroxide market, applications and production methods, also describing the factors affecting the selectivity of direct synthesis. In fact, the selective oxidation of H_2 towards H_2O_2 is followed by side reactions that lead to water. The reactions are affected by the operative conditions of the process (temperature and pressure) and the catalyst characteristics (support-metal interactions and support properties).

The second Chapter describes the materials for the experimental work. The catalysts were synthesized supporting Pd on both $Zr_xM_{1-x}O_2$ (M=La,Y,Ce) and on mechanical mixtures of CeO_2 and ZrO_2. These materials present features that could favor the hydrogen peroxide production, i.e. the oxygen mobility. The Chapter describes the experimental equipments and techniques used to carry out the catalytic experiments and characterize the samples. The catalysts were tested on a semibatch apparatus, in which reagent gases bubbled in the catalyst slurry. The catalysts were characterized by Temperature Programmed Reduction (TPR), CO chemisorption, X-Ray Diffraction (XRD) e Atomic Adsorption Spectroscopy (AAS).

The experimental results are reported in Chapter 3. The characterization analysis are presented first, focusing on how the morphological properties of the materials affect the interaction between the support and the active metal phase. Then the catalytic results are discussed, giving valuable indications on the catalyst most desirable features for hydrogen peroxide direct synthesis.

Two Appendix are added to the Thesis. The first one reports a preliminary study for the evaluation of gas-liquid mass transfer limitations. The second Appendix presents the further reduction-oxidation treatments performed on the materials and the experimental results collected.

This Thesis is the result of a collaboration between the *Dipartimento di Ingegneria Industriale dell'Università di Padova,* the *Teknisk Kemi* at *Åbo Akademi* (Turku, Finland) and the *KTH Royal Institute of Technology* (Stockholm, Sweden). The experimental activities were carried out in the the *Teknisk Kemi* at *Åbo Akademi* and supervised by Prof. Tapio Salmi and Prof. Paolo Canu. The catalysts tested were synthesized in *KTH Royal Institute of Technology.*

The research activity leads to the publication of the scientific paper:
Bernardini, a., Gemo, N., Biasi, P., Canu, P., Mikkola, J. P., Salmi, T., & Lanza, R. (2015). Direct synthesis of H_2O_2 over Pd supported on rare earths promoted zirconia. *Catalysis Today*. http://doi.org/10.1016/j.cattod.2014.12.033
A further scientific work is going to be submitted.

Chapter 1

Hydrogen peroxide: features, production and applications

Hydrogen peroxide is considered one of the most versatile chemical oxidants available and has a wide range of applications. In the last decades, the growing interest on H_2O_2 attracted the efforts of many research groups in the world, providing a large amount of literature. The drawing up of the chapter is inspired on the major reviews written on the research field: Campos-Martin, Blanco-Brieva and Fierro[1] reviewed hydrogen peroxide analyzing the large-scale conventional processes and the emerging production techniques; Samanta[2] focused on the operative aspects of direct synthesis considering the factors affecting the reactions; Centi, Perathoner and Abate[3] studied the production of peroxide from an industrial perspective; Serna *et al.*[4] evaluated the market and the prospects of the business of H_2O_2. The purpose of the chapter is to give an overview of the principal features, methods of production and applications of hydrogen peroxide.

1.1 Hydrogen peroxide and green chemistry

Hydrogen peroxide (H_2O_2) is principally used in chemical and environmental fields, although it finds applications in almost all industrial areas. Hydrogen peroxide is the simplest peroxide, a category of compounds characterized by a single bond between two oxygen atoms. This feature makes H_2O_2 reactive both as oxidizing and as reducing agent. The only degradation product of its use is water, making it a suitable reagent in environmentally friendly methods in the chemical industry.

In the last years, the environmental protection became one of the prominent aspects in designing and operating a chemical process. In 1991, Paul Anastas introduced the term *green chemistry* to define a more sustainable way to interpret the chemical industry. Green chemistry considers the application of environmental friendly chemicals and processes that result in reduced waste products, improved efficiency (high atom economy, low E-factor) and lower hazard to human health. It promotes the pollution and security prevention (safer chemicals), use of renewable feed stocks and energy efficiency. The catalysis has a central function in green chemistry considering the catalytic reagents (with high selectivity) superior to stoichiometric reagents[5].

H_2O_2 is one of the most efficient oxidizing agents by virtue of its active oxygen content (47.1%), only next to the molecular oxygen. Campos-Martin *et al.*[1] reported the reaction that hydrogen peroxide may undergo, depending on the type of substrate (Reactions 1.1-1.5).

Decomposition	$2H_2O_2 \rightarrow 2H_2O+O_2$	(1.1)
Oxidation	$H_2O_2+M \rightarrow MO+H_2O$	(1.2)
Addition	$H_2O_2+A \rightarrow AH_2O_2$	(1.3)
Reduction	$H_2O_2+R \rightarrow RH_2+O_2$	(1.4)
Substitution	$H_2O_2+RX \rightarrow ROOH+O_2$	(1.5)

The decomposition (1.1), an exothermic reaction that releases gaseous oxygen, depends on temperature and concentration of the peroxide. The rate of decomposition can be minimized by addition of stabilizers. Hydrogen peroxide can oxidize a wide variety of inorganic and organic substrates under very mild conditions (1.2). It could work also as reducing agent for stronger oxidizing compounds, such as $KMnO_4$ and Cl_2.
Hydrogen peroxide is a stable and safe chemical when handled correctly and offers the advantage to be soluble in water and many organic solvents. It is usually marketed in water solution, with added stabilizer, at concentrations of 35, 50, 70 % by weight.

1.2 Market of hydrogen peroxide

Juan Garcia-Serna *et al.* reviewed the direct synthesis of hydrogen peroxide from an engineering point of view, i.e. focusing on the costs and suitable design criteria for process development.[4] The authors described the actual situation and the prospects on the business of H_2O_2. According to the data from 2010, Solvay is the best company producer with 906 kt per year (30% of the market), followed by Evonik (19.6%) and Arkema (13.4%). China has rapidly increased the peroxide production, becoming in the last years the largest producing and consuming country in the world.
GIA (Global Industry Analysts) released a comprehensive global report on hydrogen peroxide markets[6]. It is forecast that hydrogen peroxide production will reach 4.67 million metric tons by 2017. Increased environmental pressure and pollution controls, especially in North America and Western Europe, continue to drive demand for hydrogen peroxide over chlorine products for treating process streams. The growing demand by Asian-Pacific and Latin America markets, driven by Brazil, Chile and China, will support the rapid expansion in the next years.
Juan Garcia-Serna *et al.* reported an interesting analysis on the capital (CAPEX) and operational costs (OPEX) in the direct synthesis production. During the last decades, the

direct synthesis commercialization has been limited because of the high capital expenditures due to the necessity of operate with pressurized plants. The recent research efforts have reduced the CAPEX and the OPEX decreasing the operative pressure and increasing the selectivity. It has led to further studies and trials, e.g. by Degussa-Headwaters, to build a plant for direct synthesis of H_2O_2. It has been calculated that the implementation results attractive in small on-site plant with production capacities below 10 kt per year. The maximum cost of a plant with a producing capacity of 10 kt of H_2O_2 per year is estimated in 40.3±12.1 MM$ (in 2012) to be competitive to the traditional process.[4]

1.2.1 Applications of hydrogen peroxide

The demand of hydrogen peroxide is rapidly growing due to its increasing application in the pulp/paper bleaching and water treatment industries. H_2O_2 is being used as an environmentally friendly alternative to chlorine and chlorine-containing bleaches and oxidant, avoiding halogenated products in waste streams. Figure 1.1 summarizes the major applications of hydrogen peroxide.

It is considered that more than the 80% of the hydrogen peroxide european demand is covered by paper bleaching and chemical synthesis[1].

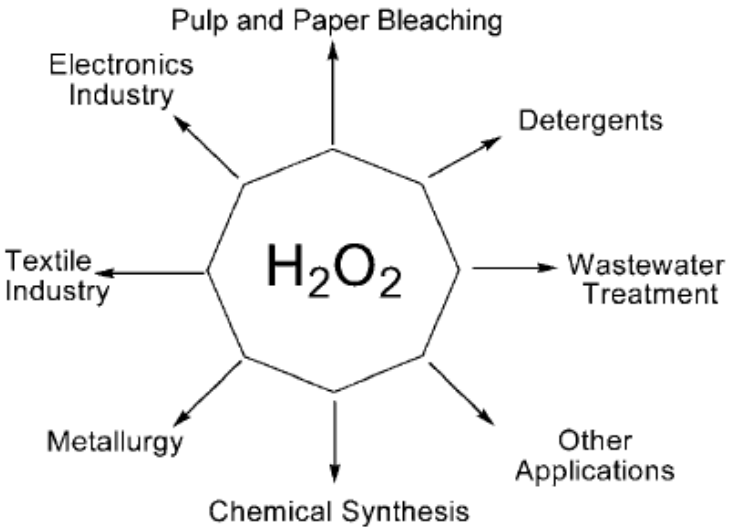

Figure 1.1. *Hydrogen peroxide uses. (Adapted for Jose M. Campos-Martin, 2006[1]).*

Samanta imputed the increased production of hydrogen peroxide as consequence of its new applications on the large volume chemical synthesis[2]. The discovery of Titanium Silicalite (TS-1) by EniChem and the tuning of the advanced propylene epoxidation (HPPO) process by Degussa/Uhde have widely contributed to the expansion of the market. TS-1 is an

aluminosilicate zeolite, ZSM-5, in which small amount of tetrahedral Si atoms are substituted by Ti atoms. TS-1 has an outstanding ability to catalyze various oxidation reactions with aqueous H_2O_2 as primary oxidant, e.g. selective oxidation of alcohols and partial oxidation of alkane.

Degussa/Uhde's propylene epoxidation, known as hydrogen peroxide–propylene oxide (HPPO) process, is a single step process with water as the only by-product. Propylene oxide (PO) is used to produce solvents, chemical intermediates, flame retardants and as starting material for polyurethane. The market growth prospects for PO are excellent; so that BASF and Dow have announced the synergic building of a plant for the synthesis of propylene oxide by a environmentally compatible HPPO route. H_2O_2 is used in the 'green' method of synthesis of caprolactam, with a process originally developed by EniChem and commercialized by Sumitomo.

In term of amount invested the textile industry is the third field of application for hydrogen peroxide[1]. It is applied as bleaching agents and it has advantages over other alternatives (sodium hypochlorite), i.e. no severe toxicity and no corrosivity. Samanta citing Jones *et al.*[7] described the use of hydrogen peroxide in production of stain free detergents. Color-safe laundries bleaches containing hydrogen peroxide have increasingly replaced bleaches containing hypochlorite. In this case hydrogen peroxide is used with stable precursors, e.g. sodium perborate, that release the peroxide when dissolved in water. The detergents result color safe, brighten colors and with a strong stain-removal capability.

The most significant environmental application of hydrogen peroxide is the treatment of a wide variety of industrial wastes and wastewaters[1]. It is used for the removal of H_2S from exhaust gases generated by chemical and pharmaceutical synthesis. H_2O_2 can efficiently destroy cyanide, nitrite, chloride and organic matter. The hydrogen peroxide is widely applied in the bioremediation of contaminated soils, e.g. in situ decontamination by injection in the ground. It consists in the utilization of H_2O_2 combined with other substances, i.e. Fe^{2+} in the *Fenton* process (Reaction 1.6), as a source of oxygen and free radicals acting on the polluting agents[8].

$$Fe^{2+} + H_2O_2 \rightarrow Fe^{3+} + OH\cdot + OH^- \qquad (1.6)$$

The $OH\cdot$ is the most reactive among these species, with a high oxidative function almost double respect H_2O_2[9].

The applications, as well important, that assimilate just a minor part of hydrogen peroxide market are several. H_2O_2 is used on the extraction, separation and purification of metal as uranium and gold. The cosmetic and pharmaceutical industries use disinfecting properties of H_2O_2. Highly pure H_2O_2 is used for purification of electronic materials (germanium and silicon semiconductors)[1].

1.3 Production of hydrogen peroxide

This section aims to give an outlook of the most diffuse and available methods to produce hydrogen peroxide. Jose M. Campos-Martin *et al.* analyzed the actual techniques and the emerging alternatives, resulting in an excellent work to overview the past, present and future of H_2O_2 technologies[1]. The anthraquinone autoxidation process (AO) is commercially the most successful since it produces H_2O_2 continuously, at moderate temperature and without H_2-O_2 contact. The technique shows also several drawbacks that could be avoided applying newer solutions. The AO process is extensively introduced in order to arrange a profitable comparison with the direct synthesis technique.

1.3.1 Anthraquinone autoxidation

The anthraquinone autoxidation involves the indirect oxidation of H_2 to H_2O_2. The process was introduced in the 1940s by IG Farben-industrie and it is composed by four major steps: hydrogenation, oxidation, hydrogen peroxide extraction and treatment of the purification working solution[1]. Figure 1.2 reports a schematic diagram of the steps of the anthraquinone method, while Figure 1.3 describes the reactions involved.

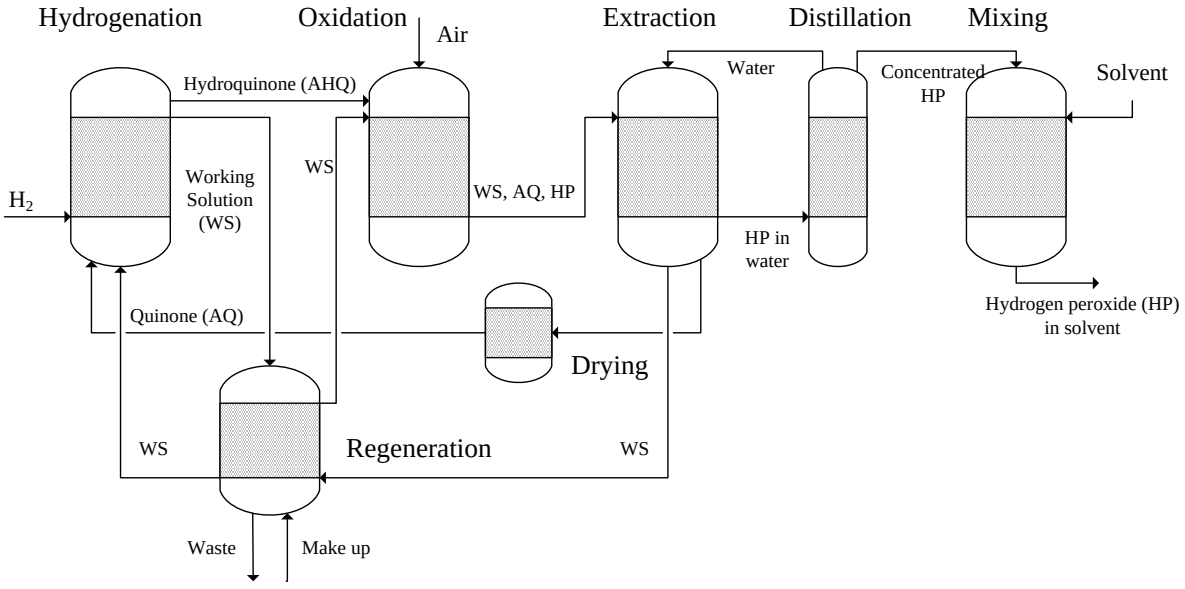

Figure 1.2. *Plant of the AO process for the synthesis of hydrogen peroxide. (Adapted from Centi, 2007[3]).*

In the first phase a 2-alkylanthraquinone (AQ) is hydrogenated catalytically to the correspond anthrahydroquinone (AHQ). The reaction is carried out in a mixture of organic solvents, e.g. ester/hydrocarbon, called working solution (WS)[2]. A side reaction suitable is the further hydrogenation of AHQ to yield the 5,6,7,8-tetrahydroanthrahydroquinone

(THAHQ). The palladium catalysts used in the reactions result selective, even if the hydrogenation by-products can't be avoided (extra consumption of hydrogen and anthraquinone). The selectivity of Pd catalysts, usually supported on Al_2O_3 and SiO_2, can be improved by adding promoters. In the subsequent phase, the solution containing the AHQ and THAHQ is separated from the hydrogenation catalyst and oxidized with air or oxygen. The oxidation produces H_2O_2 and regenerates the original anthraquinone (Figure 1.3).

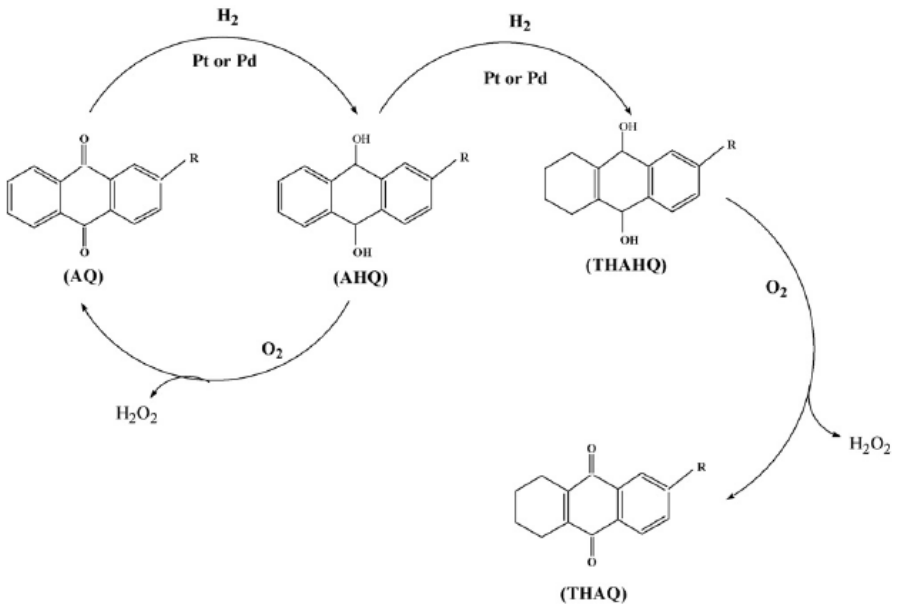

Figure 1.3. *Reactions involved in the AO process for the synthesis of hydrogen peroxide. (Adapted from Samanta, 2008[2]).*

The reaction is carried out no-catalytically by bubbling gas through the solution. AHQ and THAHQ are active in the oxidation phase with two distinct steps and mechanisms.

The hydrogen peroxide is stripped from the working solution with water in counter current to produce a solution that it is usually between 25 and 45 wt.%. The acqueous solution of H_2O_2 is then distilled to reach commercial grades for purity and concentration. It is considered to recover the 95% of the peroxide produced.

The AO method permits the production of hydrogen peroxide continuously at mild temperatures and avoiding the direct contact between O_2 and H_2. However the AO process suffers from several drawbacks, i.e. the use of a complex and toxic solvent system and the deactivation of hydrogenation catalysts. The difficulty in controlling the H_2/AQ ratio during the hydrogenation phase causes the formation of by-products. Despite the efficiency of the separation system, the use of an organic working mixture results in an unavoidable contamination of the H_2O_2 solution. The periodic replacement of costly quinone-derivative

due to non-selective hydrogenation and the requirement of energy for the removal and purification steps lead to a high capital and operating expenditures.
The AO process is economically viable only for a large-scale plant (>40x10^3 tons per year)[2]. The high costs prohibit the on-site production, then H_2O_2 is made in one location and then distributed to the end-users. The transportation creates additional safety concerns since concentrated H_2O_2 can be explosive if it violently decomposes. The solution transported must be stabilized with substances to remove before the final application of the peroxide. These issues have fascinated scientists and engineers for many years to develop a more cost-effective and cleaner process for manufacturing this large-volume environmentally friendly chemical.
An innovative concept in the industry of AO process is the reactive separation process in a sieve plate column, that combines the oxidation phase and the separation from the working solution in a single step. This approach increases the yield of H_2O_2 respect the traditional AO synthesis, because the by-products are immediately separated and avoided to participate in the equilibrium reaction. It is demonstrated that both the conversion of AHQ and the extraction efficiency from the working solution increase with the superficial velocity of O_2. The conversion of AHQ is improved as consequence of the increasing of the mass-transfer coefficient at the gas-liquid interface, that is a limitation in the oxidation phase in the conventional process[10].

1.3.2 Oxidation of alcohols

Another large-scale production for hydrogen peroxide synthesis is the partial oxidation of primary or secondary alcohols, that produces an aldehyde or ketone as a coproduct. Campos-Martin *et al.* reported the oxidation of the 2-propanol by Shell and the oxidation of methylbenzyl-alcohol by Lyondell Chemical and Repsol Quimica.
The Shell Chemical process contemplates the oxidation by an oxygen-enriched gas stream of a 2-propanol/water solution at moderate temperature (Figure 1.4).

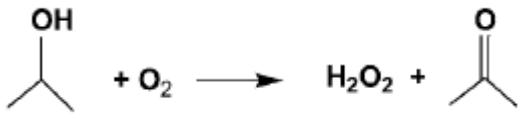

Figure 1.4. *Synthesis of hydrogen peroxide by the oxidation of 2-propanol. (Adapted from J.M. Campos Martin, 2006[1]).*

The isopropyl conversion is set under the 15% in order to reduce the formation of by-products, e.g. acetic acid. Anyway the method requires several separation phases by evaporation, distillation and solvent-extraction. The quality of H_2O_2 produced by this process is worse than that from the anthraquinone autoxidation.

Figure 1.5 displays the oxidation of the methylbenzyl-alcohol (MBA) for the synthesis of hydrogen peroxide developed by Lyondell Chemical and Repsol Quimica.

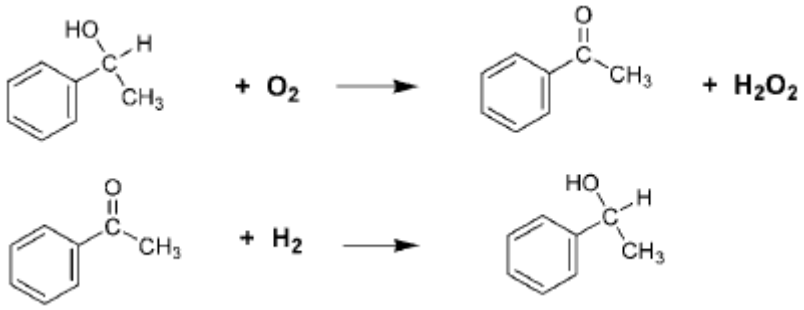

Figure 1.5. *Synthesis of hydrogen peroxide by the oxidation of methylbenzyl-alcohol. (Adapted from J.M. Campos Martin, 2006[1]).*

These companies recover the MBA as a co-product of their main processes. The reaction is operated without catalyst, although recent patents claimed that the addition of metal catalyst enhances both the reaction rate and the selectivity. The hydrogen peroxide solution must be treated by extraction and distillation units to reach the desired concentration. The distillate is hydrogenated to recycle acetophene back into methylbenzyl-alcohol[2].

1.3.3 Electrochemical synthesis

The alternative for a large-scale production of hydrogen peroxide is the electrolysis of a dilute solution of NaOH[1]. Dow Chemical performs the synthesis in an electrolytic cell. Electrolytic cell is an electrochemical cell that undergoes a chemical reaction when electrical energy is applied. The mechanism is summarized in Reactions 1.7-1.9.

$$\text{Anode: } 2OH^- \rightarrow H_2O + {}^1\!/_2\, O_2 + 2e^- \quad (1.7)$$

$$\text{Cathode: } H_2O + O_2 + 2e^- \rightarrow HO_2^- + OH^- \quad (1.8)$$

$$\text{Overall reaction: } OH^- + {}^1\!/_2\, O_2 \rightarrow HO_2^- \quad (1.9)$$

The hydroperoxide ion HO_2^- (the conjugate base of hydrogen peroxide) is synthesized by anodic oxidation of OH^- and the cathodic reduction of O_2. The cathode consists of graphite chips coated with carbon black. The peroxide is accumulated as alkaline-peroxide, HO_2Na; so that the technique is best suited with applications for which it is not necessary to separate the peroxide from the caustic soda, e.g. pulp bleaching[11]. The technology is considered to have an excessive energy requirement for large-scale production, but it could be used for on-site small production.

It finds application in wastewater treatment (electro-Fenton), but in general the catalytic route appears to be preferable in terms of costs and scale-up[3].

1.3.4 Emerging Alternatives

The large-scale production is allocated in a single site where a huge amount of peroxide is synthesized and then dispensed to end-users. The new goal of the hydrogen peroxide market is to find a process that permits the production of the commodity on the final site in order to avoid the dangerous and costly transport operations. In this category is included the direct synthesis method, to whom a wide description is dedicated.

1.3.4.1 Photocatalysis

Hydrogen peroxide can be formed on the surface of semiconductor oxides, i.e. TiO_2, under UV irradiation[1]. The illumination of an aqueous suspension of the semiconductor oxides excites an electron from the valence band to the conduction band, so that a positive hole is created in valence band. The positive hole oxidizes H_2O to form an $OH\cdot$, and the excited electron reduces O_2 to O_2^-.

Cai *et al.* proposed two formation mechanisms of H_2O_2 over TiO_2 particles[12]. The first one (Reaction 1.10) involves the oxidation by the positive hole of water and the generation of H_2O_2 by recombination of $OH\cdot$ radicals. The second mechanism (Reaction 1.11) considers the reduction of O_2 by the photogenerated electron.

$$2H_2O + 2h_{VB}^+ \rightarrow H_2O_2 + 2H^+ \quad (1.10)$$

$$O_2 + 2H^+ + 2e_{CB}^- \rightarrow H_2O_2 \quad (1.11)$$

The concentration of hydrogen peroxide achieved with this method is in the micromolar range. It can be increased by the addition of small amount of Cu^{2+}, that favored the reduction of O_2.

One of the species formed in photocatalytic reactions is $OH\cdot$, already mentioned as compound widely used for oxidation of organic substrates in liquid phase.

1.3.4.2 Fuel Cells

The industrial application of electrolytic cells for the production of hydrogen peroxide has been already introduced in this thesis (Section 1.3.3). An alternative is the utilization of fuel cells that, on the contrary of the electrolytic ones, doesn't demand electrical energy. The innovative approach simultaneously guarantees the production of H_2O_2 and generation of electricity. The simplest design of fuel cell is divided by an electrolyte membrane[13]. The anodic face of the membrane is deposited by Pt and oxides H_2; the cathode face is covered with graphite and is responsible for reducing O_2 to H_2O_2. The limiting factor of this design is the low concentration of O_2 at the cathode[13].

Newer fuel-cells setup overcomes the problem with the application of a three phase boundary (solid cathode/aqueous electrolyte/gaseous O_2). I.Yamanaka *et al.* proposed the electrochemical reduction of O_2 in an H_2/O_2 fuel cell with NaOH solution as electrolyte (Figure 1.6)[14].

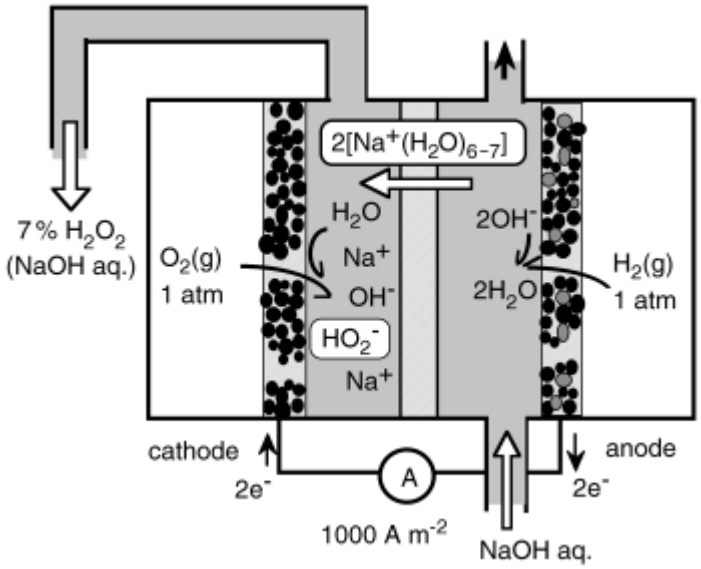

Figure 1.6. *Fuel cell scheme for hydrogen peroxide synthesis. (Adapted from I. Yamanaka et al., 2003[14]).*

The mechanism of formation of hydroperoxide ions is described by Reactions 1.12-1.14. It considers the oxidation of H_2 to H_2O at the anode, and the reduction of O_2 to HO_2^- at the cathode.

Anode: $2OH^- + H_2 \rightarrow H_2O + 2e^-$ (1.12)
Cathode: $H_2O + O_2 + 2e^- \rightarrow HO_2^- + OH^-$ (1.13)
Overall reaction: $H_2 + OH^- + O_2 \rightarrow H_2O + HO_2^-$ (1.14)

The use of porous membrane electrode derived from carbon powders allows a higher pressure of O_2 at the active site enhancing its reduction to H_2O_2 and minimizing the degradation of H_2O_2 to H_2O. Feeding pure O_2 into the cathode a 6-7 wt.% H_2O_2 concentration can be reached. The replacement of O_2 by air has a considerable cost advantage with just a slightly decrease in the cell performance[14].
The basic advantage presented by the fuel cell is that there isn't direct contact between O_2 and H_2 since they are fed separately. Despite the several good points the fuel cells utilization for hydrogen peroxide production is still far away from the industrial commercialization.

1.3.4.3 $CO/O_2/H_2O$ mixtures

The production of hydrogen peroxide is possible from $CO/O_2/H_2O$ mixtures in presence of a metal complex. The main reaction is reported in 1.15.

$$CO + O_2 + H_2O \rightarrow CO_2 + H_2O_2 \quad (1.15)$$

The reaction mechanism involves the water-gas-shift reaction ($CO+H_2O \rightarrow CO_2+H_2$), followed by the oxidation of the generated H_2 with the solubilized O_2. The method can't be considered green because of the production of CO_2.

The major field of investigation for the technological development is the synthesis of the catalyst. Both homogeneous and heterogeneous catalysts have been proposed. Campos-Martin *et al.* cited the studies on liquid-phase reactions in presence of homogeneous catalysts, as palladium triphenil-phosphate complexes. The system is rapidly deactivated by oxidation of phosphate ligands and the catalyst seems to be unsuitable for technical application. Further complexes have been proposed but not with sufficient efficiency for practical use. The breakthrough in this approach would be the detailed knowledge of the reaction mechanism in order to optimize the nature of the ligands.

The heterogeneous metal supported catalysts result reasonably active, but with a unsatisfactory selectivity. The problem is the deactivation of the catalyst through poisoning by water. Substantial improvements, especially regarding Cu/Al_2O_3 catalyst, are obtained by modification of the nature of the liquid-phase. Acetone appears to be the most appropriate solvent, increasing the transfer rate of oxygen to the catalytic site. This method is an interesting option in case a source of CO is available.

1.3.4.4 Enzymatic oxidation

The enzymatic oxidation of organic substrates is a simple and safe approach for the formation of hydrogen peroxide under mild conditions. The enzyme glucose oxidase catalyzes the oxidation of glucose by molecular oxygen, as reported in Reaction 1.16.

$$C_6H_{12}O_6 + O_2 \rightarrow H_2O_2 + C_6H_{10}O_6 \quad (1.16)$$

H_2O_2 is often generated in living organisms, but it is rapidly destroyed by oxidation to O_2 or reduction to OH^-. Peroxidase enzymes catalyze many organic oxidations with H_2O_2 as substrate and they are used for treatment of industrial waste waters, e.g. removal of phenol[15]. The main limitation to their utilization is that the enzymes work only at low concentration of H_2O_2. The instability of peroxidases can be alleviated by co-immobilization of glucose oxidase and peroxidases. The glucose oxidase is the enzyme responsible of the H_2O_2 generation through reduction of O_2 (Equation 1.16). The enzymes

are co-immobilizated in polyurethane foams affording heterogeneous biocatalysts in which the hydrogen peroxide is formed inside the polymeric matrix[16]. The reaction mechanism is reported in Figure 1.7.

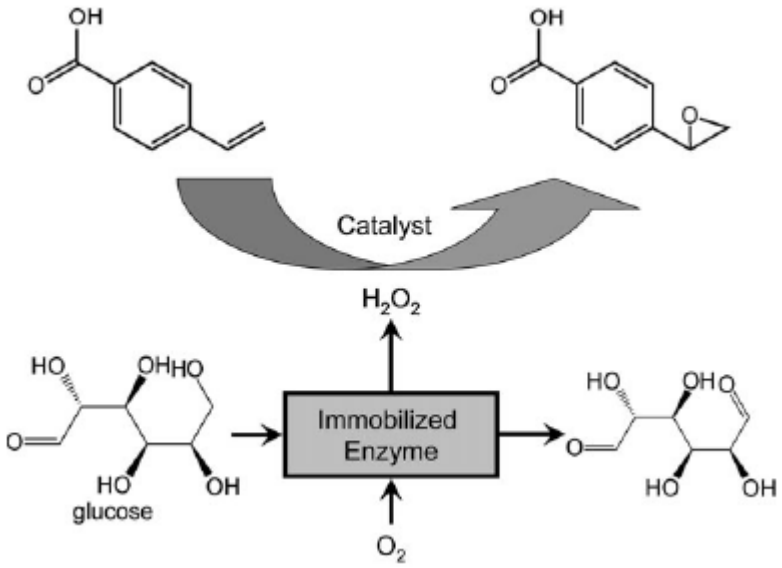

Figure 1.7. *Hydrogen peroxide synthesis by immobilized glucose oxidase. (Adapted from J.M. Campos Martin, 2006[1]).*

The immobilization of glucose oxidase on organic substrates is a profitable solution for recovery and recycle the enzyme, even if it still results a difficult operation.
The low concentration limit and the high molecular weight of enzyme lead to a low space yield. This bio-inspired approach for production of hydrogen peroxide is interesting, but not still attracting for implementation in the chemical industry.

1.3.4.5 Plasma

H_2O_2 can be synthesized with high selectivity via the gas-phase reaction of H_2/O_2 non-equilibrium plasma. The activation of H_2 and O_2 molecules is done by electric discharge at atmospheric pressure. The first synthesis of hydrogen peroxide by non-thermal plasma at atmospheric pressure and ambient temperature was reported by Zhou *et al.* using a non-explosive H_2/O_2 mixture. The authors recorded a yield of 32.8% calculated on O_2 consumption with a selectivity of 56.3%[17].
Further investigations led to notable improvement of the technique. Thevenet *et al.* investigated the synthesis of H_2O_2 with a dielectric barrier discharge ignited in a non-thermal plasma in presence of a O_2 and H_2 mixture[18]. Figure 1.8 displays the performances of the reactor after deposition of layers of SiO_2 and TiO_2 on the dielectric surfaces and insertion of SiO_2 fibres in the reactor gap.

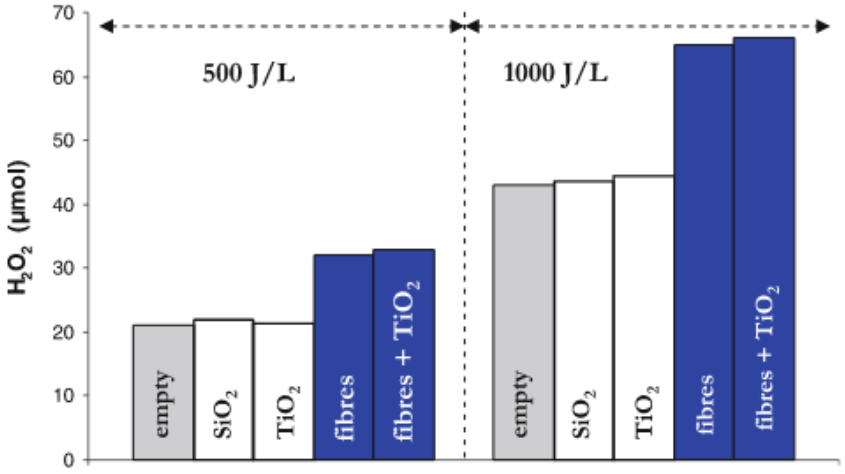

***Figure 1.8**. Amounts of H_2O_2 with (SiO_2 layers, TiO_2 layers, SiO_2 fibers and SiO_2+TiO_2 fibers) or without materials after 3 hours syntheses performed under 500 and 1000 J/L in the presence of 2.5% O_2 into H_2. (Adapted from Thevenet et al., 2010[18]).*

The fibers created physical bridges between both electrodes, consequently the discharges ignited in the presence of fibers were mainly surface discharges. The presence of simple layers on reactor walls had no effect on the reaction, but the modification of the discharge towards a surface discharge using fibrous materials considerably improved the efficiency of the process[18].

The method shows several advantages, as it is processed in a single gas phase involving only H_2 and O_2 and avoiding any mass-transfer limitation. Furthermore there is no safety concern, since the H_2/O_2 ratio that gives the best performance is far from the explosive range.

1.4 Direct synthesis of hydrogen peroxide

The first patent on hydrogen peroxide direct synthesis was presented by Henkel and Weber in 1914. The process consisted on the reaction of H_2 and O_2 on the surface of a tube completely covered by a palladium, nickel and platinum catalyst[19]. However little progress werw made after 1914 because of safety issue. The H_2-O_2 mixtures results flammable/explosive at atmospheric pressure when the molar concentration of H_2 is in the 4-94%[20].Operations inside the flammability limits have been an option for decades, but nowadays almost all the research groups work in a safer gas concentration.

Only after 1980, the increasing demand of H_2O_2 for the environmental perspectives stimulated newer researches to overcome the initial problems on direct synthesis[2]. Both academia and industry investigated direct synthesis applications, publishing a great amount of papers and patents. Between 1980s and 1990s over 100 patents were issued from

industrial researches, as reported by Centi *et al.*[3]. The most involved companies on this field are Solvay (the biggest producer of H_2O_2), Polimeri Europa/EniTecnologie, BASF, Eka Noble, Shell, Dupont and Degussa[3]. Most of the patents recently issued report results outside the explosion region, while some companies still operate inside the explosion range. BASF contemplates to work inside the explosive range considering to avoid the explosion setback with a particular reactor design, described in Figure 1.9.

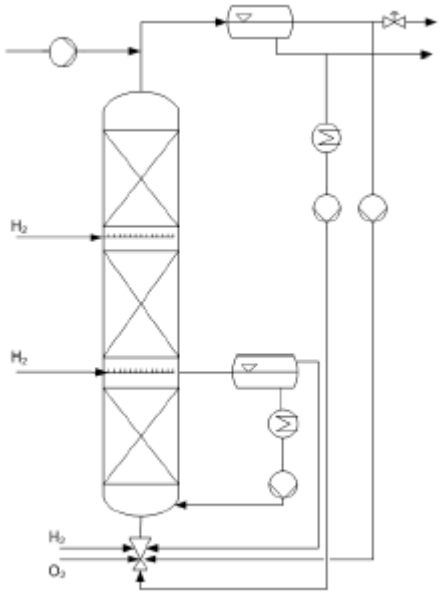

***Figure 1.9**. Scheme of the reactor proposed by BASF for direct synthesis of H_2O_2. (Adapted from Centi et al., 2013[3]).*

The reactor is composed of three layers of catalyst monolith with intermediate feed of H_2, while O_2 is dispersed from the bottom[21].

The research efforts are focused on the improvement of catalyst preparation and reaction/reactor operations, with particular attention on the safety concerns.

1.4.1 Direct synthesis reaction scheme

The direct synthesis consists in the production of H_2O_2 starting from its elements in a one-pot process. The scheme is apparently simple, but the mechanism is complicated by side and consecutive reactions. Figure 1.10 describes the reaction scheme. All the reactions are thermodynamically favored and exothermic. In particular the oxidation of H_2 to water and hydrogenation of H_2O_2 are more favored than the selective oxidation to hydrogen peroxide.

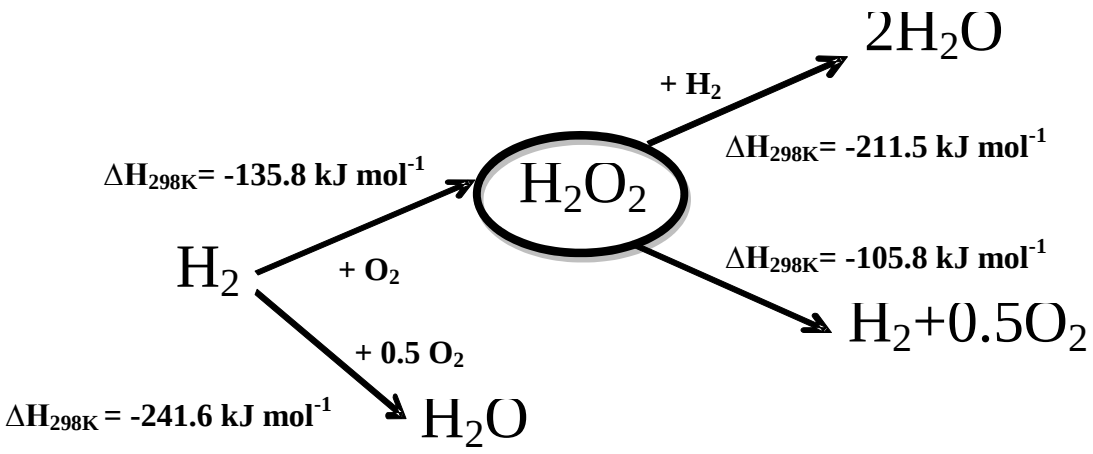

Figure 1.10. *Reactions involved in the direct synthesis of H_2O_2. (Adapted from J.M. Campos Martin, 2006[1]).*

Therefore, the selectivity towards H_2O_2 is still the first issue for a viable industrial application, since the catalysts active for the peroxide production are also active for the side reactions. The two main research areas are the actual mechanism of synthesis and the controlling factors that affect the rates of the reactions. The study and definition of the operative conditions, kinetics and mass transfer limitations could contribute to minimize the unwanted reactions.

1.4.1.1 Reaction kinetics and mass transfer

The direct synthesis reaction is a heterogeneous three-phase reaction that involves gases (H_2, O_2, diluent gas), a reaction liquid medium and a solid catalysts. The external transport phenomena that can occur in the process are described with these steps in series: (a) convection in the gas phase; (b) gas-liquid equilibrium at the interphase; (c) convection in the bulk liquid; (d) adsorption H_2 and O_2 on catalyst surface; (e) surface reaction between adsorbed reagents; (f) desorption of H_2O_2 to bulk liquid phase; (g) convection in the bulk liquid phase[4]. The study of the kinetics and the mass transfers can lead to the identification of the steps limiting the overall reaction conversion.

The main research efforts are focused on rationalizing the rate of the four reactions involved in the synthesis network (Figure 1.10) and developing a model to study the overall mechanism[22,23,24]. Voloshin and Lawal performed an extensive experimental campaign to define a kinetic rate expression for design and modeling a microreactor for direct synthesis of H_2O_2. The experiments were carried out using a 2% Pd/SiO_2 in a microreactor consisted of stainless steel tubing with 765 μm ID[25]. The strategy was to isolate the single reactions and then combine the rates of each reaction to define the overall rate of H_2O_2 formation. In Voloshin *et al.* (2007) is described the kinetic rate of

synthesis[26], while the rate of decomposition reaction is studied in Voloshin *et al.* (2008)[27]. The reduction reaction was isolated feeding a mixture of H_2-N_2 and suppressing the decomposition reaction adding NaBr[25]. The Langmuir-Hinshelwood-type mechanism was evaluated appropriate for the complete description of the rates of reactions. In the mechanism two molecules adsorb on neighboring sites and the adsorbed molecules undergo a bimolecular reaction. The expressions take in account the effects of adsorption and desorption considering the surface reaction steps determining the overall reaction rate.
In Voloshin and Lawal (2010), the authors defined a micro-reactor model that involved the four component reactions as well as mass transfer effects. The model and the rate equations were verified by comparison with experimental data. Experimental data points were acceptably close to the calculated point, thus the model could be used to calculate the optimum operating conditions for the process and predict the performances of the reactor[22].
Gemo *et al.* proposed a multiphase model for a batch slurry reactor for direct synthesis of H_2O_2 taking in account the reaction kinetics and the effect of mass transfer[24]. The authors conducted a preliminary study on the H_2 solubility in methanol with presence of gaseous CO_2 and O_2[28]. The lack of data on vapour-liquid equilibria would have hampered the complete and precise description of the mechanism of a reaction in which H_2 acts as limiting reagent. The kinetics experiments were carried out on a 5% Pd/C catalyst in a 600 ml batch reactor. Hydrogenation and decomposition experiments were performed with N_2 replacing O_2 or H_2, respectively. The kinetics mechanism was based on the hypothesis that hydrogen and oxygen dissociatively adsorb on the Pd catalyst surface, surface hydroxyls are formed leading to formation of hydrogen peroxide and water. The Table 1.1 summarizes the mechanism proposed.

Table 1.1 *Reaction steps used in modeling of the direct synthesis kinetics (Adapted from Gemo et al., 2012[24]).*

	Step
$H_2 + 2* = 2H*$	I
$O_2 + 2* = 2O*$	II
$O* + H* = OH* + *$	III
$OH* + OH* = HOOH* + *$	IV
$OH* + H* = H_2O* + *$	V
$HOOH* + * = H_2O* + O*$	VI
$HOOH* + 2H* = 2H_2O* + *$	VII
$HOOH* = H_2O_2 + *$	VIII
$H_2O* = H_2O + *$	IX

The steps I, II and VIII, IX coincided with the adsorption and desorption phase that were assumed to be enough rapid to reach quasi-equilibria. The steps considered to limit the overall rate were the surface reactions (IV, V, VI, VII). The mass transfer resistances between gas-liquid and between liquid-solid catalyst surface were predicted a priori using the best available correlations.

The model was compared with the experimental data, as displayed in Figure 1.11 and Figure 1.12.

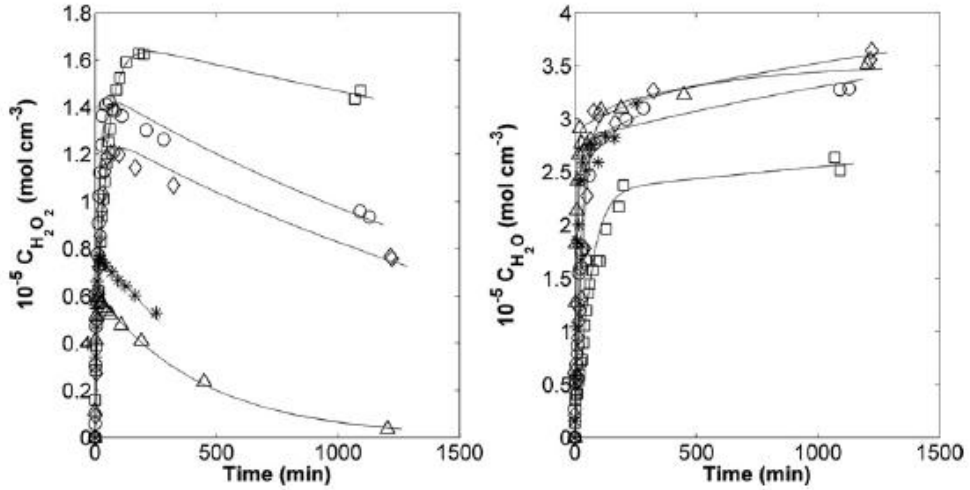

Figure 1.11. *Experiments of direct synthesis of H_2O_2. Δ, 297K; *, 283K; ○, 273K; ◊, 268K; □, 258K; solid line, model. (Adapted from N.Gemo, 2012[24]).*

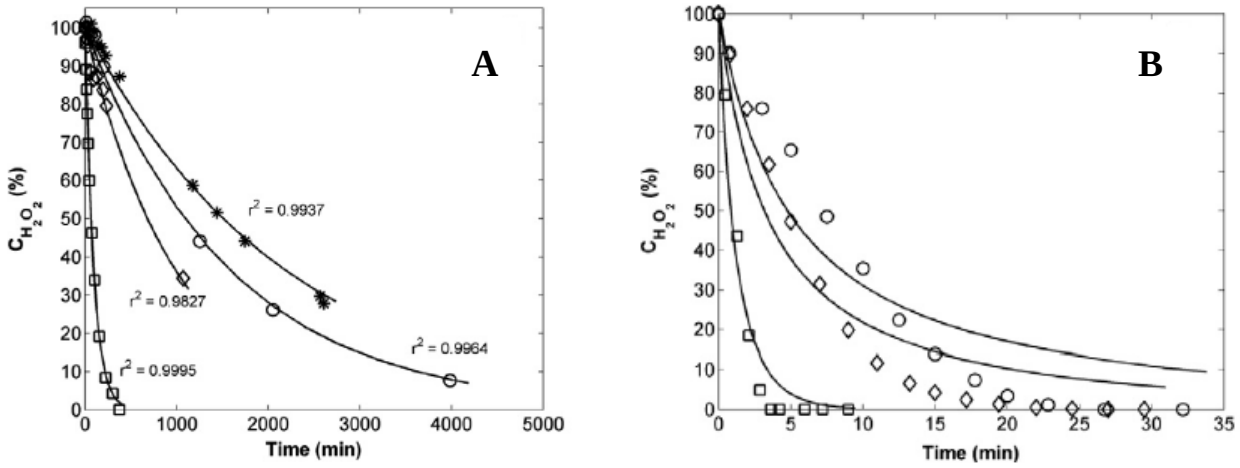

Figure 1.12. **A.** *Normalized experimental and calculated H_2O_2 concentration in experiments of decomposition. *, 268 K; ○, 273K; ◊, 283K; □, 313K; solid line, model.* **B.** *Normalized experimental and calculated H_2O_2 concentration in experiments of hydrogenation. ○, 273K; ◊, 283K; □, 313K; solid line, model. (Adapted from N.Gemo, 2012[24]).*

The model was in good agreement with experimental results in case of direct synthesis (Figure 1.9) and reaction of decomposition (Figure 1.10A) with values of r^2 really close to one. Only in case of hydrogenation experiments the model resulted not adeguate (Figure 1.10B). The fitting of the experimental data provided the four irreversible reaction rate constants *k* for every temperature. The linear fitting of the *k(T)* permitted the calculation of the Arrhenius constants (pre-exponential factors and activation energy) for each reaction. The reaction rates were related to the one of direct synthesis (Figure 1.13).

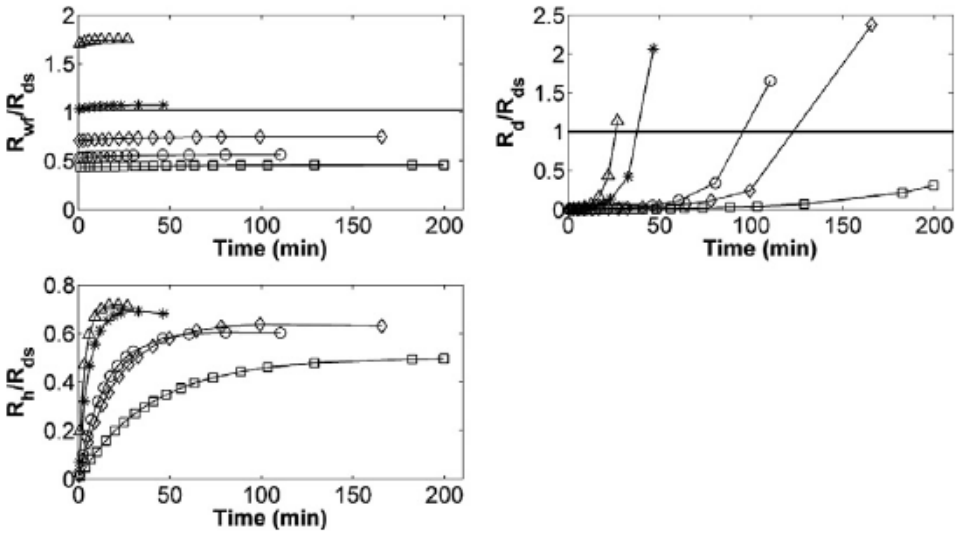

Figure 1.13. *Ratio of each reaction rate to the direct synthesis during the reaction course.* Δ*, 297K; *, 283K;* ○*, 273K;* ◊*, 268K;* □*, 258K. (Adapted from N.Gemo, 2012).*

The decomposition reaction was slow compared to the direct synthesis and became important only at a high H_2 conversion. The hydrogenation reaction increased as H_2O_2 became available, but it was always slower than direct synthesis. The formation of water competed with the direct synthesis, prevailing at high temperature but getting slower than direct synthesis at low temperature[24].

1.4.2 Experimental devices for direct synthesis

The device setup used to operate the direct synthesis of H_2O_2 influences the results that can be obtained, acting on mass transfer and contact time. In most cases the reaction are conducted in batch and semi-continuous, stirred reactors. From the industrial application the most suitable plant for three-phase reaction are continuous slurry bubble columns and trickle bed reactors. Other systems are applied such as micro-reactors and catalytic membranes[4]. An application that can be considered as direct synthesis is the fuel cell, described in Section 1.3.4.2, in which the only reagents involved are hydrogen and oxygen.

1.4.2.1 Batch and semi-continuous reactors

Batch reactors are extensively used in direct synthesis of hydrogen peroxide[29,30]. In literature glass reactors are generally utilized for experiments under mild conditions and stainless vessels at high pressure. The catalyst is commonly introduced as a slurry before closing the vessel and feeding the gaseous reactants. It implies that the reaction starts when the gases enter the system. The setup presents difficulties in controlling the initial composition, that it is estimated with the pressure of the gases. The concentrations of the gas and liquid phases change during the experiment, which makes the kinetic analysis more complicate. The mixing reduces the mass transfer and allows for a good temperature control.

Semi-continuous reactors are commonly conceived as batch for the liquid and continuous for the gas phase[31,32]. The catalyst can be added before close the reactor or after all liquids and gases have been charged. In the second configuration the reaction starts when the catalyst is added[32]. The gas phase is continuously bubbled in the liquid and the pressure is controlled with a back pressure valve. The plant permits the control of the pressure and to achieve high hydrogen peroxide concentrations, since H_2 is continuously provided. A diluent gas is usually added, i.e. nitrogen, carbon dioxide or argon, in order to control the H_2/O_2 ratio and work in safe conditions.

1.4.2.2 Fixed bed reactor

In fixed bed reactors the liquid and the gases continuously flow through a bed of solid catalyst. The downflow for both liquid and gas is the best configuration in production of hydrogen peroxide, since the contact between fresh H_2 and H_2O_2 should be avoided. Biasi *et al.* reported values of H_2O_2 up to 1.2 wt.% in a trickle bed reactor (TBR) over a 5% Pd/C commercial catalyst[33]. The name *trickle bed* comes from the special liquid operation mode, in which the liquid trickles down over the solid particles in the form of droplets and rivulets[34]. In TBRs different flow regimes are distinguished, depending on gas and liquid flow rates, fluid properties and packing characteristics. Most of the industrial three–phase fixed beds operate in trickle to pulse flow regime. Figure 1.14 displays the flow regimes in an industrial trickle bed reactor.

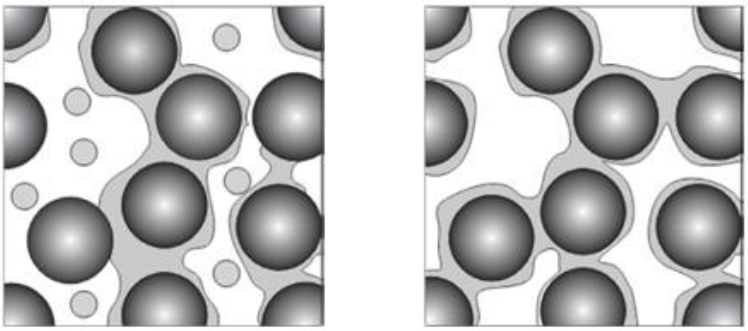

Figure 1.14. *Flow regimes in an industrial trickle bed: tickle regime on the left and pulse regime on the right.*

Trickle flow regime is a low interaction regime where the gas is present as continuous phase while liquid represents the semi–continuous one. Pulse flow is a high interaction regime, where both the gas and liquid phase are considered semi-continuous. Pulse regime presents an higher heat and mass transfer than trickle flow[34].

The major advantage presented by this structure is the enormous mass transfer area between the phases. TBRs and the slurry bubble column are the two most evident options for the large-scale implementation of direct synthesis of H_2O_2[4].

1.4.2.3 Microreactors

The application of micro-reactors is a recent innovation in the synthesis of hydrogen peroxide. These reactors are characterized by high heat dissipation and rapid mass transfer. It makes micro-reactors a safe structure for operate reactions that are exothermic and involve explosive mixtures, like H_2O_2 synthesis. The low volume of apparatus requires the use of miniature catalyst particles to avoid clogging[4].

Inoue *et al.* applied different Pd supported catalysts for the direct synthesis of H_2O_2 in glass micro-reactors at room temperature and atmospheric pressure. They obtained a 10 wt% aqueous hydrogen peroxide solution with a selectivity up to 73%[35]. It demonstrates that micro-reactor technology can achieve high concentration of H_2O_2 in safer and milder conditions compared with those used in conventional reactors. Nevertheless the low capacities of the system make this approach suited just for small-scale applications, while the cost is too high for larger scale reactors.

1.4.2.4 Membranes

The use of membrane catalysts in direct synthesis is an elegant approach that avoids safety concerns, keeping the O_2 and H_2 separated. Choudhary *et al.* developed a dense palladium membrane (Figure 1.15) that displayed conversions up to 100% and selectivity over

60%[36]. The membrane separated hydrogen from the reaction liquid, where the oxygen was bubbled. Only H_2 atoms were able to penetrate the membrane and react with O_2 on the palladium surface.

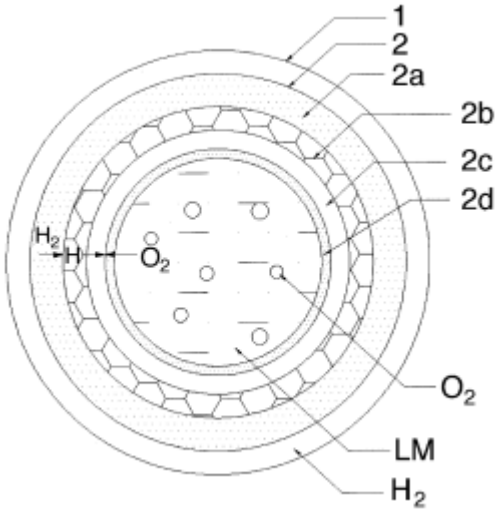

Figure 1.15. *The H_2-permselective membrane developed by Choudhary (2001)[36]. It consists of thin films of Pd–Ag alloy (2b) and oxidized Pd (2c), a hydrophobic polymer membrane (2d) supported on a tubular membrane (2a) within a reactor wall (1). Hydrogen atoms permeate through the membrane and react with molecular O_2 in a liquid medium (LM).*

The major process limit was the slow diffusion of H_2 through the membrane.[36] More recent studies investigated the effect of application of higher differential pressure. Melada *et al.* successfully used a carbon-coated ceramic membrane containing palladium for the synthesis of hydrogen peroxide[37]. These membranes were designed to feed hydrogen from inside the membrane towards the external part, where an oxygen-saturated methanol solution came in contact with the Pd active phase. The selectivity obtained at 1 bar was below those of industrial interest, but the experiments carried out over 65 bar gave satisfactory productivity and selectivity results[37].

1.4.3 Affecting factors

The direct catalytic oxidation of H_2 over an active catalyst will preferentially form H_2O than H_2O_2. This is mainly because the catalysts active for the formation of hydrogen peroxide could also support its depletion. Several factors strongly influence the hydrogenation and decomposition reactions, affecting the selectivity and productivity of the direct synthesis. The most considered parameters in literature are the active metal, the addition of promoters, the nature of catalyst supports and solvents, the pressure and the temperature.

1.4.3.1 Active metal and oxidation state

The catalysts utilized in direct synthesis are based on noble metals supported on different substrate materials. In most catalyst formulations palladium is applied as active metal. The performances of the supported metal depend on a series of parameters, such as the dimension and morphology of the active particles[4]. Zhou *et al.* reported that nanoparticles presenting a high number of Pd atoms with a low degree of coordination are the most suitable for the synthesis hydrogen peroxide (Figure 1.16) [38].

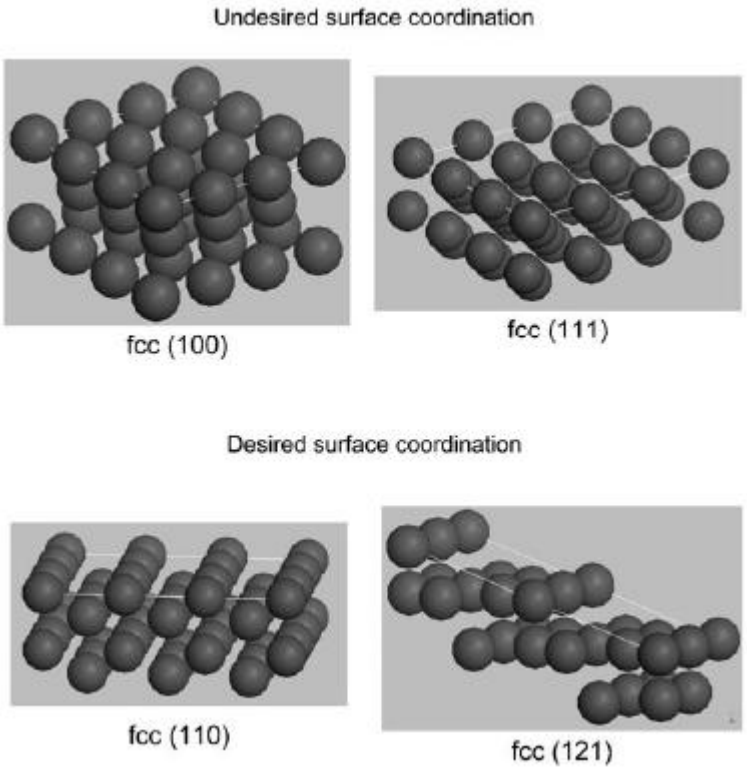

Figure 1.16. *Desired and undesired surface coordinations of metal particles for the synthesis of H_2O_2 from H_2 and O_2.*

It is demonstrated that crystalline geometry like fcc(1 0 0) and fcc(1 1 1) are undesired, while crystallites with fcc(1 1 0) and fcc(1 2 1) are active and selective for the production of H_2O_2[38].

The oxidation state of the active metal phase results to play an important role in the catalyst performance. Samanta demonstrated that supported PdO catalysts are more selective but less active than the corresponding Pd^0 catalysts. The higher selectivity of PdO catalysts is due to the lower activity in decompose and hydrogenate H_2O_2 compared to Pd^0 surface[39]. On the other hand, numerous scientists claimed that the Pd^0 is the active phase in the direct formation of H_2O_2 and can provide higher selectivity and productivity respect PdO catalysts[40,41].

Different research groups presented enhancement of performances in catalyst activity when Pd is combined with another noble metal. Landon *et al.* reported that the addition of Au or Pt to Pd significantly improved the catalyst stability and selectivity in the direct synthesis[42]. Particular attention has been paid to the bimetallic Pd-Au, that has been found to be superior compared to Pd-only and Au-only catalysts[23,30]. Despite the numerous investigation the real mechanisms of modification of Pd catalysts by addition of Au is still unclear. It was proposed that the electronic effect created between the two metals and the support is responsible for the enhancement of the catalyst performance[4]. Menegazzo *et al.* studied the effect of the addition of Au in zirconia and ceria supported Pd catalysts. The authors evidenced that the presence of Au profoundly changed the Pd particle morphology, electron density and dispersion on the support. Furthermore the addition of Au decreased the Pd particle size increasing the catalyst productivity, while at the same time maintaining a significant proportion of low energy sites that ensure a high selectivity[23]. The less energetic metal sites can chemisorb O_2 without dissociation, that is a necessary condition for the selective synthesis of hydrogen peroxide[43].

1.4.3.2 Supports

The nature of the support can significantly influence the catalyst activity. The interaction between the metal and the support can affect different catalyst properties, such as the metal particle size, morphology, metal dispersion and electronic state[44]. The most used Pd supports in direct synthesis are activated-C, SiO_2, Al_2O_3, TiO_2, Fe_2O_3 and ZrO_2. Acidic supports such as carbon, zirconia and zeolite usually show the better results due to the higher stability of hydrogen peroxide on an acidic environment[45]. Abate *et al.* studied the deactivation of Pd catalyst supported on silica. The presence of deactivation, which can be correlated to the loss of accessible active metal surface area, is due to sintering of Pd. The authors underlined the fundamental function of a stable support to delay or eliminate the sintering effect[46]. Fu *et al.* emphatized the importance of the application of an hydrophobic support. The catalysts supported on hydrophobic are more selective since the removal of H_2O_2 from the active sites are favored, avoiding the decomposition[47].

The addition of different dopants to the supporting material has been investigate with promising results[48]. Melada *et al.* reported the benefits of support sulfonation for ceria and zirconia supported Pd catalysts[23,31]. Resins functionalized with sulfonic groups have been presented as suitable supports for hydrogen peroxide synthesis[49].

1.4.3.3 Promoters

The use of promoters, i.e. halides and acids, inhibits the unwanted catalytic activity for H_2 oxidation to water and decomposition/hydrogenation of H_2O_2. Their utilization is considered crucial in direct synthesis of hydrogen peroxide. Halides act as catalyst poisons

retarding water production, while acids limit the base-catalyzed decomposition and hydrogenation of H_2O_2[4]. Ishihara *et al.* reported a higher peroxide formation in acidic conditions and no formation in basic conditions[45]. Choundary *et al.* employed Pd supported catalysts in aqueous acidic medium containing different halide anions (F^-, Cl^-, Br^- or I^-) to study their influence in direct synthesis of H_2O_2. The presence of I^- was found to completely deactivate the catalyst due to poisoning. Cl^- and, especially, Br^- resulted the most effective promoter for the selective oxidation of H_2 to H_2O_2[50]. It is believed that halides block the more active sites responsible for the dissociative chemisorption of O_2 and re-adsorption of H_2O_2[23]. An optimum value of halide concentration has to be fixed in relation to the number of metal active sites, in fact an excess of Br^- leads to indiscriminate poisoning of the surface and it is detrimental to overall catalytic activity[37,48,51]. Choudhary *et al.* claimed that the presence of halide ions alone is not enough to promote the selectivity towards H_2O_2. The halide ions together with H^+ ions reduce the non-selective oxidation of H_2 to water and decrease the decomposition/hydrogenation of H_2O_2 formed[50]. Hydrogen halides, HCl and HBr, are commonly chosen as promoter combining the effect of the acidic proton with the halide ion. The specific role of H^+ ions in directing the H_2/O_2 reaction towards H_2O_2 is still not completely clear. Abate *et al.* proposed a possible reaction pathway on monometallic Pd catalysts considering the effect of H^+ (Figure 1.17)[52].

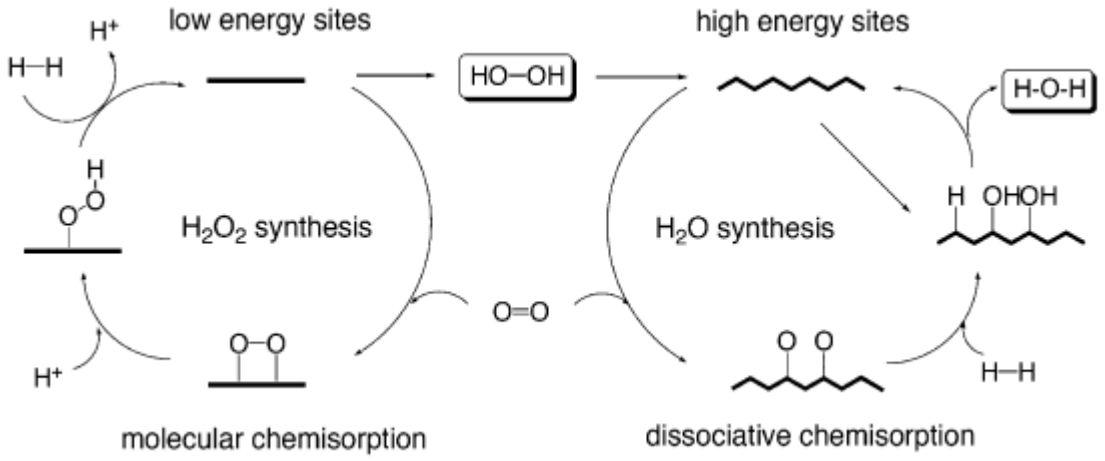

Figure 1.17. *Possible pathway for the synthesis of H_2O_2 and H_2O. (Adapted by F.Menegazzo et al., 2008[23]).*

According to this proposal, oxygen can chemisorb with or without dissociation depending on the energy of the site. The mechanism involves the protonation (from external H^+) of non-dissociated chemisorbed O_2 followed by reaction with non-chemisorbed H_2, leading to the formation of H_2O_2 and the regeneration of H^+ ions. At the same time more energetic and defective sites dissociatively chemidsorb O_2 and re-adsorb H_2O_2. The presence of

chemisorbed hydrogen leads to the formation of water by reaction with O_2 or with the OH fragments deriving from H_2O_2. This interpretation is consistent with data reported in several papers[23,43].

The presence of an acid in reaction medium may cause the corrosion of reactor materials and leaching of active metal from the catalyst. These problems can be avoided by addition of halide ions directly into the catalyst or by using solid acid supports. The industrial applications try to avoid the implication of chlorine ions because it could present safety problems forming dangerous Cl_2[3].

1.4.3.4 Solvents

The most suitable solvent for direct synthesis is water because it is safety, no toxic and miscible with hydrogen peroxide. The major drawback is the low solubility of reagent gases that limits the rate of production of H_2O_2. Krishan *et al.* compared the performance of a Pd supported catalyst in different organic solvents[53]. The authors observed that the formation of H_2O_2 in water depended on the acid added, i.e. HCl showed the best qualities suggesting a strong halide effect. Alcohols in general were found to be the best solvents for the peroxide synthesis, in particular methanol gave the highest rate of reaction. The alcohols as reaction medium are able to dissolve promoters and have a high solubility of the gases, favoring the formation rate of H_2O_2[47,53]. Centi *et al.* indicated that increasing the chain length of alcohols improves the H_2 and O_2 solubility, reporting for ethanol better performances than methanol[3,54]. However, ethanol doesn't result attractive for industrial production, since it is not suited to be used in the consecutive application. For this reason nearly all the patents focus on the use of methanol[3].

During the direct synthesis reaction the H_2/O_2 mixture is commonly diluted by CO_2 or N_2. CO_2 forms carbonic acid in water and expands different solvents, reporting a beneficial effect on selectivity and productivity in direct synthesis of H_2O_2[55]. An interesting application is the use of supercritical CO_2. The solvent is considered green, since no-flammable and no-toxic, and has an high solubility of the reaction gases[2]. The use of $scCO_2$ presents advantages due to its acidification effect and the enhancement it causes in the mass transfer between the gas and the liquid phase[56]. The technical, safety problems and the necessity of finding a suitable soluble catalyst lead to contradictory conclusions about the use of $scCO_2$ in industrial application[2].

1.4.3.5 Pressure and temperature

The influence of pressure is related to the mass transfer of the gases to the liquid phase. The increasing of total pressure of the system improves the solubility of the gases and decreases the bubble sizes, enhancing the mass transfer. The higher mass transfer and partial pressure of gases in reaction medium increases the H_2O_2 synthesis yield[47,57].

Numerous scientists demonstrated the direct dependence of productivity of H_2O_2 on temperature[24,56]. The reaction temperature range of investigation is between -10°c and 60°C. Biasi *et al.* studied the kinetic temperature dependence in a batch system using a 5 % Pd/C catalyst, reporting the best selectivity at -5°C and the worst at 40°C (Figure 1.18) [58]. At low temperatures, the decomposition of H_2O_2 was almost suppressed probably due to the low activity of palladium[58].

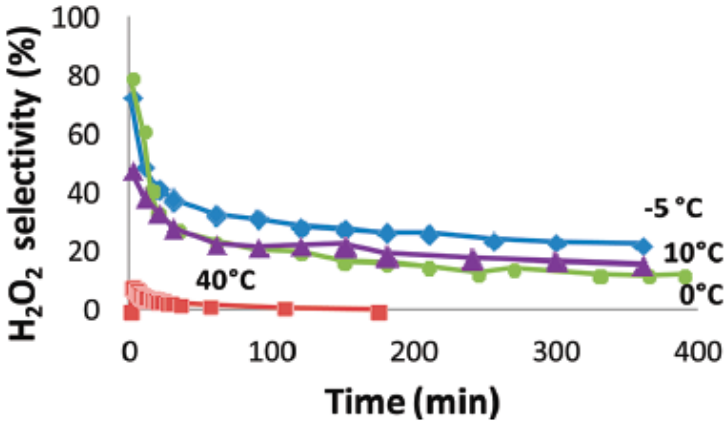

Figure 1.18. *Selectivity towards H_2O_2 at 18 bar and different temperature: ◊, -5°C, Δ, 10°C; ○, 0°C; □, 40°C. (Adapted by P.Biasi et al., 2012 [58]).*

From an industrial point of view working below 35°C is not feasible as it would be difficult remove the heat produced in the reaction.

1.4.3.6 Factors affecting decomposition and hydrogenation of H_2O_2

The study of the parameters affecting the reactions responsible for the depletion of H_2O_2 formed is of primary interest. Choudhary and co-workers provided an intense experimental campaign on the understanding of the factors influencing decomposition and hydrogenation of H_2O_2. The pure H_2O_2 is stable with weak decomposition, but the contact with a catalyst causes its conversion to H_2O, producing gaseous O_2 and heat. It's reported that maximum stability of hydrogen peroxide is in acidic environment (pH 3.5-4.5)[2,47]. The major factors affecting the decomposition reaction has been already introduced in the previous sections. The presence of H+ ions and halides in the reaction medium[23,37,50,51], hydrophobicity of catalyst[46], oxidation state of Pd[39,40,41] and operative temperature[24,55,58].

H_2O_2 can be converted to water in presence of hydrogen. Hydrogenation is the preferred path of H_2O_2 degradation as its reaction rate rapidly increased with H_2 conversion[24]. The main factors affecting the hydrogenation reaction are: reaction medium, catalyst amount and H_2O_2 concentration. Melada *et al.* proved that the rate of hydrogenation reaction in

water is higher than in methanol, even though the solubility of H_2 is higher in methanol[37]. It is believed that the formation of surface species on catalyst blocks the most reactive Pd sites, responsible for HO–OH bond breaking. Choudhary *et al.* reported that the rate of hydrogenation appears to increase proportionally with the amount of catalyst[59]. The hydrogenation reaction mechanism requires the adsorption on the catalyst surface of both H_2O_2 and H_2[60]. The concentration of H_2O_2 in the reaction medium is an influencing factor in the reaction rate of hydrogenation. Huerta *et al.* proved that hydrogenation is more severe at low concentrations of hydrogen peroxide, since the catalyst sites are available to H_2 adsorption. At high H_2O_2 concentrations, the rate of hydrogenation competes with synthesis reaction (O_2 adsorption) or limited by mass transfer[60].
The definition of the optimum catalyst structure and operative reaction condition that favor the selective oxidation of H_2 to H_2O_2 is the major challenge in direct synthesis of H_2O_2.

1.4.4 Comparison between direct synthesis and anthraquinone auto-oxidation process

The comparison between the direct synthesis and the anthraquinone process (AO) can be summarize in the Table 1.2. The principles of both the methods have been widely described in the previous sections. The major terms of comparison are the costs, the safety concerns and the performances of the process. Juan Garcia-Serna *et al.* proposed an simplified cost evaluation based on direct costs only, that primarily comprise raw materials, utilities, man labor and maintenance[4]. The AO process is composed by 4-5 sub-units: hydrogenation, catalyst recovery, oxidation, extraction and product concentration. The running of the plant occupies at least 4 to 6 employees. The direct synthesis is one step operation requiring at maximum 2 people. The AO process needs a steam utility for the distillation columns. Furthermore in direct synthesis the extraction of H_2O_2 from the medium solvent is not always required, e.g. methanol for propylene oxidation application, simplifying the purification steps and reducing the costs[1]. On the other hand the consumption of electricity in direct synthesis is much higher due to the costly compression of the gases. Regarding the raw material consumption, hydrogen represents one of the major products needed in both the applications. In the case of direct synthesis also oxygen must be considered, that it is expensive and used in large excess. It is the key parameter in estimating the economic competitiveness of the direct synthesis process. The costs could appreciably reduce replacing O_2 using air or recycling the off-gases. The direct synthesis can be operated on-site in small scale and on demand production, so that the costs and safety precautions related to the transportation are avoided.

Table 1.2 *Comparison between AO process and direct synthesis of hydrogen peroxide. (Adapted from P.Biasi Phd thesis, 2013[61]).*

Process	Indirect synthesis AO process	Direct synthesis
Principle	Sequential hydrogenation and oxidation of organic molecule, recycle of the organic molecules	$H_2+O_2 \rightarrow H_2O_2$
General feature	A well known and complex process	A very simple process
Catalyst	Pd in hydrogenation step	Pd based catalyst
Reaction environment	Working solution of a mixture of organic molecules	H_2O, MeOH or CO_2 used as co-solvent
Reactor system	A complex system that counts numerous and sequential steps	Synthesis done in one reactor
Selectivity	High	It is an issue
Safety	Safe	Can be made safe
On site production	Impossible	Possible

From an economic point of view, direct synthesis process could compete only avoiding the cost of further concentration steps, so producing H_2O_2 solutions equivalent to the traditional technology after dilution. The technology related to direct synthesis is considered more environmental friendly than AO process, considerably reducing the amount of waste. The direct synthesis is still not well enough developed to be considered as a valid alternative to AO process, but the research efforts will be helpful to solve the selectivity and the safety issues of direct synthesis process.

Chapter 2

Materials and Methods

The first part of the chapter is focused on the description of the materials and methods used for the preparation of the catalysts. The section includes a definition of the techniques applied for the characterization of the catalysts. The catalysts used are Pd supported on $Zr_xM_{1-x}O_2$ (M=La,Y,Ce) and mechanical mixtures of ZrO_2 and CeO_2 in different compositions. All the catalysts have been synthesized and characterized by Professor R. Lanza in *KTH-Royal Institute of Technology*, Stockholm.
The second part of the chapter is dedicated to the presentation of the reactor setup, the experimental procedure and analysis techniques.

2.1. Supports for the metal particles

The catalysts synthesized and tested are based on zirconia (zirconium (IV) oxide – ZrO_2) promoted by rare earths. Rare earths are a set of 17 elements, specifically scandium, yttrium and the 15 lanthanides. The rare earths utilized in catalysts synthesis are cerium, yttrium and lanthanum in their oxide form, ceria (cerium(IV) oxide – CeO2), yttria (yttrium(III) oxide – Y_2O_3), lanthana (lanthanum(III) oxide – La_2O_3), respectively. The most of the presented samples are based on a zirconia and ceria solution. ZrO_2-CeO_2 solid solution is a promising eco-friendly catalyst that played an important role in heterogeneous catalysis applications during the last years[62]. It inspired several lines of research providing a wide and exhaustive literature production.
Zirconia is a white crystalline derived by calcination of zirconium compounds. Calcination is a thermal treatment process in the absence or limited supply of air or oxygen. ZrO_2 presents a high thermal stability and is described as a material with tunable porosity and surface area. The surface acidity/basicity is easily controlled by addiction of different dopants[31]. It results interesting properties for direct synthesis of hydrogen peroxide, since numerous authors, e.g. Burato *et al.*[63], reported promising results over acidic supports.
Ceria is a pale yellow-white powder, formed by calcination of cerium compounds. Damyanova *et al.* widely analyzed CeO_2 performances describing several advantages as promoter for supported noble metals catalysts. The oxygen mobility and storage/release capacity (OSC), the stabilization of the metal dispersion and the promoting of the oxidation and reduction of the supported noble metal make ceria a suitable catalyst for a large

number of industrial reactions[64]. It is used in many catalytic reactions with oxygen as a reactant based on its redox nature at lower operating temperature compared to other oxides. The good redox property of ceria is due to its capacity to switch easily between two oxidation states ($Ce^{+3} \leftrightarrow Ce^{+4}$). Ceria can store oxygen in aerobic conditions and release it in anaerobic conditions[65]. The common utilizations are on automotive exhaust gas conversion, hydrogen production and water-gas shift reactions. The most remarkable application of CeO_2 is probably in Three-Way Catalysts (TWC) for automotive exhausts, where its redox properties results essential. Madier *et al.* described properly the function of ceria in this application, citing also the recent employment of zirconia-ceria mixed oxides[66]. TWC simultaneously have to oxidize CO and hydrocarbons (HC) to CO_2 and reduce NO_x to N_2. Both oxidation and reduction reactions may take place at the same time if a stoichiometric mixture is employed. For that reason the ratio between oxidizing (O_2, NO_x) and reducing agents (H_2, CO, HC) should be maintained close to one. Ceria is systematically added to TWC to face possible oscillations around the stoichiometry of the system. According to its redox properties, ceria can store O_2 during an oxygen-rich phase and release it when the O_2 partial pressure decreases. In this way the catalyst can balance the domain variation from the stoichiometry. Nowadays, ceria tends to be replaced by $Ce_xZr_{(1-x)}O_2$ mixed oxides. These oxides have both better thermal stability and larger OSC, limited in ceria by the lack of surface area. High thermal stability is an essential requirement for these materials employed as supports in automotive converters. In fact, TWC can meet temperatures up to 1000 °C[66].

The reducibility of a support of a metal catalyst is connected with its ability to generate oxygen vacancies and transfer the oxygen on the metal particles[64]. ZrO_2-CeO_2 system displays better reducibility properties at low temperature than ZrO_2, shifting the temperature of the surface reduction process to lower temperature. The improved reducibility and OSC of the zirconia-ceria solid solution could due to the generation of a high concentration of structural defective sites on the zirconia surface[64]. Nagai *et al.* proposed that the homogeneity of the ZrO_2-CeO_2 solution is an influencing factor on the oxygen storage capacity. The formation of a homogeneous solid solution favors the reducibility and the redox proprieties of zirconia-ceria solution[67].

Pudukudy and Yaakob described these materials as really versatile and tunable depending on the different method of preparation and conditions. The authors deeply studied the effect of metal loading[62]. The introduction of transition metal or rare earth elements in the zirconia-ceria solid solutions results in promoting the oxygen storage capacity and the redox property at low temperature. In particular the doping with rare earths (La and Y) causes the increasing of surface area and the improving of the thermal stability[62].

McGuire *et al*. considered the role of lanthana studying a CeO_2-La_2O_3-ZrO_2 (17-5-78 wt%) solid solution[63]. Zirconia presents both weakly acidic and basic sites. The addition of

lanthana, a basic oxide, causes a reduction of the overall acidity of the support. However the nature of the acidity is different, i.e. lanthana significantly reduces the number of Lewis acid sites leaving active the Brönsted ones[68]. In hydrogen peroxide production not just the total acidity of the support is important, but also the kind of acidity. Enhancing the ratio between the number of Brönsted and Lewis sites, the hydrogen peroxide yield results improved[69].

The notable features listed inspired the utilization of these materials on the hydrogen peroxide direct synthesis. In particular the good oxygen mobility and storage capacity of the CeO_2-ZrO_2 solid solution were supposed to improve the supported metal activity. The Thesis aims to find connection between the properties of the supports and the catalyst performances.

2.1.1 Catalyst preparation

Seven Pd catalysts were prepared by incipient wetness impregnation. Most of the supports were provided by MEL Chemicals, while others were obtained by mixing, crushing together and calcining ceria and zirconia powders supplied by Evonik and Alfa Aesar, respectively. Prior to the impregnation, each support was calcined in air at 550 °C for 5 hours, with a heating rate of 5 °C/min. According to MEL Chemicals, their supports form a solid solution upon calcination at 500-550 °C. The calcination conditions were chosen in order to assure the formation of a solid solution between ceria and zirconia.

The incipient wetness impregnation (dry impregnation) is a common technique for the synthesis of heterogeneous catalysts. Typically, the active metal precursor is dissolved in an aqueous solution. Thereafter, the metal-containing solution is added to a catalyst support characterized by the same pore volume as the volume of the solution that was added. Palladium (II) nitrate hydrate 99.9%, from Alfa Aesar, was used as metal precursor dissolved in de-ionized water. The catalyst is then dried and calcined to drive off the volatile components within the solution, depositing the metal on the catalyst surface. The metal loading was 0.3 wt.% for the samples prepared using MEL Chemicals supports and 0.6 wt.% for the remaining ones. A higher metal loading was chosen for the latter samples to assure a high enough activity, since they are not expected to form a solid solution. All the supports used and their composition are listed in Table 2.1. The procedure of preparation of catalysts required multiple steps. A single step consisted in an impregnation phase and a drying phase. The repetition of the single step is needed to reach the expected loading content[70]. The impregnation procedure was done in 3 steps on samples that display an higher pore volume (Pd2, Pd4, Pd5 and Pd8). The support Pd7 needed 6 steps, while the samples with lower pore volume (Pd3 and Pd6) required 7 steps. The values of pore volume of the bare samples are reported in Table 3.1.

Table 2.1 *List, composition and suppliers of the materials used.*

Label	Support (wt.%)	Supplier	Product code/CAS
Pd2	ZrO_2/CeO_2 82.5/17.5	MEL Chemicals	XZO 802
Pd3	Ce doped ZrO_2	MEL Chemicals	XZO 0857
Pd4	ZrO_2/CeO_2 50/50	Evonik/Alfa Aesar	
Pd5	ZrO_2/CeO_2 17.5/82.5	Evonik/Alfa Aesar	
Pd6	ZrO_2/Y_2O_3 92/8	MEL Chemicals	XZO 1012
Pd7	$ZrO_2/CeO_2/La_2O_3$ 77.5/17.5/5	MEL Chemicals	XZO 892
Pd8	CeO_2	Evonik	VP AdNano® Ceria 50
	ZrO_2	Alfa Aesar	1314-23-4

The powders were dried at 90 °C in a ventilated oven for 2 hours after each impregnation step. Finished the impregnation procedure, all the samples were calcined in air at 500 °C for 4 hours, increasing the temperature at a rate of 5 °C/min. Finally, before the catalytic tests, all the catalysts were reduced in a furnace in pure H_2 flow (50 Nml/min) at 300 °C for 2h. Starting from room temperature, the samples were heated up at 300°C at a rate of 5 °C/min in 50 Nml/min argon flow.
A 1 wt.% Pd/C commercial catalyst purchased by Sigma Aldrich was used as benchmark.

2.1.2. Catalyst characterization techniques

The characterization of a sample investigates the structure and properties of the material. It is a fundamental examination in the field of catalysis, without which no scientific understanding of tested materials could be ascertained. The catalysts were characterized by nitrogen adsorption analysis, X-ray diffraction, CO chemisorption and temperature programmed reduction.

2.1.2.1 Brunauer, Emmett and Teller (BET) area and pore volume

The surface area of catalysts and porosity were calculated by data collected with N_2 physisorption on the bare supports. The analysis consist in measuring the volume of nitrogen gas adsorbed by the catalyst sample. A static volumetric measuring system is used to obtain sufficient equilibrium points on each branch of the isotherm to adequately define the adsorption and desorption branches. The tests were performed with a Micromeritics ASAP 2000 unit. The samples were de-gassed by evacuation at 250 °C for a minimum of 4-5 h prior to analysis. Data were collected at liquid nitrogen boiling temperature (77 K) and various low pressure levels. Figure 2.1 displays the isotherms relative of sample Pd2 (ZrO_2/CeO_2 82.5/17.5 wt.%).

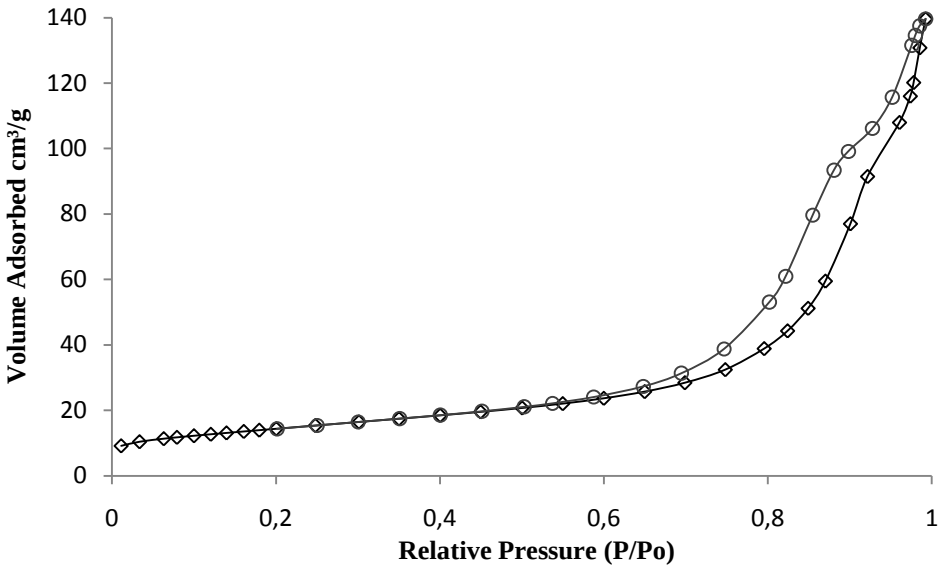

Figure 2.1. *Adsorption (◊) and desorption (○) of N_2 isotherms relative to ZrO_2/CeO_2 82.5/17.5 wt.% (sample Pd2). Analysis bath at 77.35K.*

The plot reports the volume of N_2 adsorbed at the corresponding relative pressures. The relative pressure is defined as the ratio between the partial vapor pressure (P) and the saturated pressure (P_0) of adsorbate gas. The isotherms in Figure 2.1 are typical of no-porous or mesoporous supports, characterized by an indefinite multi-layer formation after completion of the monolayer[71].

The surface area was calculated by the linear BET (Brunauer–Emmett–Teller) method considering data collected at relative pressures between 0.06 and 0.2. BET is an extension to multilayer adsorption of the Langmuir theory for monolayer molecular adsorption. The following assumption are made in the definition of the method: (a) a molecular layer is not required to be completed before an upper layer formation starts; (b) there is no lateral interaction between molecules and the molecules in a layer act as adsorption sites for molecules of upper layer; (c) the uppermost layer is in equilibrium with the vapor phase, i.e. adsorption equal to desorption rate; (d) at the saturation pressure, gas molecules can adsorb in layers infinitely[71].

Equation 2.1 represents the BET adsorption isotherm.

$$\frac{1}{\left[V_a\left(\frac{P_0}{P}-1\right)\right]} = \frac{C-1}{V_m C}\frac{P}{P_0} + \frac{1}{V_m C} \qquad (2.1)$$

where V_a is the volume of gas adsorbed at standard temperature and pressure [$m^3 \cdot (g)^{-1}$]; P_0, the saturated pressure of adsorbed gas at the considered temperature [Pa]; P, the partial vapour pressure of gas in equilibrium with the surface at the considered temperature [Pa]; V_m, the volume of adsorbed gas to form a monolayer on the sample [$m^3 \cdot (g)^{-1}$]; C, dimensionless constant related to the enthalpy of adsorption of the gas on the sample.
V_a is measured at different relative pressure (P/P_0). Then the term on the left is plotted against P/P_0 according to Equation 2.1 as showed in Figure 2.2.

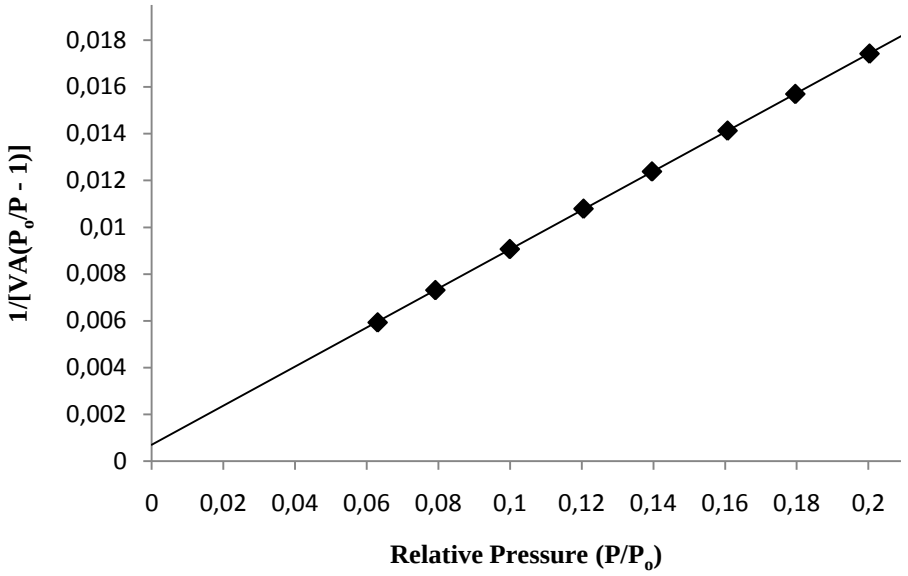

Figure 2.2. *BET surface area plot relative to ZrO_2-CeO_2 82.5/17.5 wt.% (sample Pd2). The Y-intercept is 0.0007 and the slope 0.08358. The C value results equal to 121.0059 and V_m 11.8664 cm^3/g.*

This plot returns a straight line, where it is possible to define the slope and the intercept values by linear regression. It leads to the calculation of V_m and C. From the value of V_m, the specific surface area can be determined with the Equation 2.2.

$$S_{BET} = \frac{V_m N a}{V} \tag{2.2}$$

where S_{BET} is the specific surface area [$m^2 \cdot (g)^{-1}$]; N, Avogadro's number [6.022×10^{23} molecules$\cdot (mol)^{-1}$]; a, cross-sectional area of one adsorbed gas molecule [0.168 nm^2 for nitrogen molecule]; V, volume occupied by one mole of adsorbed gas [$m^3 \cdot (mol)^{-1}$].

The total pore volume was calculated by data collected by N_2 physisorption (Figure 2.1). The pore diameter distribution was determined using the BJH (Barrett-Joyner-Halenda) method[71]. It gives acceptable results in mesopore (2-50 nm) and small macropore ranges.

A careful definition of the relative pressure is required to properly apply the model. A pressure closes to saturation (P/P_0=0.99) is usually chosen because it corresponds to the saturation of the mesopore by the liquid. For the calculation it is generally applied the desorption isotherm, i.e. the gas released decreasing the pressure, although also adsorption data can be used. The pore radius in BJH model is defined using the modified Kelvin equation, that consider also the fluid wall interaction[71]. Equation 2.3 defines the pore radius as the sum of the Kelvin radius and the thickness of the film adsorbed on the pore wall.

$$r_{pore} = r_{Kelvin} + t \tag{2.3}$$

The Kelvin model assumes that pores have a cylindrical shape and that at the initial relative pressure the pores are completely filled of liquid. The Kelvin equation defines the radius of a pore in which the adsorbed specie spontaneously evaporates at a given relative pressure. The boiling point, the molar volume of liquid and the surface tension of the adsorbed specie must be known. For nitrogen as adsorbate the Equation results as 2.4.

$$r_{Kelvin} = \frac{4.15}{\log\left(\frac{P_0}{P}\right)} \tag{2.4}$$

This model also requires the definition of the thickness of the adsorbed film [Å]. The method uses a mathematical representation of multi-layer adsorption[71]. The thickness-values are calculated as function of the relative pressure by statistical t-curve equations, i.e. De Boer and Halsey. In the considered study the Halsey equation (2.5) has been used[72].

$$t = 3.54\left[\frac{5}{\ln\left(\frac{P_0}{P}\right)}\right]^{1/3} \tag{2.5}$$

The thickness of an adsorbate layer increases with increasing pressure. The obtained pore radius is finally applied in BJH equation for pore size distribution to get the volume.

2.1.2.2 X-ray diffraction (XRD)

X-ray crystallography is used to identify the atomic and molecular structure of a crystal.
The crystalline structure diffracts the beam of incident X-rays into many specific directions. The X-rays have wavelengths on the order of a few angstroms, the same as

typical interatomic distances in crystalline solids. By measuring the angles and intensities of these diffracted beams, a crystallographer permits to characterize the solid samples. Figure 2.3 reports a schematic functionality of a crystallographer.

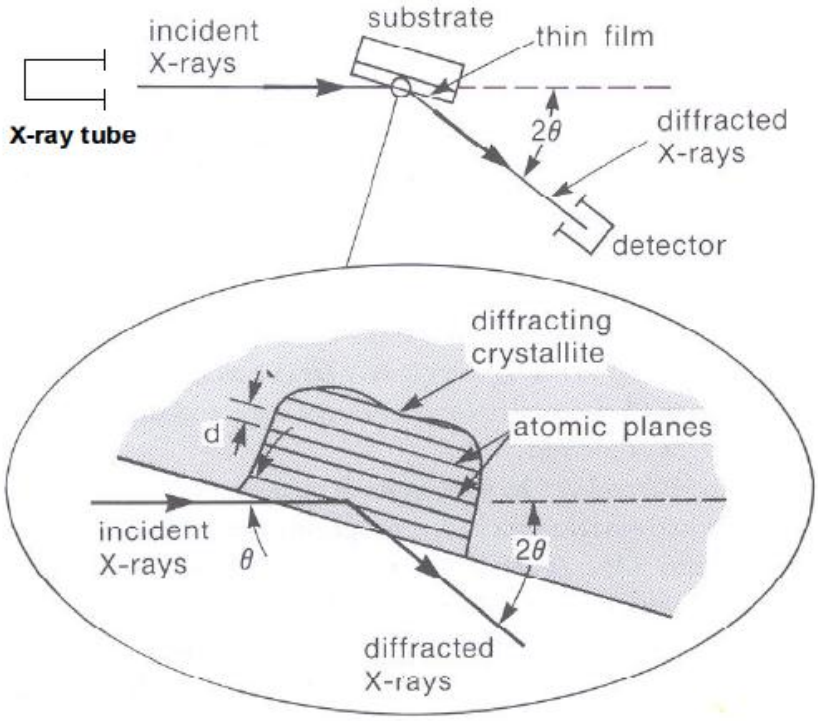

Figure 2.3. *Schematic of a diffractometer functionality. θ is the angle between the substrate and the incident ray. The diffraction angle between the diffracted and incident rays result 2θ.*

X-rays are produced when a high-speed beam of electrons emitted by a hot filament collide with a metal target (copper). The incident beam will ionize electrons from the K-shell (1s) of the target atom and X-rays are emitted as the resultant vacancies are filled by electrons dropping down from the L (2P) levels. In this case the Kα radiation is emitted, as shown in Figure 2.4. Kβ emission occurs when an electron transitions to the K shell from a M orbital[73].

The diffraction occurs when the Bragg's law, reported in Equation 2.6, is satisfied for constructive interference from planes with spacing *d* [Å].

$$\lambda = 2d\sin\theta \tag{2.6}$$

where λ is the wavelength of the metal radiation [Cu - 1.5418 Å]; θ is the angle between the incident rays and the atomic plane. Since the wavelength and the angle are known, it is possible to calculate the spacing between planes that characterizes the structure of the crystalline.

When the beam of radiation is diffracted with a constructive interference the detector registers a peak of intensity on the XRD plot. The plot reports the Bragg peaks at the correspondent incident ray angle. Comparing the pattern with the ones collected in appropriated database it is possible to characterize the unknown sample.

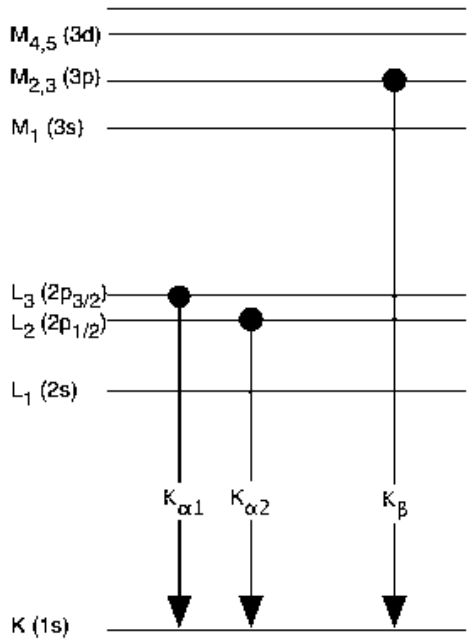

Figure 2.4. *Atomic levels involved in copper Kα and Kβ emissions.*

The X-ray diffraction patterns (XRD) were obtained using a Siemens D5000 diffractometer. The D5000 model measured atomic spacings in crystals using an approximately monochromatic x-radiation. A Cu Kα monochromatic radiation was used. It was used a scanning range 2θ between 10° and 90° with a step size of 0.02° and a time/step ratio of 1.0 s.

2.1.2.3 CO chemisorption and Atomic Absorption Spectroscopy (AAS)

The metal dispersion and average metal particle size were estimated by means of CO chemisorption. The chemical between the adsorbed molecule (CO) and the metal site takes place with a specific stoichiometry. The stoichiometric ratio CO/Pd is assumed equal to 1 (gas molecules per surface metal atom). The pulse dosing procedure contemplates the injection of variable volumes of CO into the carrier gas stream, which continuously flows over the sample. The detector measures the volume of gas that remains unadsorbed by the sample, defining the amount of gas adsorbed. Multiple injections are performed till the complete saturation of the exposed metal on sample. Equation 2.7 permits the evaluation of the metal surface area.

$$A = \frac{V_m N a_m}{V_{molar} S m} \tag{2.7}$$

where A is the metal surface area [$m^2 \cdot (g_{sample})^{-1}$]; V_m is the volume of gas chemisorbed at monolayer [m^3]; N, the Avogadro number [molecules·$(mol)^{-1}$]; S is the stoichiometric factor; a_m, the surface area occupied by a metal atom [$m^2 \cdot (\text{metal atoms})^{-1}$]; V_{molar} is the volume occupied by a mole of gas [0.0224 $m^3 \cdot (mol_{gas})^{-1}$ at STP] and m, the mass of the sample [g]. The specific metal surface area is defined as [$m^2 \cdot (g_{metal})^{-1}$]. It is calculated from the surface area (A) as described in Equation 2.8.

$$A_m = A\frac{100}{L} \tag{2.8}$$

where A_m is the metal surface area [$m^2 \cdot (g_{metal})^{-1}$] and L is the metal loading expressed as ratio between the mass of the metal loaded and the sample [wt.%]. In supported metal catalysts, it is important to know what fraction of the active metal atoms is exposed and available to catalyze a surface reaction. Those atoms that are located inside metal particles do not participate in surface reactions, and are therefore wasted.
The dispersion represents the exposed metal atom as a percentage of the total number of metal atoms in the sample[74].

$$D = \frac{V_m M 10^4}{V_{molar} SmL} \tag{2.9}$$

where D is the dispersion [%] and M, the atomic weight of the metal [$g_{metal} \cdot (mol)^{-1}$].
For the CO chemisorption was used a Micromeritics ASAP 2020 unit. Prior the tests, the samples were evacuated in helium at 100 °C for 30 min, then at 350 °C for 15 min to eliminate adsorbed moisture. After the evacuation, the powder was reduced with H_2 at 350 °C for 2 hours. A further evacuation step was carried out to quickly strip excess reducing gas. The analysis was performed dosing CO at 35 °C.
The samples metal loading L was measured by atomic absorption spectroscopy (AAS). This technique is used in several applications, e.g. water and clinical analysis, to control the amount of heavy metals in a solution. The analytical application is based on the fact that metal atoms of different elements adsorb characteristic wavelengths of light. The wavelengths correspond to the amount of energy needed to promote electrons to a more energetic level. The investigation of a definite chemical specie means select the lightsource issuing the proper wavelengths. Analyses on a particular element are done using light emitted from that element[75].
The tests were carried out with a Perkin Elmer 1100 B equipped with a Pd Lumina Hollow Cathode Lamp (HCL). The HCL is the common source of light. It contains a tungsten anode and a cylindrical cathode made of the element to be determined. The lamp is filled

by inert gas that is ionized applying a potential difference between the anode and the cathode. The gaseous ions bombard the cathode that eject metal atoms in a process called sputtering. Some sputtered atoms are in excited states and emit radiation characteristic of the metal as they fall back to the ground state. The shape of the cathode concentrates the radiation into a beam. Figure 2.5 shows the schematic functionality of a HCL lamp.

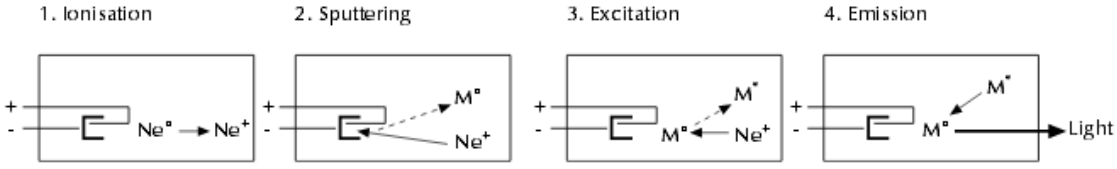

Figure 2.5. *Atomic levels involved in copper Kα and Kβ emissions.*

The sample preparation consisted in dissolving 20 mg of dried catalyst in an acquaregia solution and then diluted with deionized water. The quantitative analysis was carried out evaluating the amount of specific radiation adsorbed.

2.1.2.4 Thermal Programmed Reduction (TPR)

Temperature Programmed Reduction (TPR) determines the number of reducible species present on the catalyst surface and reveals for each of them the most efficient reduction condition. An oxidized catalyst is submitted to a temperature ramp while a reducing gas mixture is flowed over it. The tests were performed with a Micromeritics Autochem 2910 equipped with a thermal conductivity detector (TCD). The TCD is used to measure the composition of the gaseous mixture at the exit of the sample container. The detector senses changes in the thermal conductivity on the column in which the sample flow, and compares it with the reference flow. This information yields the volume of hydrogen needed for the reduction of the sample. The samples were flushed in helium at 250 °C for 2 hours prior to analysis and cooled down to room temperature. The analysis was run using 5% H_2 in Argon up to 700 °C, with a heating rate of 5 °C/min.

2.2. Reactor set up

The reactor used to perform the direct synthesis experiments was a 300 ml-stainless steel autoclave (Parr) operated in semibatch mode. A schematic of the apparatus is given in Figure 2.6. The mixing was performed by a Heidolph RZR 2021 rotor. The temperature inside the autoclave was monitored by a K-type thermocouple. A cooling/heating unit (B.Braun, Thermomix UB/Frigomix) fitted to a thermal jacket around the vessel maintained a constant temperature during the experiments.

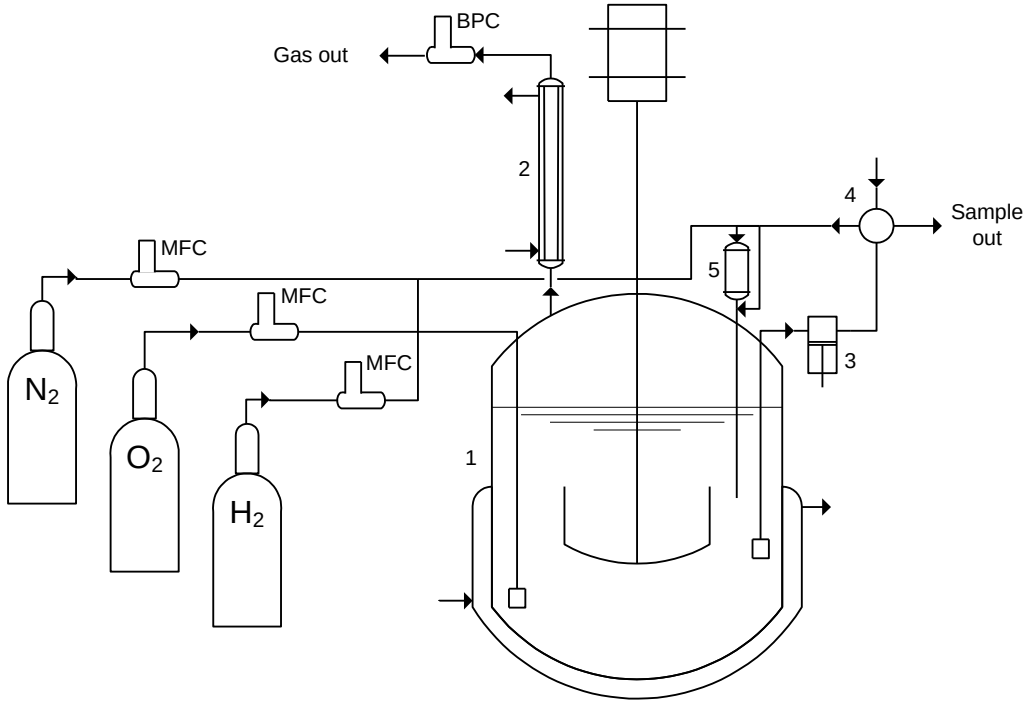

Figure 2.6. *Schematic of the experimental apparatus: 1- reactor; 2 - condenser; 3 - high pressure pump; 4 - sampling valve; 5 - catalyst chamber; MFC - mass flow controller; BPC - back pressure controller.*

The pressure inside the reactor was aquired by a Keller PA-21R pressure transducer and kept constant via a back pressure controller. The gases were provided directly from cylinders via mass flow controlers (Brooks Instruments) to ensure a constant and reproducible stream. An important phase in the plant setting was the calibration of the flow mass controlers. The procedure was to open the controlers at different percentages of full scale and register the flux value with a bubble flow meter (Figure 2.7).

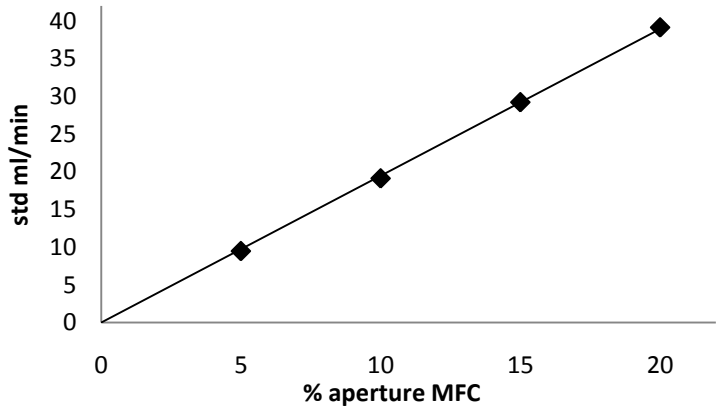

Figure 2.7. *Calibration plot relative to the MFC used to control the flow of H_2.*

The calibration returned a linear correlation that allowed the definition of the flow rate relative to the opening percentage of the mass flow controler.
A system of on/off valves was arranged after the gas cylinders to ensure a separation between the cylinders and the reactor. The reagents loading was achieved bubbling the gases in the liquid by a 2 µl gas diffuser to reduce the bubble size. The gas composition at the outlet was analyzed by gas chromatography. The gas outlet was equipped with a condenser (operating at -18°C) to ensure that no methanol left the reactor with the outgoing gas flow. The refrigerant liquid was also used to pre-cool the gases incoming the reactor. The efficiency of the condenser was verified by gas chromatography analysis, and no methanol was detected in the gas flow leaving the system.
The apparatus implementation is showed in Figure 2.8.

Figure 2.8. *View of the semibatch apparatus. It is recognizable: 1- Agitator motor; 2 – Injection chamber; 3 – Condenser; 4 – High pressure pump; 5 – Flow mass controller; 6 – reactor and cooling jacket fitted in an isolating cover. On the left of the reactor, the on-off valves for the gases introduction appear. Between the pump and the reactor there is the 6-ways valve for the liquid sampling.*

The catalyst was introduced in the reactor by a dedicated chamber. The use of a particular injection instrumentation was necessary since the addition of the catalyst was performed in a pressured system. In fact the introduction happened after that all the gases had been charged and the liquid-vapor system had reached the phase equilibrium. The catalyst was

added last to ensure no in situ oxidation/reduction of the catalyst due to a potential contact with the reagents before the beginning of the experiment. Moreover, this procedure allowed for a very precise identification of the beginning of the reactions. The procedure of injection is described below and guarantees the whole catalyst to be successfully added in the liquid phase. A high pressure pump recirculated (20 ml/min) the liquid through an external loop into a six-way GC valve. Liquid samples were withdrawn through this valve and collected at increasing time up to 5h. The liquid probe inside the reactor was equipped with a 7 µl filter to prevent any block of the sampling valve and pump by catalyst particles.

2.2.1. Operative conditions and procedure

Before the experimental program was started, a 5 hours passivation treatment was performed on the reactor using 30 vol% nitric acid at 40°C. The apparatus was periodically tested for decomposition and hydrogenation of hydrogen peroxide at the same operative conditions of experimental tests. A 0.5wt% H_2O_2 in methanol was tested without detecting any decrease of hydrogen peroxide concentration.

The catalysts were tested in a slurry methanol solution (200 ml). Methanol was introduced in the reactor first, followed by the gas reagents. No addictive and promoters were used during the tests. Throughout the experiments, the gas mixture was continuously bubbled into the static liquid phase. The gas composition was 76-20-4 mol% N_2-O_2-H_2, respectively, with a total flow of 300 Nml/min. Before the introduction of the catalyst, the temperature was set at 10 °C and stirring started (1000 rpm), allowing the pressure to reach the desired value (50 bar). The temperature of 10°C was optimal for the experimental campaign intent. The operative pressure of 50 bar was chosen to improve the solubility of the reagent gases in the methanol and thus the reaction rate. For every experiment eventual pressure leakage were controlled and detected. After the stabilization of pressure and temperature, the vapor-liquid equilibrium of the system had to be achieved before the test was initiated. The gas phase at the outlet was repetitively analyzed by gas chromatography, until the gas composition at the outlet resulted equal to the one at the inlet. The vapor-liquid equilibrium was reached when the two gas composition corresponded. Figure 2.9 describes the typical evolution of the outlet gas composition during an experiment. The time *zero* corresponds to the injection of the catalyst and the starting of the catalytic test. The axis of ordinates at the left is relative to the molar fraction of N_2 and O_2, while the y-axis on the right concerns the molar fraction of H_2. The plot reports the gas composition in relation to the experimental time. The data before zero display the development of the system to reach the vapor-liquid equilibrium. The *full* points correspond to the gas composition at the starting of the catalytic test (76-20-4 mol% N_2-O_2-H_2). After

approximately 90 minutes, the gas composition at the outlet is comparable with the one supplied at the inlet and the vapor-liquid equilibrium is reached.

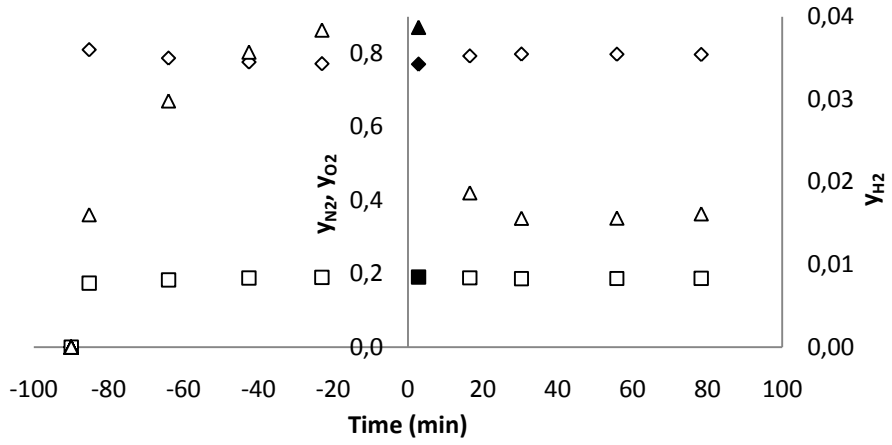

Figure 2.9. *Typical evolution of gas phase composition before and after the starting of the catalytic experiment: ◊, N_2; □, O_2; Δ, H_2.*

The evident decrease of the molar fraction of H_2 is due to the after time zero is due to the proceeding of the catalytic reaction.

The catalyst (60 mg) was introduced via the dedicated chamber. The dedicated chamber consists of a pipe, filled by a slurry of catalyst and methanol, connected by a three way valve to the reactor. A schematic is shown in Figure 2.10, displaying two separate loops.

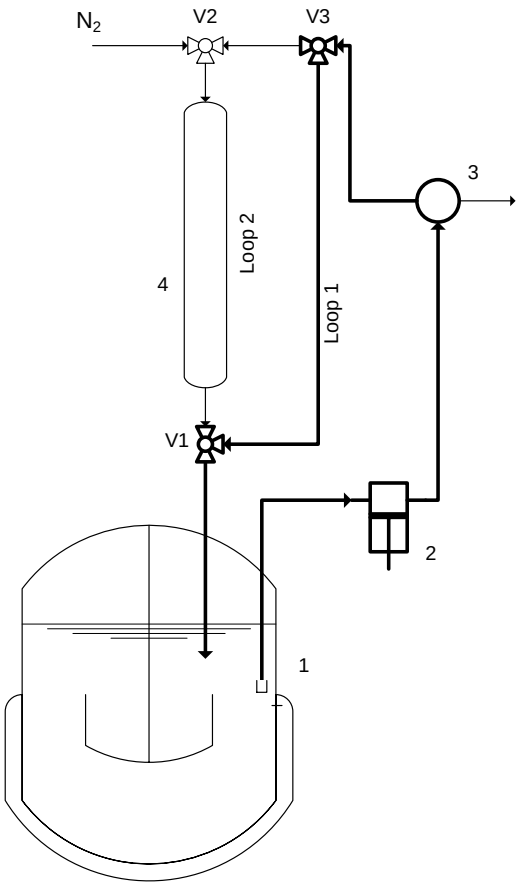

Figure 2.10. *Schematic of the injection chamber: 1- reactor; 2 – high pressure pump; 3 – sampling valve; 4 - catalyst chamber; V1, V2, V3 – three ways valves.*

Loop 1, highlighted in figure by the bold line, was used during the standard experimental running. The liquid was recirculated by the pump (2) to the reactor by-passing the injection chamber (4). *Loop 2* was only used during the injection phase, providing the recirculation of the solvent to the reactor through the chamber.
The procedure for the catalyst addition started opening valve V1 and connecting the chamber to the reactor. After that, the recirculated liquid flow was switched from *Loop 1* to *Loop 2* permitting the passage through the chamber. Flushing alternatively nitrogen and solvent, the whole catalyst was injected and active in the reaction ambient.
At the end of each test the apparatus tools and the reactor were washed in an ultrasonic bath and left overnight in a 30% nitric acid solution to remove any trace of residual catalyst. In preparation of the next experiment every part of the system was washed with deionized water, dried and then rinsed with methanol to remove any possible moisture.

2.3 Instrumentations and analysis

2.3.1 Gas analysis

Only hydrogen, nitrogen and oxygen needed to be analyzed in the gas samples. The gas chromathography can perform qualitative and quantitative analyses. Each of the three components was characterized by a specific retention time (Table 2.2). The gas chromatogram returns a peak for each component, whose area is proportional to the molar concentration. The internal normalization method permits to make the peaks comparable and proportional to their concentration. It is usable if all the components of the mixture are known and present in the chromathogram. The method uses a corrective factor for each component that is multiplied by the correspondent peak area detected in the gas chromatograph. In this way the corrected areas are found and they can be compared finding the mixture composition. The procedure for calculate the corrective factors requires the injection in the GC a mixture of the interested components at known composition. One of the component is considered of reference, i.e. hydrogen, whom corrective factor will be 1. The corrective factor is defined comparing the areas of the peaks of the reference component and the other substances. Table 2.2 reports the values of GC corrective factors for the considered substances.

Table 2.2 *GC corrective factors and retention times for each gas components.*

	H_2	O_2	N_2
Retention time *(min)*	8:54	8:12	9:36
Response factor	1.000	6.290	8.277

The specific values of the corrective factors depend on several variables, e.g. operative conditions, instrument features and column type.

All the analyses were carried out with a Agilent Technologies 6890N gas chromatograph (GC). Figure 2.11 provides a schematic of the gas chromatograph functionality.

The GC was equipped with a HP-Plot Molecular Sieve 5A GC column J&W Scientific. This is a 30 meter column commonly used to separate permanent gases through its molecular sieves, since different molecules have distinct retention times due to their dimensions. Molecular sieve columns can easily absorb water and methanol which, over time, can results in changing the retention time. The provider reports a GC program at 200°C for 7 hours to regenerate the column.

A 10 µl syringe was used to inject the sample. The temperature of the injector was set at 250°C.

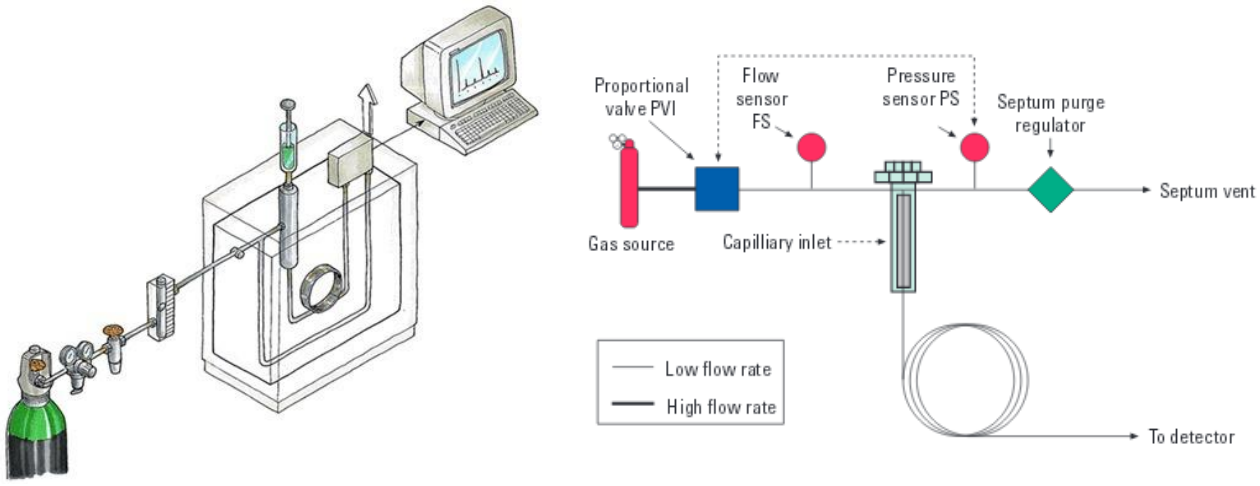

Figure 2.11. *Schematic of the GC functionality (left) and the injection phase (right). (Adapted from Agilent 6890N network GC User Manual).*

After the injection the sample was carried through the column permitting the separation. The column was installed in a oven at 40°C for the whole program. This temperature gave a good compromise between low retention time and good separation. The carrier gas was

argon, it permitted all the substances present in the sample to be visible in the cromatoghram.

The detector was a thermo-conductivity detector (TCD). As already explained in this Thesis, the TCD is a detector based on the different thermal conductivity of gases. It is composed by two heated wires: one flowed by the pure carrier, the other by the gas exiting the sampling column (carrier + gas sample). The wires are part of a Wheastone bridge (a balanced electric circuit) and maintained at constant temperature in carrier flow. The temperature of the wire connected to the column changes when it is reached by the gas sample, since the examined gases have different thermal conductivity from the pure carrier. The temperature change causes the variation of the electric resistance of the wire and an imbalance on the Wheastone bridge. The detector registers this imbalance and reports with an electric signal (μV) the passage of a substance different from the carrier. The temperature of the detector was set at 250°C.

2.3.2 Liquid analysis

H_2O_2 and H_2O concentrations were determined by iodometric and Karl-Fischer titrations, respectively.

The iodometric analysis consists on the indirect titration of the molecular iodine produced from the oxidation reaction between hydrogen peroxide and potassium iodide (KI) in an acid ambient and catalyzed by molybdenum.

The materials used in the titration were:

(a) Potassium iodide (KI): prepared dissolving 10 g of KI (Sigma-Aldrich) in 100 ml of deionized water. It must be prepared fresh before every experimental test, since it is easily degraded by contact with air and light.

(b) Molibdate (Mo): 0,125 g of ammonium molybdate tetrahydrate ($(NH_4)_6Mo_7O_{24}\cdot 4H_2O$ - Fluka) dissolved in 100 ml of deionized water with the adding of 2,4 ml of concentrated sulfuric acid (H_2SO_4 – J.T. Baker). It is the catalyst of the reaction between KI and H_2O_2.

(c) Water solution of sodium thiosulfate: the concentration of depends on the expected concentration of hydrogen peroxide in sample solution. In this titration it was used 0,8 g of pentahydrate sodium ($Na_2S_2O_3\cdot 5H_2O$) in 500 ml of deionized water (0.645E-6 mol/ml). It was periodically standarized with a standard solution of potassium dichromate ($(NH_4)_2Cr_2O_7$ - Riedel de Haen). Thiosulfate tritates the iodine released in the reaction.

(d) Starch solution: starch (Sigma-Aldrich) is dissolved in deionized water, stirred at 60°C overnight to get a homogeneus solution. The starch is used to evidenciate the end point of the reaction.

Iodide has weak reducing behaviors and it is easily oxidized to iodine by strong oxidant, i.e. hydrogen peroxide, as reported in Reaction 2.1.

$$H_2O_2 + 2KI + H_2SO_4 \xrightarrow{Mo} I_2 + K_2SO_4 + 2H_2O \quad (2.1)$$

The solution becomes yellow due to the presence of iodine. The iodine is titrated with a standard solution of sodium thiosulfate, that reduces it to iodide (Reaction 2.2).

$$I_2 + 2Na_2S_2O_3 \rightarrow Na_2S_4O_6 + 2NaI \quad (2.2)$$

Close to the end-point, the starch is added and the sample solution turns purple. The titration process is resumed till the solution becomes transparent. The thiosulfate is used before the starch in order to remove most of the iodine before the starch is added. The starch is employed as last because of the insolubility of the starch-iodine complex which may prevent some of the iodine reacting with the titrant.
The stoichiometric ratio between H_2O_2, I_2 and $Na_2S_2O_3$ is 1:1:2. Hence, the hydrogen peroxide is calculated through Equation 2.10.

$$M_{H_2O_2} = \frac{1}{2}\frac{M_{Na_2S_2O_3}V_{Na_2S_2O_3}}{m_{H_2O_2}\rho_{solution}} \quad (2.10)$$

where $M_{H_2O_2}$ is the molarity of the hydrogen peroxide solution [$mol_{H_2O_2} \cdot l_{solution}$]; $M_{Na_2S_2O_3}$, thiosulfate molarity; $V_{Na_2S_2O_3}$, volume of titrant used; $m_{H_2O_2}$, the analyzed volume of the H_2O_2 solution; $\rho_{solution}$ is the density of the sample solution.
The analysis was performed adding 5 ml of KI and 2 ml of Molibdate to a known amount of liquid sample. The sample was maintained agitated and the thiosulfate was dosed drop by drop with a semiautomatic titrator. In this phase two drops of the starch indicator was added and the titration resumed till the solution became transparent. The iodometric titration is affected of different experimental error, e.g. the equilibrium point is detected by the operator view. The volatility of iodine is a source of error for the titration, this can be effectively prevented by ensuring an excess of potassium iodide.

The water content was automatically determined by Karl Fischer titration (KF) with a Titrino GP 736 titrant from Metrohm (Figure 2.12). The titration procedure developed by Karl Fisher was conducted in methanol with the presence of a base capable to neutralize the sulfuric acid released in the reaction. The reaction occurs in two steps: at first, in Reaction 2.3, the methanol reacts with sulfurous anhydride to produce methyl-sulphite, that is successfully oxidized by iodine in Reaction 2.4.

$$CH_3OH + SO_2 + B \rightarrow [BH]SO_3CH_3 \quad (2.3)$$

$$[BH]SO_3CH_3 + I_2 + H_2O + 2B \rightarrow [BH]SO_4CH_3 + 2[BH]I \quad (2.4)$$

where B is the base used, diethanolamine. The diethanolamine can be used in excess since its fundamental function is to create a buffer solution that stabilize the pH of the reagent ambient. The equilibrium point is automatically detected by amperometric way with a double Pt electrode immerged in the anionic liquid. When the sample is injected the testing liquid contains a lot of I^- and a little amount of I_2; that permits the passage of current between the electrodes. At the equilibrium point there is an excess of molecular iodine that provoke a voltage drop.

Figure 2.12. *Automatic titrator 736 GP Titrino for quantitative analysis of water. Adapted from Instructions for Use 736 GP Titrino (Metrohm).*

Hydranal methanol (Fluka) and Composite 2 (Fluka) were used as titrants. The titration cell was prepared by addition of 5 ml of hydranal methanol which are enough to cover the tip of the Pt electrode. The cell was isolated with a rubber ring because the instrumentation was particularly sensible and any kind of humidity source, e.g. air, could influence the titration. The titrator had to be calibrated every time a new experiment was started. The calibration consisted in titrate 10 µl of deionized water. The procedure had to be done three times, then it was considered the average value of the amount of titrant used.

The sample was added to the cell through a plug set on the top of the cell. The addition of the sample with a micropipette was carried out opening the cell, the operation had to be as rapid as possible to avoid excessive air contamination.

The KF titration is affected by several systematic errors, e.g. umidity adsorption by the sample and the liquid in the cell. Their influence on the titration results can be mitigated following the same procedure for every test.

The concentrations were rescaled on the moles of Pd to take in account the different content of active metal in the catalysts. H_2O_2 selectivity (S_{H2O2}) and specific conversion (C_{H2O2}) were calculated as in (2.11) and (2.12) respectively.

$$S_{H_2O_2} = \frac{[H_2O_2]}{[H_2O_2]+[H_2O]}100 \tag{2.11}$$

$$C_{H_2O_2} = \frac{[H_2O_2]+[H_2O]}{\dot{n}_{H_2} t}100 \tag{2.12}$$

where $[H_2O_2]$ and $[H_2O]$ are the specific molar concentration of peroxide and water, respectively, V^L is the liquid volume in the reactor and $\dot{n}_{H_2}$ is the inlet molar flow of H_2, t is time. Prior to the introduction of the catalyst, water content of the liquid phase was measured and deducted from the subsequent analyses.

Chapter 3

Results and discussion

In this section the analyses and the experimental results are discussed. The first part reports a thorough interpretation of the outcomes of characterization tests on the catalysts. The second part of the chapter is focused on the experimental tests and in depth analysis of results. An interesting relation between the characteristics of the materials and their performances is described.

3.1 Characterization results

The experimental results reveal the different characteristics of the supports provided by MEL and the ones mechanically mixed and crushed. The effects of the distinct structures on the reducibility of the support-metal systems are outlined. The metal particle size and dispersion are discussed in relation to the morphological properties of the support.

3.1.1 BET surface and porosity analysis

The first analysis reported are relative to the BET surface and the pore volume. The tests were carried out on bare supports. Being different in composition, the calcined supports exhibit a wide range BET surface area, from 30 to over 100 m^2/g.

The average pore diameter range is quite wide, from about 5 up to 28 nm, as well as the total pore volume that affected the number of steps necessary for the impregnation of the Pd precursor. As expected, samples with higher surface area present low pore volume and pore diameter (Table 3.1).

The samples present low surface areas and pore volumes. As reference the 1 wt% Pd/C used as benchmarks in the experimental tests report a surface area of 1746 m^2/g and a pore volume of 1.00 cm^3/g.

Table 3.1. *Surface features of the supports used.*

Sample	BET area (m^2/g)*	Pore Volume (cm^3/g)*	Pore Ø (nm)*	AAS metal loading (%)	Dispersion (%)	Particle size (nm)	Metal surf. area (m^2/g_{metal})
Pd2	51.7	0.216	16.7	0.29%	48.5	2.3	216
Pd3	93.4	0.115	4.9	0.34%	55.6	2.0	248
Pd4	31.4	0.198	25.2	0.66%	61.9	1.8	276
Pd5	44.2	0.310	28.0	0.62%	80.7	1.4	359
Pd6	71.6	0.125	7.0	0.26%	52.5	2.1	234
Pd7	102.0	0.118	4.7	0.30%	42.4	2.6	189
Pd8	71.3	0.290	16.3	0.54%	99.1	1.1	441

*bare support

3.1.2 XRD

XRD spectra of catalysts prepared using MEL supports (Pd2, Pd3, Pd6 and Pd7) are shown in Figure (3.1). All the supports formed a solid solution between zirconia and the promoter present in the powder.

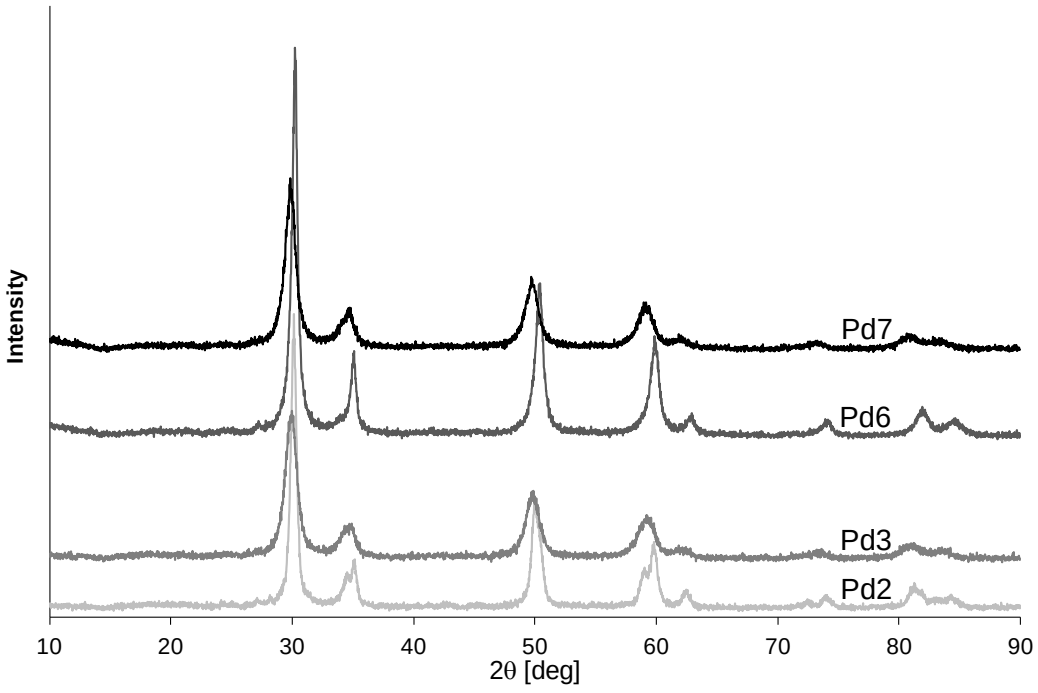

Figure 3.1. *XRD patterns of the Pd samples supported on MEL Chemicals powders. Pd2: ZrO_2/CeO_2 82.5/17.5 wt%, Pd3: Ce doped ZrO_2, Pd6: ZrO_2/Y_2O_3 92/8 wt%, Pd7: $ZrO_2/CeO_2/La_2O_3$ 77.5/17.5/5 wt%.*

Both Pd2 (ZrO_2/CeO_2 82.5/17.5 wt%) and Pd3 (Ce doped ZrO_2) show peaks of tetragonal $Zr_{0.84}Ce_{0.16}O_2$ as main phase. Pd2 also shows some low peaks due to residual amounts of ZrO_2, which are not present in the pattern of Pd3. The residual presence of ZrO_2 reduces the overall homogeneity of the support. Pd6 (ZrO_2/Y_2O_3 92/8 wt%) shows the formation of tetragonal $Zr_{0.9}Y_{0.1}O_{1.95}$, while the Pd7 sample ($ZrO_2/CeO_2/La_2O_3$ 77.5/17.5/5 wt%) exhibits overlapping peaks originated by the formation of cubic zirconium lanthanum oxide ($Zr_{0.9}La_{0.1}O_{1.95}$).

The patterns of the samples Pd4, Pd5 and Pd8 are reported in Figure 3.2, along with two references patterns. The first reference, named CeO_2-ZrO_2 mix, is a sample of ceria and zirconia that were mixed and crushed together, but not calcined. The pattern on top of the figure is relative to the second reference and it is representative of a solid solution between ceria and zirconia. The comparison with the two reference patterns simplifies the interpretation and recognition of the phases[64,67].

The spectra in Figure 3.2 show that these samples are more crystalline compared to those prepared with MEL supports. Indeed the peaks in Figure 3.1 are broader and less intense, probably due both a loss of crystallinity and a decrease of the particle size of the supports, as already reported for this kind of materials by R. Pèrez-Hernàndez *et al.*[76].

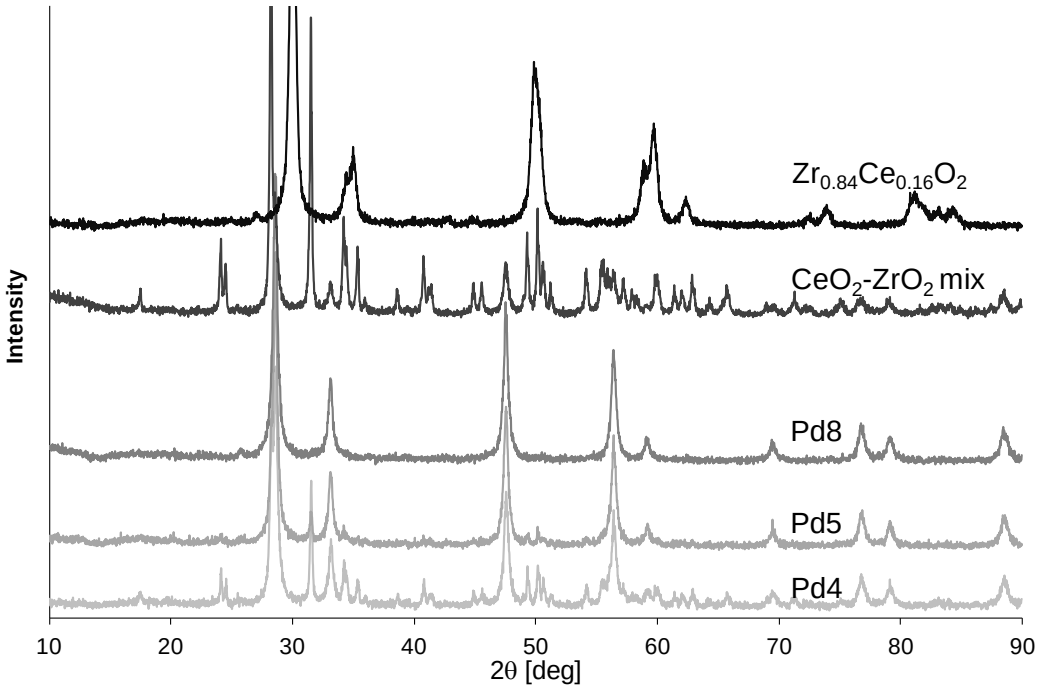

Figure 3.2. *XRD patterns of the Pd samples supported on ceria-zirconia mixtures. Pd4: CeO_2/ZrO_2 17/83 wt%, Pd5: CeO_2/ZrO_2 50/50 wt%, Pd8: CeO_2. For comparison, the pattern of a non calcined CeO_2/ZrO_2 17/83 wt% is also reported, as well as the pattern of a solid solution of ceria and zirconia.*

As expected, the samples prepared by mixing, crushing and calcining different amounts of ceria and zirconia did not form a solid solution, but rather maintained distinct phases. However, both the patterns of Pd4 (CeO_2/ZrO_2 17/83 wt%) and Pd5 (CeO_2/ZrO_2 50/50 wt%) show a marked reduction of the peaks due to pure ZrO_2. This can be noted mainly by observing the peak at 31.54° and the pair of overlapping peaks at 24.1 and 24.5°, which becomes much smaller in the spectra of Pd4 and Pd5. The main peaks are due to the presence of cubic ceria and monoclinic ZrO_2. No peaks of Pd were detected, due to both the small particles size and the low amount of metal loaded on the samples.

3.1.3 CO chemisorption and the Atomic Absorption Spectroscopy

As highlighted in Table 3.1, the support physical features considerably affect the metal dispersion and the average particle size. In general, the dispersion of all the samples is very high, ranging from 50 up to almost 100%. The MEL supports showed bigger particles size with a range from 2.0 to 2.6 nm. Apparently, the Pd dispersion is proportional to the pore diameter and inversely proportional to the surface area of the support, as demonstrated in Figure 3.3.

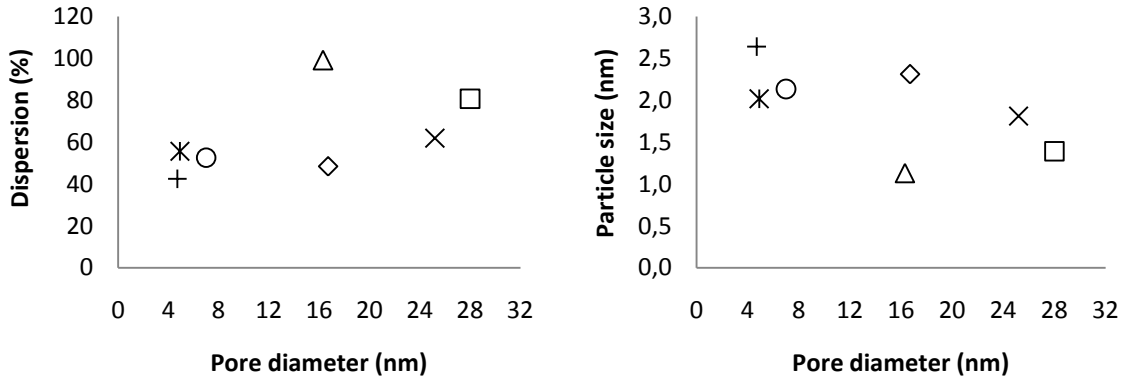

Figure 3.3. *Dispersion and particle size in relation to the pore diameters: ◊, Pd2; *, Pd3; x, Pd4; □, Pd5; ○, Pd6; +, Pd7; Δ, Pd8; - Pd/C commercial.*

It appears that supports with larger pore diameter allowed the formation of smaller particles, thus favoring the metal dispersion. On supports with smaller pores, the Pd particles appears less likely to disperse and grow outside the pores resulting in bigger particles.

The results of the measurement of the metal loading in Table 3.1 show that for all the samples the actual loading is rather close to the nominal; this being 0.3 wt.% for the samples supported on MEL Chemicals powders and 0.6 wt.% for the remaining samples.

The measurements were repeated 5 times on each sample and the relative standard deviation was always smaller than 2%.

3.1.4 TPR

The TPR profiles of the samples supported on MEL are reported in Figure 3.4, while Figure 3.5 displays the patterns relative to samples Pd4, Pd5, Pd8. The dashed lines in the plots are relative to the reduction of bare supports. All the prepared samples show a clear negative peak centered around 70 °C. This peak is due to the decomposition of Pd β–hydride[77]. Melada *et al.* outlined this behavior of palladium at low temperature[31]. The PdO can be reduced at temperatures as low as -15 °C, leading to the formation of β–hydride. The reduction of PdO occurs before the analysis starts, when H_2 is dosed at room temperature until the TCD base line stabilizes. When the TPR run starts and the temperature increases, the freshly formed hydride decomposes, originating the negative peaks at around 70 °C. The amount of H_2 released from the hydride decomposition has been quantified and related to the amount of Pd available. The moles of H_2 released are divided by the moles of Pd and scaled on the measured metal dispersion, since the hydride forms on the surface of the Pd particles (Table 3.2).

Table 3.2. *Calculated amount of H_2 released by the b-hydride decomposition. The value for the sample Pd7 is not available.*

Sample	H_2 release ($\mu mol_{H2}/mmol_{Pd}$ exposed)
Pd2	42.5
Pd3	33.2
Pd4	7.1
Pd5	9.4
Pd6	39.9
Pd7	n.a.
Pd8	10.9

It must be noticed that the higher H_2 release values are characteristic of the samples with larger Pd particle size (Table 3.1). It could be interpreted as a better ability by larger metal particles to store hydrogen, with possible enhancing of the catalytic activity.

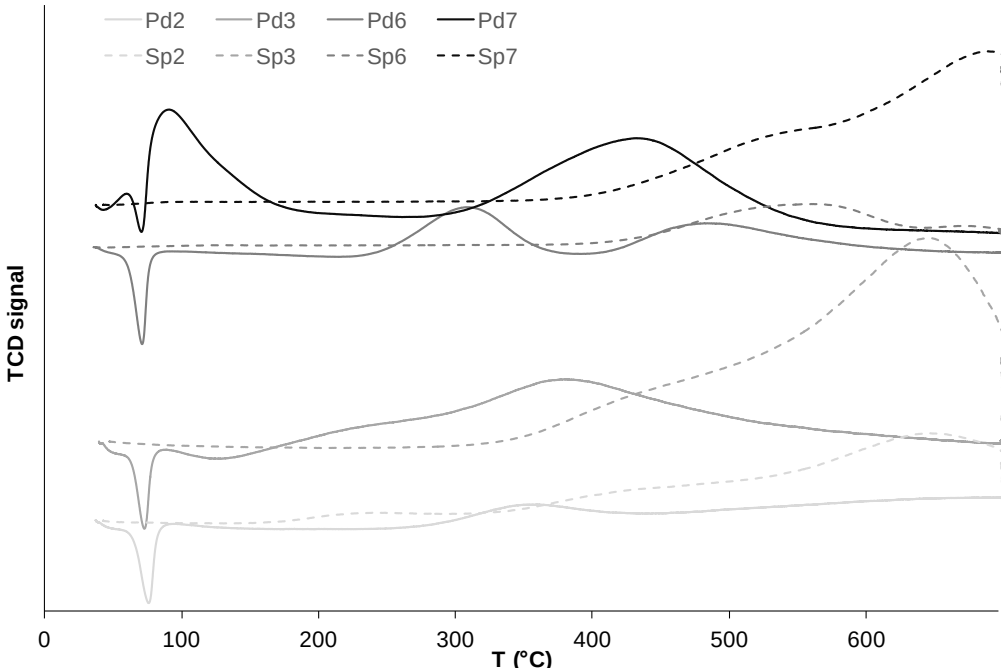

Figure 3.4. *TPR curves of the fresh samples and of the supports for the 0.3% Pd samples.*

For the samples supported on MEL (Figure 3.4), distinct palladium reduction peaks are detected at varying temperatures. Indeed, Pd2 shows a peak between 300 and 400 °C; Pd3 shows a peak starting at about 170 °C and overlapping with another very wide one at 400 °C, the latter likely due to the support. Pd6 shows a reduction peak centered at 307 °C, while sample 7 exhibits a peak at 93 °C.

The peaks between 80 and 350 °C are due to Pd(II) non reducible at room temperature[31]. In particular the high temperature reduction peaks can be assigned to two dimensional PdO that can be formed on the surface in case of low Pd content. This kind of PdO structure is formed in presence of highly dispersed metal, due to small crystallite size. This is in agreement with the high dispersion values detected and the consequent low particles size of the examined samples.

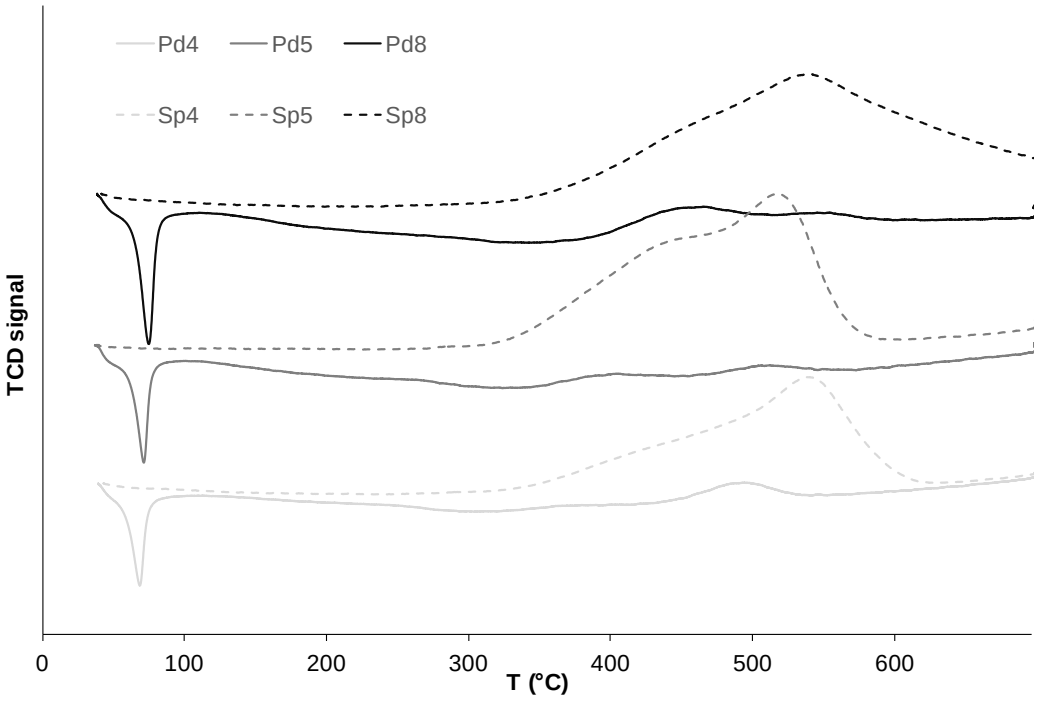

Figure 3.5. *TPR curves of the fresh samples and of the supports for the 0.6% Pd samples.*

Interestingly, no Pd reduction peaks are detected for the samples with higher Pd loading (Figure 3.5). Only a more pronounced negative peak at 75 °C is detected. Other peaks are detected at much higher temperature, but they are very small and they seem to correspond to those obtained in the reduction of the bare supports. It appears that the loaded Pd is suppressing the reduction of the support. As already mentioned there seems to be a connection between the reducibility of the support and its homogeneity. The MEL samples that create a homogeneous solid solution are more reducible. The mechanically-prepared samples that remain in distinct phases show lower reduction peaks.

3.2 H_2O_2 direct synthesis experimental results

During the experiments, the reagents were continuously bubbled through the static liquid phase. The gas phase was assumed as a continuous stream reactor, where the composition at the outlet is equal to the composition inside the reactor. Prior to the experimental campaign, the reactor setup was tested for eventual external mass transfer limitations (Figure 3.6). Given that the gas to liquid mass transfer is independent of the specific catalyst, increasing amounts of a commercial 5% Pd on carbon catalyst (Degussa) were tested in similar reaction conditions. Since a high H_2 conversion was the aim of these experiments, a catalyst with a higher Pd content compared to our synthesized materials was

deliberately chosen. A linear conversion of H_2 (the limiting reagent) was observed up to 80%, confirming that the reaction was not affected by gas to liquid transport limitations.

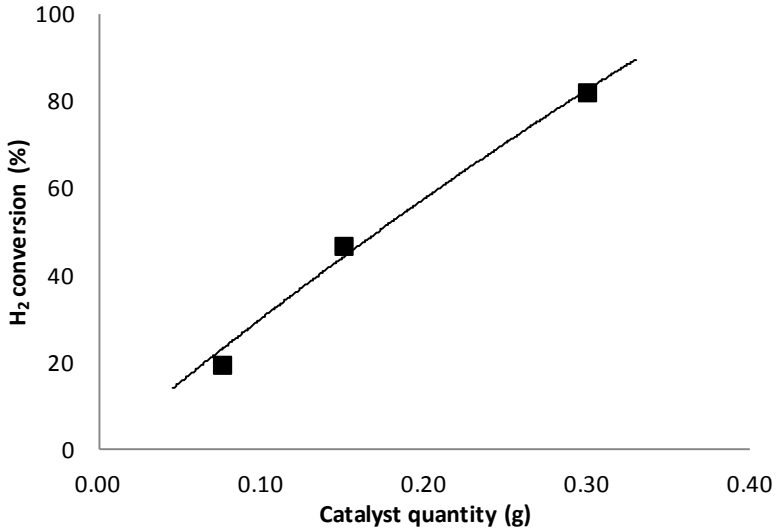

Figure 3.6. *H_2 conversion with increasing amount of a commercial 5% Pd on carbon catalyst.*

If the mass transfer had interfered with the reaction the correlation between quantity of catalyst and conversion wouldn't have been linear. Hence, all experiments herein reported were carried out at H_2 conversion below 80%. Experimental results are reported in Figure 3.7 in terms of hydrogen peroxide and water specific concentration, selectivity and conversion as a function of time.

In all experiments, hydrogen peroxide concentration leaned towards a steady state value. At the same time, the selectivity dropped, meaning that the water concentration (Figure 3.7B) steadily increased. This is expected, since hydrogen peroxide is a reaction intermediate and water is the final product; in a semibatch apparatus the accumulation of peroxide leads to an increase of the hydrogenation and disproportionation rates, so that H_2O_2 concentration reaches a steady value. Interestingly, the conversion decreased with the time on stream (Figure 3.7C), which is in apparent contradiction with the increasing peroxide (and water) concentrations.

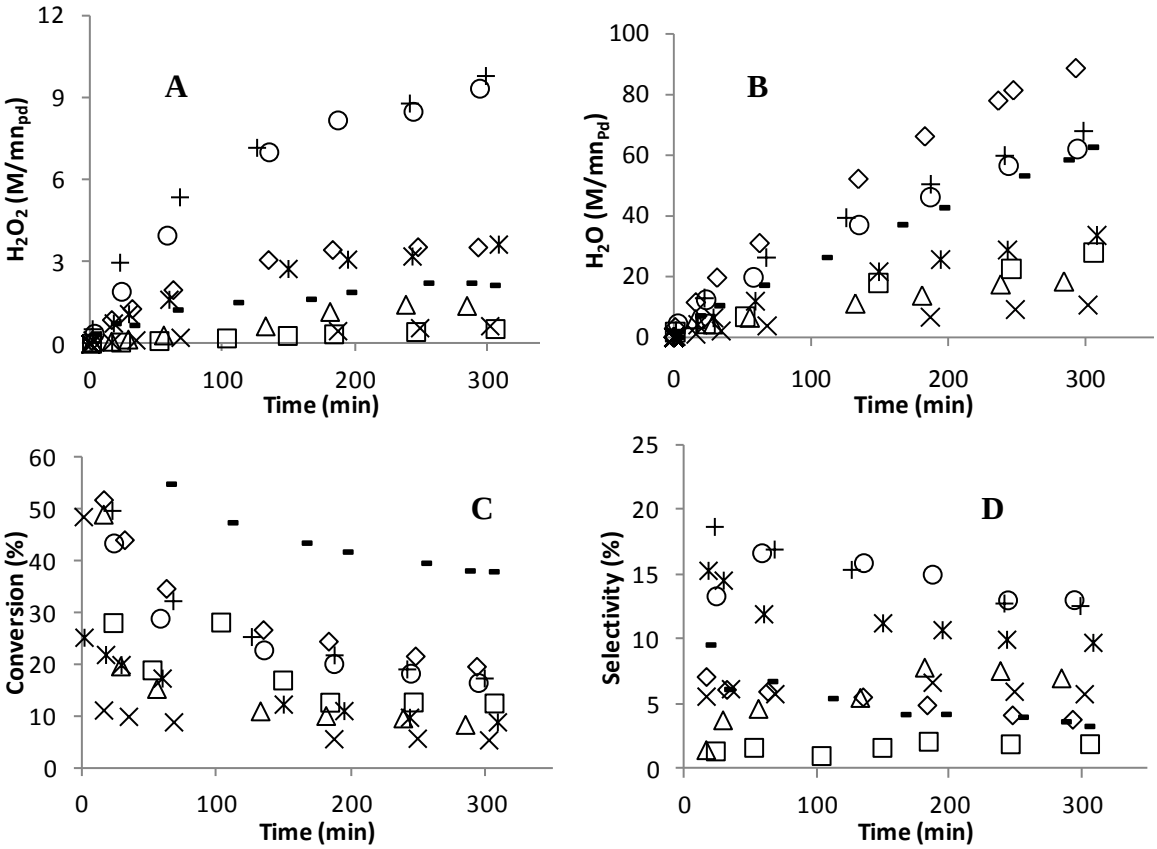

Figure 3.7. *Experimental results in terms of specific H_2O_2 concentration (A), specific H_2O concentration (B), conversion (C) and selectivity (D): ◊, Pd2; *, Pd3; x, Pd4; □, Pd5; ○, Pd6; +, Pd7; Δ, Pd8; - Pd/C commercial.*

This effect is due to the solubility of H_2 in the liquid phase. As soon as the catalyst was introduced, H_2 started to react, creating a sink of H_2 that was refilled by the inlet gas flow. Because of the reactions, the liquid phase goes through a transient from a higher to a lower H_2 (and O_2) content, that caused a decreased in the H_2 conversion. Moreover, the decreased composition in the liquid phase caused a reservoir of H_2 in the methanol. This quantity of H_2 was available to the reactions but is not included in the definition of conversion given in Section 2.3.2, that considers only the inlet H_2 molar flow. This contributed to the very high conversion values observed at low contact time (< 10 min). The H_2 buffer is soon consumed and its effect is only noticeable at low time on stream. Including the effect of the H_2 reservoir requires the precise knowledge of the vapor-liquid equilibrium of the complex system H_2-O_2-N_2-methanol and numerical modeling of the reactor. Nonetheless, the reported conversion values are significant to quantitatively evaluate the activity of the synthesized catalysts.

A 1 wt.% Pd on carbon commercial catalyst was tested as a benchmark. Apparently, all our synthesized catalysts had a lower conversion. However, the Pd content of the commercial was much higher, so that the conversion compare well with the tested original catalysts

when normalized. Furthermore, most catalysts reached a much higher peroxide specific concentration and selectivity, with values up to 4 times larger.

3.2.1. Discussion

The catalysts supported on MEL supports (Pd2, Pd6, Pd7) showed the highest H_2 conversion. In particular, the catalysts Pd2, Pd6 and Pd7 had the same conversion throughout the experiment, reaching values around 20% after 5h of reaction, whereas the other catalysts showed 9% conversion. Note that the catalysts prepared on MEL supports had half the Pd content of the others (Table 3.1), so that their relative activity is actually much higher than the other catalysts. The average conversion values are apparently rather low. A comparison with literature values is quite difficult, since different experimental conditions are often used. Menegazzo *et al.* found H_2 conversions values between 45% and 54% at 5h reaction of a 1.5 wt.% Pd/SiO_2 catalyst working at atmospheric pressure[43]; the same research group reported values between 40% and 90% with Pd catalysts (2.5 wt.%) supported on Zirconia and Ceria at 1 bar and 20°C (5h reaction)[23]. However, in the present study the experimental conditions (in particular the ratio between the H_2 flow rate and the catalyst quantity) were chosen so that the conversion never exceeded 80% for high time on stream to avoid any possible mass transfer limitation. Moreover, the conversion strongly depends on the total active metal used in the experiments, so that values are more significant when normalized. Hence, specific conversions in the range of 46-100 $[mol_{H_2}^{consumed} \cdot (mol_{H_2}^{supplied} \cdot mmol_{Pd})^{-1}]$ were obtained at 5h time on stream, whereas in the mentioned studies the specific conversion was between 24 and 40.

The same catalysts Pd2, Pd3, Pd6 and Pd7 also showed the highest H_2O_2 specific concentration (Figure 3.7A), with values of 3.5 and 8.5 $[M_{H_2O_2} \cdot (mmol_{Pd})^{-1}]$ for the groups Pd2, Pd3 and Pd6, Pd7, respectively. Lower values are normally reported in the literature. For instance, Abate *et al.* obtained peroxide specific concentrations in the range 2.1-5.2 $[M_{H_2O_2} \cdot (mmol_{Pd})^{-1}]$ at 4h contact time in a 6.5 bar semibatch apparatus[78]; Menegazzo *et al.* obtained values between 0.2 and 4.2 $[M_{H_2O_2} \cdot (mmol_{Pd})^{-1}]$ at 5h contact time, depending on the catalyst[23,43]. However, a higher peroxide concentration value is expected in a system as it is examined. Indeed, due to the higher pressure (50 bar), a higher reagent concentration was reached, allowing for a higher reaction rates. Interestingly, the catalysts with the highest specific peroxide concentration showed also the highest selectivity (Figure 3.7D). Nonetheless, the selectivity was quite low compared to the values obtained in the literature. It is worth noticing that in most of literature studies promoters and stabilizers (such as bromine and/or acids) were introduced in the reaction slurry to enhance selectivity and productivity. No such chemicals were used in this study, in order to isolate the effect of the catalyst properties on the selectivity.

In the following, the experimental results are discussed in relation to the properties of the catalysts. The catalysts showing the best yields are the ones supported in MEL materials, reporting better reducibility and homogeneity. Interestingly, the sample with the lowest Pd content (Table 3.1) showed the highest selectivity and specific hydrogen peroxide concentrations. More specifically, this relates to the interaction between the active metal and the support, where smaller pore diameters allowed the formation of larger Pd particles. In order to quantify this effect, in Figure 3.8 the selectivity and the specific peroxide concentration are reported as a function of the Pd particle size. Since the measurements varied with time, comparisons were carried out at 1h and 5h time on stream. Selectivity and peroxide concentration evolutions were independent on the contact time, suggesting that the choice of the reaction time for the comparison can be arbitrary. The larger the Pd particle, the higher the concentration and the selectivity towards the desired product obtained. This suggests that larger particles of the active metal suppressed the formation of water, favoring the production of the peroxide.

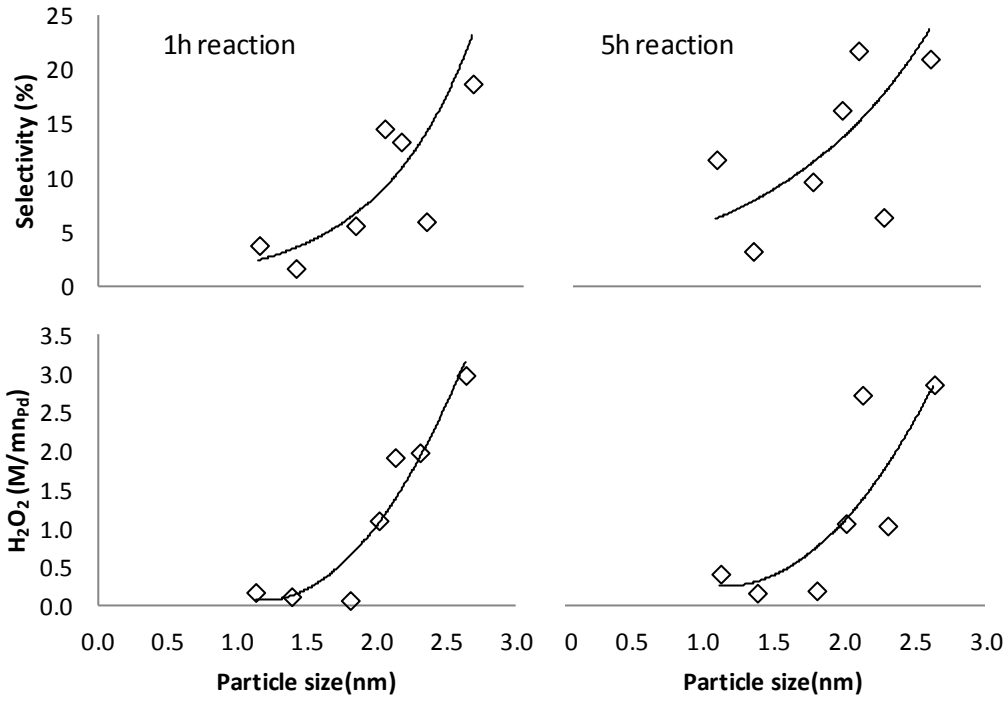

Figure 3.8. Selectivity (top) and specific peroxide concentration (bottom) after 1h (left) and 5h (right) time on stream as a function of the Pd particle size of the catalyst.

Menegazzo *et al.* proposed that O_2 adsorbs associatively on less energetic Pd particles, thus favoring H_2O_2 formation[43]. On the contrary, highly unsaturated sites, such as Pd atoms at a corner or an edge cleave the O-O bond, leading to the non-selective production of H_2O. The morphological properties of the catalysts presented in this work support this hypothesis, where large and thus less energetic particles favored the direct synthesis of H_2O_2.

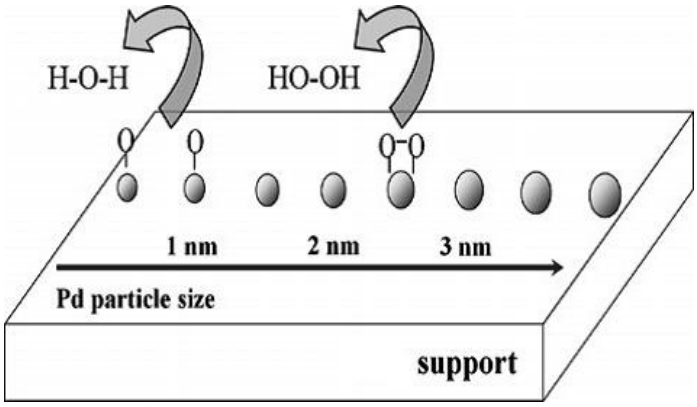

Figure 3.9. *Oxygen activation on Pd particles with different sizes.(Adapted from Menegazzo et al,. 2012[43]).*

The advantage of the samples supported on solid solutions of ZrO_2 is evident. Indeed, the samples that perform better are those that presented a $Zr_xM_{1-x}O_2$ structure (M= La, Y, Ce). The Pd2 sample seems to be an exception, since it exhibits activity and selectivity towards the values obtained with the samples that did not form a solid solution. The reason for the lower performance of Pd2 might be the presence of residual amounts ZrO_2 in its support structure, that reduced its overall homogeneity. This fact can also be correlated with the redox behavior of the samples. Indeed, Pd2 shows a much smaller Pd reduction peak than any other sample that forms a solid $Zr_xM_{1-x}O_2$ solution. Conversely, Pd2 shows a TPR profile that is closer to that of the samples supported on mechanical mixtures of ceria and zirconia, which in turn show much lower activity and selectivity. It is corroborated the concept that metallic catalysts supported on homogenous solid solution of ZrO_2 with promoters such Ce, Y and La, become more reducible[62]. The redox properties of the metal/support system are very important in determining the final performance of the catalyst. Observing the supports features reported in Table 3.1, it is clear that ceria did not have an as good surface and metal stabilizing effect for the Pd2 sample as for the Pd3 one. Indeed, the Pd2 surface area is only 52 vs 93 m^2/g for Pd3. Accordingly, the average pore diameter and the total pore volume are also different. Looking closer, one can note that the better performing samples (Pd3, Pd6 and Pd7) present a very low average pore diameter (5-7 nm). On the contrary, the remaining samples, whose performance are lower, present an average pore diameter in the range of 16-30 nm. The same observation stands for the total pore volume, with the better performing catalysts showing a value that is about half or less than the remaining samples.

It is concluded that both the support physical features and the global redox properties strongly affect the behavior of the catalyst, with bigger metal particles and higher reducibility favoring the production of H_2O_2.

Conclusion

Novel catalysts for the hydrogen peroxide direct synthesis were prepared and tested. The catalysts were synthesized supporting Pd on mixed oxides (ZrO_2 and CeO_2) and rare earth elements (Y_2O_3 and La_2O_3). These materials were chosen for their capacity of increasing both the metal dispersion and the O_2 storage. The homogeneity and the related high reducibility of the support enhanced the oxygen mobility favoring the active metal activity. XRD analysis showed the formation of $Zr_xM_{1-x}O_2$ (M= La, Y, Ce) solid solutions for the supports supplied by MEL Chemicals, contrary the persistence of two separate phases for the supports prepared by mixing and calcining different amounts of ceria and zirconia. All the samples achieved very high dispersion (50-99%) resulting from a very small average particle size (1-2.6 nm). TPR analyses showed that the supports features affect the reducibility of the metal-support system, resulting in rather different catalytic performance. Hydrogen peroxide direct synthesis was performed in a high pressure semibatch apparatus in the absence of promoters and stabilizers. H_2 conversion and peroxide concentration obtained were higher than usually reported in the literature using similar apparatus. Specific conversion and selectivity up to 4 times higher compared to a commercial Pd/C catalyst were achieved. Larger Pd particles were obtained upon supports with smaller pore diameters. In turns, the larger Pd particles were more selective towards the peroxide, suggesting that highly unsaturated sites, such as Pd atoms at a corner or an edge largely present on small particles, cleave the O-O bond, leading to water. Furthermore, supports with higher reducibility favored the production of H_2O_2, probably due to an easier reduction of the active metal. These observations lead to conclude that highly reducible supports giving larger metal particles are most desirable in the preparation of catalysts for the H_2O_2 direct synthesis.

Appendix 1

Mass transfer study

The knowledge of the gas to liquid transport is required in order to set a proper model of the experimental apparatus. In this sense, a series of data were collected on the H_2 dissolution rate in methanol in presence of gaseous N_2 and O_2. A simple model of the reactor has been formulated, with the scope of a further implementation in a numerical computing software (Matlab). Mass transfer coefficients can be evaluated by fitting the experimental data with the model proposed. The coefficients calculation is a proposal for further studies. This Appendix reports the experimental results and the species mass balances for each phases.

1.1 Experimental results

The experimental test were carried out in the same apparatus and operative conditions described in Section 2.2. The semi-batch reactor was filled with methanol (200 ml) and set at the temperature of 10°C and pressure of 50 bar. Initially, the gas mixture bubbling in the liquid was composed by N_2 and O_2 only. H_2 was introduced in the reactor only after the system O_2-N_2-methanol had achieved the vapor-liquid equilibrium, checked via GC analysis

The addition of H_2 in the inlet gas flow marked the starting of the experiment (time zero). The composition of the N_2-O_2-H_2 gas mixture was 76-20-4 mol%, respectively. During the test the hydrogen concentration in the outlet gas was measured by gas chromatographic analysis. The experiments were carried out at different total gas flow rate and stirring rate, since these two factors are considered to influence the transfer rate of H_2 from the gas to the liquid phase.

At constant stirring rate, if the H_2 is supplied at a higher flow than allowed by the gas to liquid mass transfer, then H_2 should be immediately detected at the outlet, because at least part of the H_2 supplied bypasses the liquid phase. On the contrary, if H_2 is supplied at a lower flow than allowed by the gas to liquid mass transfer, no H_2 should be detected at the outlet, because it is all dissolved, until the complete liquid saturation. The former situation is undesired, because it does not allow determining the time needed for the liquid saturation.

Figure 1 displays the H_2 composition profiles at constant stirring rate (1000 rpm) and different total gas flow rates.

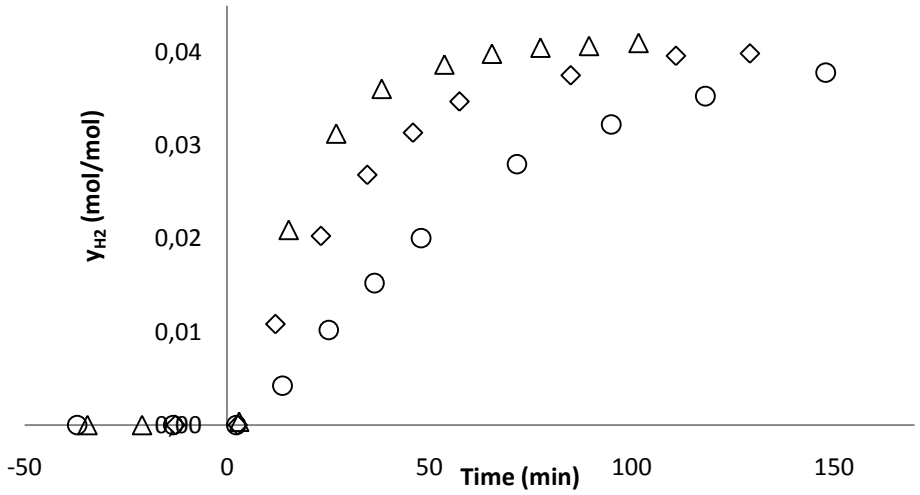

Figure 1. *H_2 dissolution at constant stirring rate (1000 rpm) and at different total gas flow rates (ml/min): ○, 150; ◊, 300; Δ, 450.*

Clearly, initially H_2 is not detected at the outlet, then it slowly increased up to the same value of the inlet gas stream (4 %mol). The time required to saturate the liquid strongly depends on the gas flow rate.

In Figure 2 the H_2 compositions are presented for different stirring rates and at constant total gas flow rate (300 ml/min). It is expected that a high stirring rate would provide a better mixing, hence reducing the time to reach the complete saturation of the liquid phase.

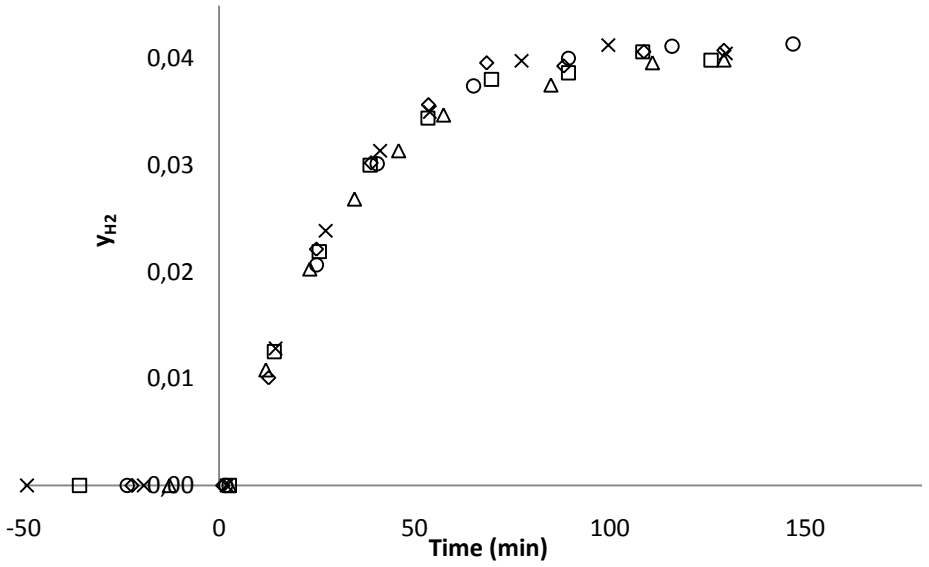

Figure 2. *H_2 dissolution at constant total gas flow rate (300 ml/min) and at different stirring rate (rpm): ◊, 0; ○,500; X, 750; Δ, 1000; □, 1250.*

The experimental results show that, in the considered apparatus, the stirring rate doesn't affect the dissolution of H_2.

The reason could be related to the presence of a large gas volume in the headspace, which has to be filled before H_2 can be detected at the outlet. If the gas volume above the liquid is too large, than the time required to fill it becomes comparable with (or higher than in the worst scenario) the time required for the saturation of the liquid. Hence, the experimental results (Figure 2) suggest that the experimental campaign should be repeated diminishing the gas volume in the headspace; this could be achieved increasing the liquid inside the reactor.

1.2 Mathematical model

The reactor considered is a semi-batch, with the gases continuously bubbling in the liquid static phase. Both the liquid and gas phase are assumed well-mixed. Three control volumes are considered: liquid, bubbles and headspace gas. The species mass balances on each phase are written in Equations 1,2 and 3.

Liquid: $$\frac{dC_i^L}{dt} = \frac{K_i^{L,B} A^{L,B}}{V^L}\left(C_i^{L,B} - C_i^L\right) \qquad i = H_2, O_2, N_2 \tag{1}$$

Bubbles: $$\frac{dC_i^B}{dt} = \frac{\dot{n}_i^{B,in}}{V^B} - \frac{\dot{n}_i^{B,out}}{V^B} - \frac{K_i^{L,B} A^{L,B}}{V^B}\left(C_i^{L,B} - C_i^L\right)$$

$$\frac{\dot{n}_i^{B,out}}{V^B} = \frac{\dot{n}^{B,out}}{n^{B,out}} C_i^{B,out} = \frac{\dot{n}^{B,out}}{V^B \rho^B} C_i^B \tag{2}$$

$$\frac{\dot{n}^{B,out}}{V^B} = \frac{\dot{n}^{B,in}}{V^B} - \sum_{j=i}^{NC} \frac{K_i^{L,B} A^{L,B}}{V^B}\left(C_i^{L,B} - C_i^L\right)$$

Gas: $$\frac{dC_i^G}{dt} = \frac{\dot{n}^{G,in} C_i^{G,in}}{V^G \rho^G} - \frac{\dot{n}^{G,out} C_i^{G,out}}{V^G \rho^G} \overset{\dot{n}^{G,in} = \dot{n}^{G,out}}{=} \frac{\dot{n}^G}{V^G \rho^G}\left(C_i^{G,in} - C_i^G\right) \tag{3}$$

C_i^L and C_i^B are the concentrations of the component *i* in the liquid and bubble phase [$mol_i \cdot (cm^3)^{-1}$]; $K^{L,B}$ is the gas-liquid mass transfer coefficient [$cm \cdot (s)^{-1}$], while $A^{L,B}$ is the bubble-liquid surface. V and $\dot{n}$ are respectively volumes [cm^3] and molar flows [$mol \cdot (s)^{-1}$].

The species concentrations at the gas-liquid interface are calculated by the Henry's solubility law (Equation 4).

$$C_i^{L,B} = C_i^B H_i \tag{4}$$

where H_i is the Henry's constant for the component *i* [ad.].
Equation 3 reports the mass balance relative to gas volume above the liquid, assumed as a CSTR where the composition at the outlet is assumed equal to the composition inside the reactor. C_i^G is the concentration of the component *i* in the gas phase [$mol_i \cdot (cm^3)^{-1}$]; $\dot{n}^G$ is the gas molar flow [$mol \cdot (s)^{-1}$]; V^G and ρ^G are the gas volume [cm^3] and molar density [$mol \cdot (cm^3)^{-1}$], respectively.
$C_i^{G,in}$, inlet concentration of the component *i* in gas phase, corresponds to the concentration of the gas exiting the bubbles phase, $C_i^{B,out}$ (Equation 5).

$$C_i^{G,in} = C_i^{B,out} \tag{5}$$

The following initial conditions are defined:

$$C_{O_2}^L\Big|_{t=0} = C_{O_2}^B H_{O_2} \qquad C_{O_2}^B\Big|_{t=0} = C_{O_2}^{B,0} \qquad C_{O_2}^G\Big|_{t=0} = C_{O_2}^B H_{O_2}$$
$$C_{O_2}^L\Big|_{t=0} = C_{O_2}^B H_{O_2} \qquad C_{N_2}^B\Big|_{t=0} = C_{N_2}^{B,0} \qquad C_{O_2}^G\Big|_{t=0} = C_{O_2}^B H_{O_2}$$
$$C_{H_2}^L\Big|_{t=0} = 0 \qquad C_{H_2}^B\Big|_{t=0} = C_{H_2}^{B,0} \qquad C_{H_2}^G\Big|_{t=0} = 0$$

An important effect to consider in the modeling of the reactor is the induced gas rate through the impeller. The gas entrainment impeller is employed in the reactor for obtain the maximum gas dispersion into the liquid system. This is achieved with a hollow stirring shaft through which gases are continuously recirculated from the head space above the liquid into the liquid phase (Figure 3)[79].

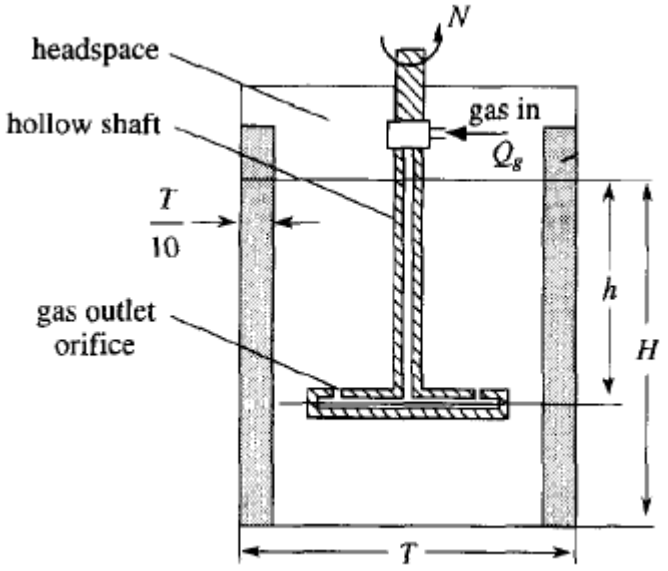

Figure 3. *Geometry of the gas-inducing impeller. The headspace gas is continuously recirculated in the liquid phase. (Adapted from Forrester et al., 1997[76]).*

When the impeller speed is zero the level of the liquid in the hollow pipe and in the vessel is the same. As the impeller starts rotating the level in the pipe starts decreasing (Figura 4). This happens due to the increasing of the speed of the impeller, that creates a reduced pressure region in the vicinity of the stirrer[80].

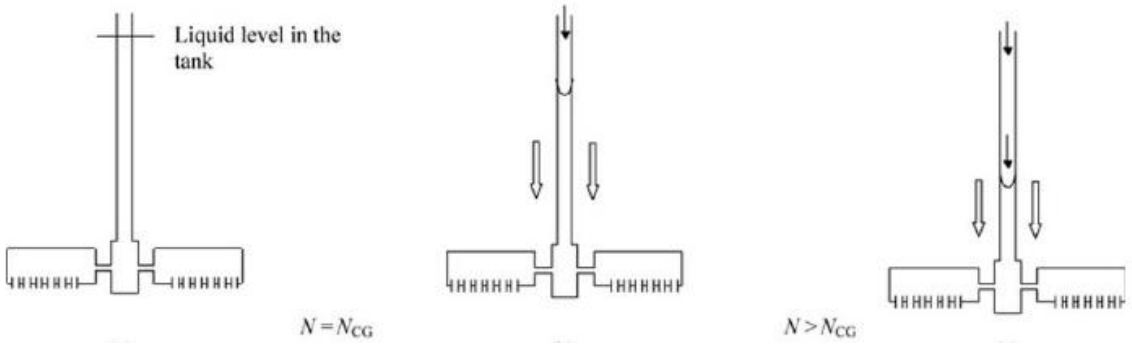

Figure 4. *Mechanism of gas induction. At the critical impeller speed, N_{CG}, the level of liquid in the pipe decreases and the headspace gas starts to be inducted. (Adapted from Deshmukh et al., 1997[77]).*

The pressure difference between the stirrer blades surface and the headspace produces a gas induction effect. Gas induction commences when the reduction in pressure at the blade orifice is sufficient to overcome the static head of liquid. The stirring speed at which this occurs is defined the *critical impeller speed* (N_{CG})[79]. The works reported in literature principally focus on the understanding of the gas induction mechanism. Martin *et al.* proposed a semi-theoretical model assuming that the dominant pressure loss along the gas pathway is across the outlet orifice of the impeller blade[81]. Evans *et al.* showed that the pressure drop at the orifice is only around the 30% of the total, and there are other significant pressure losses in the system. Their model is based on an energy balance equating the total pressure driving force for the gas induction to the sum of the pressure losses along the gas pathway[82]. The energy balance of the gas flow is described in Equation 6.

$$-\Delta P_D = \Delta P_{KE} + \Delta P_P + \Delta P_o + \Delta P_\gamma \tag{6}$$

where ΔP_D is the total pressure driving force ($P_{orifice}$-$P_{headspace}$); ΔP_{KE} is the pressure loss due to the kinetic energy imparted to the liquid during the bubble formation process; ΔP_P is the frictional pressure loss along the pipe; ΔP_O is the pressure loss at the orifice and ΔP_γ is the pressure loss due to the work done against the surface tension at the bubble surface.

Forrester *et al.* improved the Evans's model with a more detailed study of how the gas bubbles grow and detach at the outlet orifices on the impeller blades. The equations (7) proposed for the gas flow rate through a single orifice is:

$$Q_o = \frac{4\pi(r_d^3 - r_o^3)}{3t_d} \qquad t_d = \frac{(r_d + r_o)}{U_o} \tag{7}$$

Q_O is the gas flow rate through one orifice [$m^3 \cdot (s)^{-1}$]; r_d and r_o are the bubble radius at the detachment and the orifice radius respectively [m]; t_d is the detachment time [s] and U_o is the liquid velocity over the orifice [$m \cdot (s)^{-1}$].
The total induced gas flow rate can be derive multiplying Q_o for the number of blades of impeller, n_b (Equation 8).

$$Q_g = n_b Q_o \tag{8}$$

A significant increase in the induced gas rate is observed by adding more outlet orifices to each blade.[79]

Appendix 2

Reduction cycles: Experimental results

The novel solid mixtures employed in the synthesis of the catalysts, present a high thermal stability and tunable properties (surface area, pore volume, particle size) changing the preparation procedure[62]. A series of treatments were carried out on the same catalysts so far studied (Section 2.1.1, Table 2.1). The processing was expected to improve the catalyst characteristics acting on Pd particle size control and reducibility of the metal-support system. The samples were then tested for direct synthesis of hydrogen peroxide, so that the effects of the treatments on the materials performances could be evaluated.

A series of reduction and oxidation cycles were performed on the catalysts. The cycles were carried out in a vertical tubular oven furnace where a glass tube was installed and maintained at fixed temperature. The tube containing the catalyst was equipped with a thermocouple to monitor the temperature. The gas flow was controlled by rotameters.
In the reduction stage, a heating ramp (5°C/min) was performed in 50 Nml/min argon flow up at 300 °C. Then pure H_2 (50 Nml/min) was flowed for 2h. The temperature was then decreased till room conditions in 50 Nml/min argon flow. The heating and cooling ramps were carried out in argon in order to avoid the contemporary presence of H_2 and air moisture on the catalyst, which can lead to Pd sintering[83].
The oxidation was carried out flowing synthetic air (50 Nml/min) at 400 °C for 2h, increasing the temperature at 5 °C/min. The temperature was then decreased till room temperature in 50 Nml/min.
3 and 6 reduction/oxidation cycles were carried out on each catalyst. All the samples were finally characterized and tested.

The catalytic tests were carried out in the same apparatus and with the same operative procedure described in Section 2.2.

Figure 1 shows hydrogen peroxide and water specific concentration profiles, conversion and selectivity for the catalyst Pd3 (Ce doped ZrO_2) with 3 and 6 redox cycles (the results obtained with the reduced catalyst are also reported as a reference).

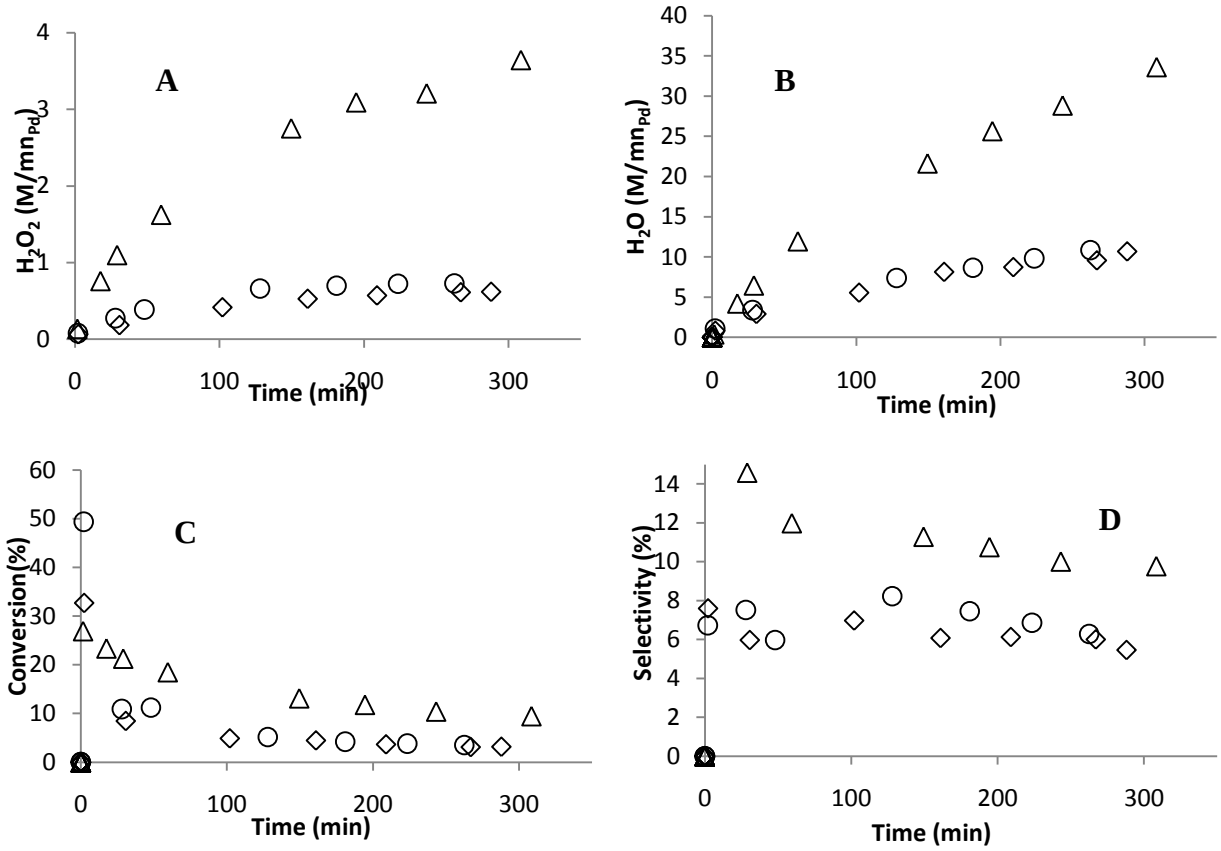

Figure 1. *Experimental results relative to catalyst Pd3 in terms of specific H_2O_2 concentration (A), specific H_2O concentration (B), conversion (C) and selectivity (D): Δ, reduced; ○, 3 redox cycles; ◊, 6 redox cycles.*

The same qualitative results were measured in the Pd6, Pd7, Pd8 samples (experimental data not shown), that is a marked worsening of catalytic performances.

The reduction-oxidation processing had a different effect on catalyst Pd2 (ZrO_2/CeO_2 82.5/17.5). Figure 2 reports the experimental results in term of hydrogen peroxide and water specific concentrations, selectivity and conversion.

After three redox cycles of treatments, the catalyst showed an improvement of selectivity compared to the sample reduced one time. H_2O_2 concentration was increased, whereas water was decreased.

Six redox cycles drastically reduced selectivity and conversion, limiting both the production of hydrogen peroxide and water.

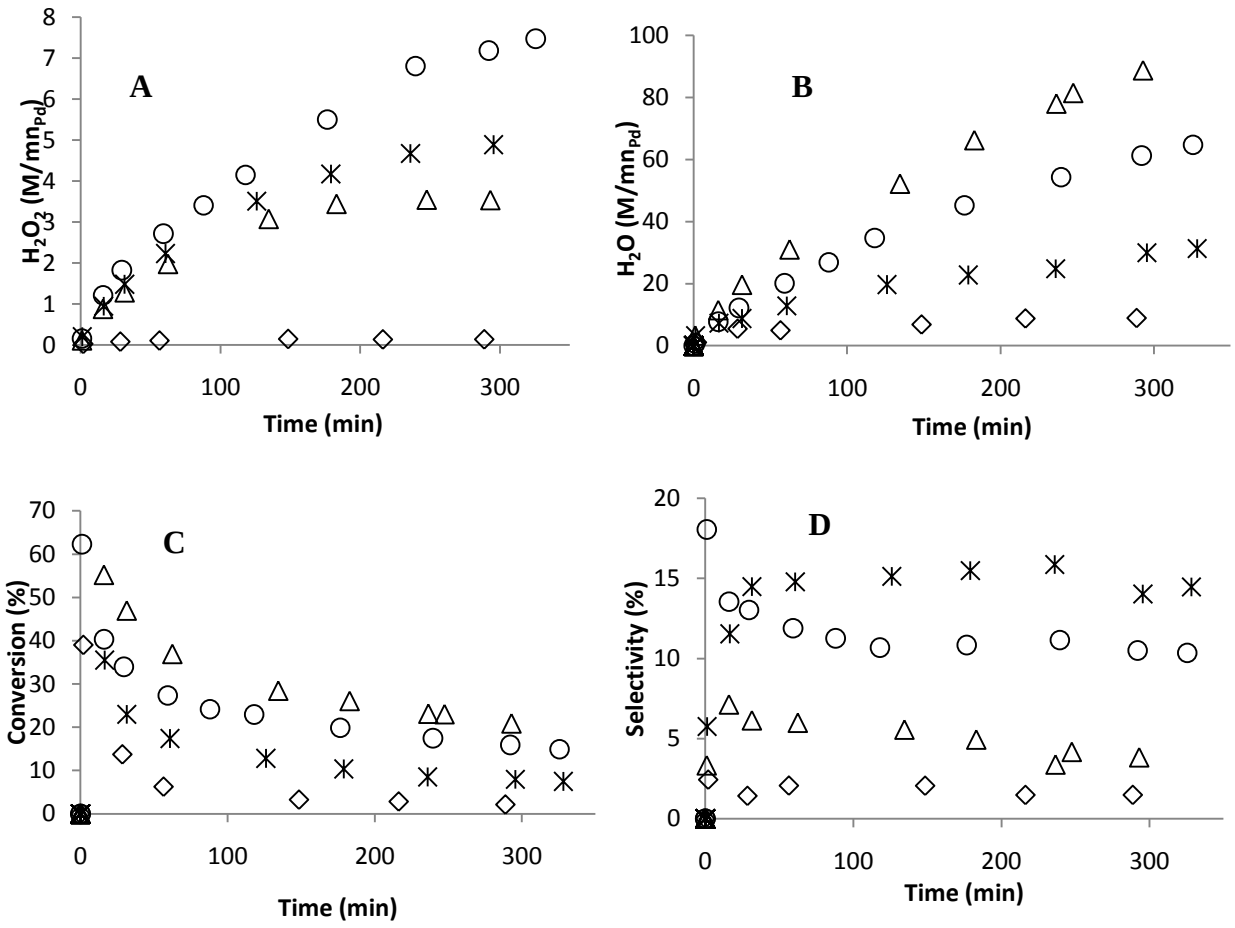

Figure 2. *Experimental results relative to catalyst Pd2 in terms of specific H_2O_2 concentration (A), specific H_2O concentration (B), conversion (C) and selectivity (D): Δ, reduced; ○, 3 redox cycles; *, 3 redox cycles + partial oxidation; ◊, 6 redox cycles.*

After 3 redox cycles, a further oxidation was performed on the sample Pd2. The oxidation was carried out flowing synthetic air (50 Nml/min) at 70°C for 1h, increasing the temperature at 5 °C/min in 50 Nml/min.

The oxidized catalyst (*, in Figure 2) showed a lower conversion, but an higher selectivity towards hydrogen peroxide, respect to the correspondent sample not oxidized (○). It seems to be in agreement with the observations advanced in literature that the oxidized form of Pd is more selective but less active than the corresponding reduced form[31,39].

Figure 3 reports the specific concentration of H_2O_2 and H_2O, selectivity and conversion for catalyst Pd4 (ZrO_2/CeO_2 50/50) after 3 and 6 cycles of reductions.

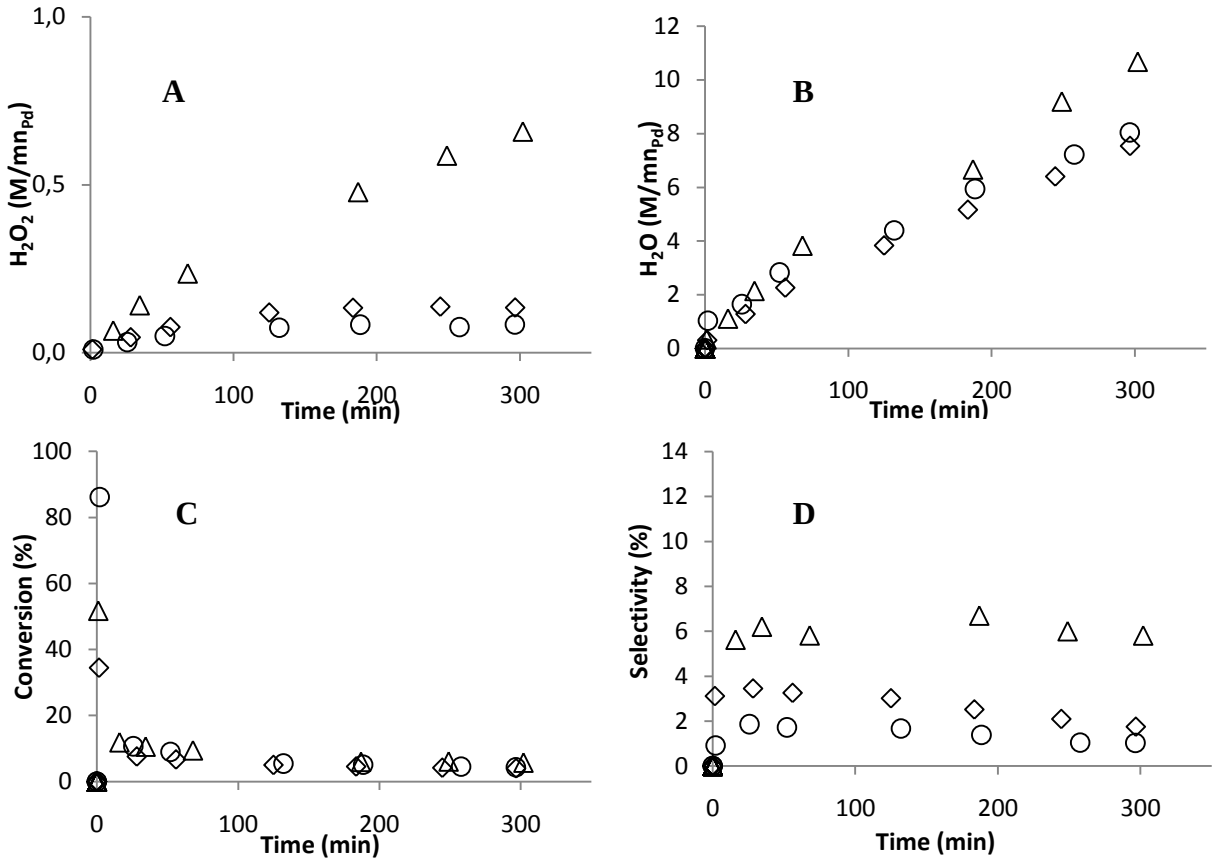

Figure 3. *Experimental results relative to catalyst Pd4 in terms of specific H_2O_2 concentration (A), specific H_2O concentration (B), conversion (C) and selectivity (D): Δ, reduced; ○, 3 redox cycles; ◊, 6 redox cycles.*

Hydrogen peroxide concentration strongly decreased, while water remained unchanged: the treatments had a negative effects on the materials, causing a marked drop of selectivity. Catalyst Pd5 (ZrO_2/CeO_2 17.5/82.5) showed a different trend respect the other catalyst (Figure 4). The sample 3 times reduced reported a considerable decrease both in selectivity and conversion. The sample after 6 redox cycles produced hydrogen peroxide concentrations comparable with the catalyst reduced only one time, but better limiting the water formation. Hence, the selectivity towards hydrogen peroxide resulted enhanced by the cycles treatments.

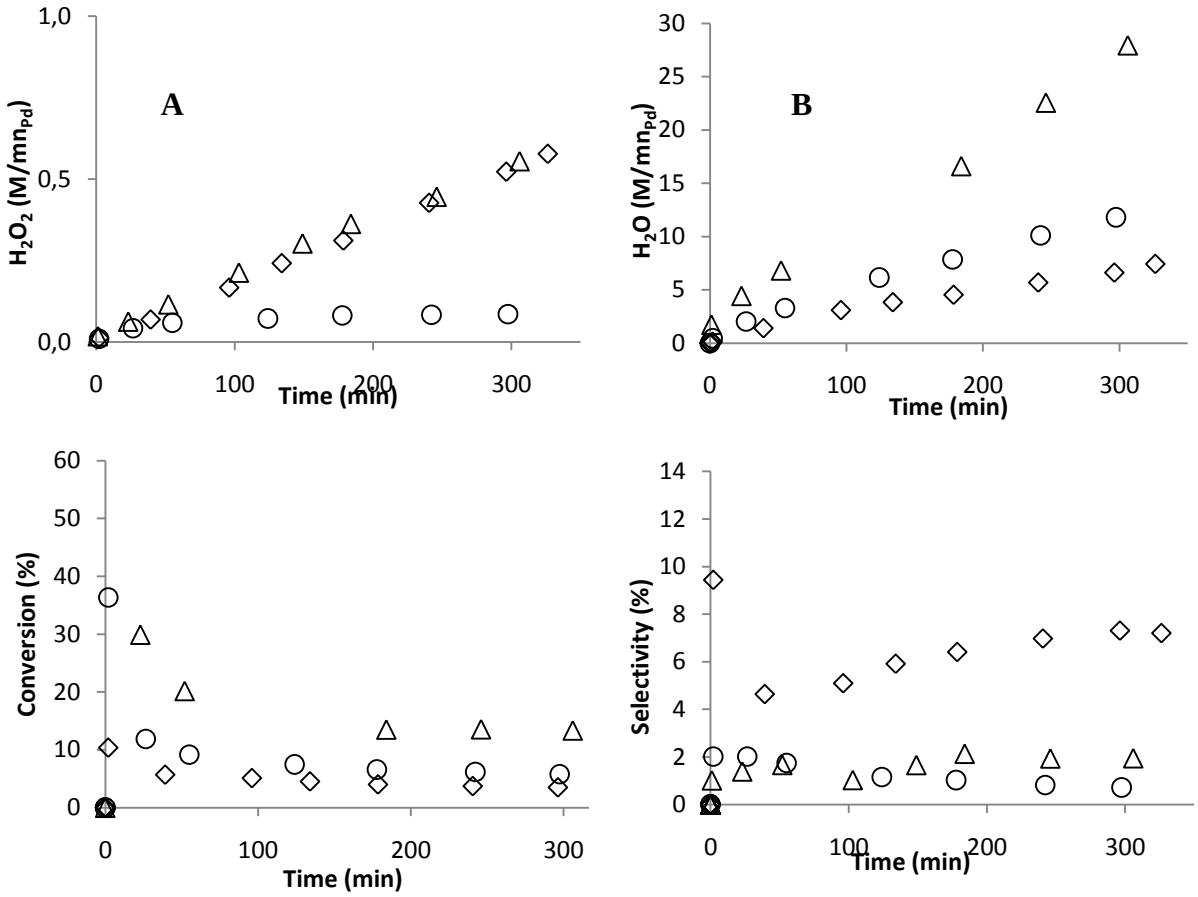

Figure 4. *Experimental results relative to catalyst Pd5 in terms of specific H_2O_2 concentration (A), specific H_2O concentration (B), conversion (C) and selectivity (D): Δ, reduced; ○, 3 redox cycles; ◊, 6 redox cycles.*

At the moment, further analyses on the catalyst are being performed, including TPR, TPO, CO chemisorption and XRD. The techniques have been explained in Section 2.1.2. Without a complete and critical investigation of the characterization results, the reasons of such different behaviors can be only hypothesized.

One of the possibilities is that the treatments result in *stressing* the catalyst structure, compromising their activity. The redox cycles could act on the support-Pd interaction re-arranging the metal particles in a more or less favorable conformation for hydrogen peroxide production[4,38].

The exhaustive description of the phenomena investing the materials is a proposal for a subsequent scientific publication.

Bibliography

[1] Campos-Martin, J. M., Blanco-Brieva, G., & Fierro, J. L. G. (2006). Hydrogen peroxide synthesis: An outlook beyond the anthraquinone process. *Angewandte Chemie - International Edition*, *45*(42).

[2] Samanta, C. (2008). Direct synthesis of hydrogen peroxide from hydrogen and oxygen: An overview of recent developments in the process. *Applied Catalysis A: General*, *350*(2), 133–149.

[3] Centi, G., Perathoner, S., & Abate, S. (2009). Direct synthesis of hydrogen peroxide: recent advances. *Modern Heterogeneous Oxidation cataòlysis*, Wiley-VCH Handbook, 1–33.

[4] García-Serna, J., Moreno, T., Biasi, P., Cocero, M. J., Mikkola, J.-P., & Salmi, T. O. (2014). Engineering in direct synthesis of hydrogen peroxide: targets, reactors and guidelines for operational conditions. *Green Chemistry*, *16*(5), 2320–2343.

[5] Anastas, P.T., Warner, J.C. (1998). Green Chemistry: Theory and Practice. *Oxford University Press*, New York.

[6] Hydrogen peroxide – A global strategic business report. (2014) *Global Industry Analysts, Inc. (GIA)*

[7] Jones, C.W. (1999). Applications of Hydrogen Peroxide and Derivatives. *Royal Society of Chemistry*, London.

[8] Goldstein, S., Meyerstein, D., & Czapski, G. (1993). The Fenton reagents. *Free Radical Biology and Medicine*, *15*(4), 435–445.

[9] Huang, C.P., Dong, C., Tang, Z. (1993). Advanced chemical oxidation: Its present role and potential future in hazardous waste treatment. *Waste Management*, 13(5-7), 361-377.

[10] Lü, S., Mi, Z., Wang, L., Wang, Y., Zhu, Z., & Fu, S. (2005). Experimental investigation and simulation of gas-liquid-liquid reactive extraction process for the production of hydrogen peroxide. *Chemical Engineering Science*, *60*(22), 6298–6306.

[11] Gopal, R. (2003). Electrochemical synthesis of hydrogen peroxide. US 2003019758, The Electrosynthesis company.

[12] Cai, R., Baba, R., Hashimoto, K., Kubota, Y., & Fujishima, a. (1993). Photoelectrochemistry of TiO_2 particles: efficient electron transfer from the TiO_2, particles to a redox enzyme, *360*, 237–245.

[13] Otsuka, K., Yamanaka, I. (1990) One step synthesis if hydrogen peroxide through fuel cell reaction. *Electrochim. Acta*, 35, 319-322.

[14] Yamanaka, I., Onizawa, T., Takenaka, S., Otsuka, K. (2003). Direct and Continuous Production of Hydrogen Peroxide with 93 % Selectivity Using a Fuel-Cell System. Angewandte Chemie 115, 3781-3783; Angewandte Chemie International Edition 2003, 42, 3653-3655.

[15] Aitken, M. D. (1993). Waste treatment applications of enzymes: opportunities and obstacles. *The Chemical Engineering Journal*, *52*(2), B49–B58.

[16] van de Velde, F., Lourenco, N. D., Bakker, M., van Rantwijk, F., Sheldon, R. A. (2000) Improved operational stability of peroxidases by coimmobilization with glucose oxidase. *Biotechnology and Bioengineering* 69, 286 – 291.

[17] Zhou, J., Guo, H., Wang, X., Guo, M., Zhao, J., Chen, L., Gong, W. (2005) Direct and continuous synthesis of concentrated hydrogen peroxide by the gaseous reaction of H_2/O_2 non-equilibrium plasma. *Chemical Communications*, 1631 – 1633.

[18] Thevenet, F., Couble, J., Brandhorst, M., Dubois, J. L., Puzenat, E., Guillard, C., & Bianchi, D. (2010). Synthesis of hydrogen peroxide using dielectric barrier discharge associated with fibrous materials. *Plasma Chemistry and Plasma Processing*, *30*(4), 489–502.

[19] Henkel, H., Weber, W. (1914). Manufacture of hydrogen peroxide. US1108752 A, Henkel & CIE.

[20] Lewis, B., Guenther von Elbe, G. (1987) The Reaction between Hydrogen and Oxygen. *Combustion, Flames and Explosions of Gases (Third Edition)*, 25 – 77.

[21] Fisher, M., Karbel, G., Stammer, A., Flick, K., Quaiser, S., Harder, W., Massoume, K. (2002). Process for the manufacture of hydrogen peroxide. US6375920, BASF (Germany).

[22] Voloshin, Y., & Lawal, A. (2010). Overall kinetics of hydrogen peroxide formation by direct combination of H2 and O2 in a microreactor. *Chemical Engineering Science*, *65*(2), 1028–1036.

[23] Menegazzo, F., Burti, P., Signoretto, M., Manzoli, M., Vankova, S., Boccuzzi, F., … Strukul, G. (2008). Effect of the addition of Au in zirconia and ceria supported Pd catalysts for the direct synthesis of hydrogen peroxide. *Journal of Catalysis*, *257*(2), 369–381.

[24] Gemo, N., Biasi, P., Canu, P., & Salmi, T. O. (2012). Mass transfer and kinetics of H_2O_2 direct synthesis in a batch slurry reactor. *Chemical Engineering Journal*, *207-208*, 539–551.

[25] Voloshin, Y., & Lawal, A. (2009). Kinetics of hydrogen peroxide reduction by hydrogen in a microreactor. *Applied Catalysis A: General*, *353*(1), 9–16.

[26] Voloshin, Y., Halder, R., & Lawal, A. (2007). Kinetics of hydrogen peroxide synthesis by direct combination of H2 and O2 in a microreactor. *Catalysis Today*, *125*(1-2), 40–47.

[27] Voloshin, Y., Manganaro, J., Lawal, A. (2008). Kinetics and mechanism of hydrogen peroxide decomposition over Pd/SiO_2 catalyst. *Industrial and Engineering Chemistry Research* 47, 8119–8125.

[28] Gemo, N., Biasi, P., Salmi, T. O., & Canu, P. (2012). H_2 solubility in methanol in the presence of CO_2 and O_2. *Journal of Chemical Thermodynamics*, *54*, 1–9.

[29] Salmi, T., Gemo, N., Biasi, P., & Serna, J. G. (2014). Product distribution analysis of the hydrogen peroxide direct synthesis in an isothermal batch reactor. *Catalysis Today*.

[30] Edwards, J. K., Solsona, B. E., Landon, P., Carley, A. F., Herzing, A., Kiely, C. J., & Hutchings, G. J. (2005). Direct synthesis of hydrogen peroxide from H2 and O2 using TiO2-supported Au-Pd catalysts. *Journal of Catalysis*, *236*(1), 69–79.

[31] Melada, S., Rioda, R., Menegazzo, F., Pinna, F., & Strukul, G. (2006). Direct synthesis of hydrogen peroxide on zirconia-supported catalysts under mild conditions. *Journal of Catalysis*, *239*(2), 422-430.

[32] Bernardini, A., Gemo, N., Biasi, P., Canu, P., Mikkola, J. P., Salmi, T., & Lanza, R. (2015). Direct synthesis of H2O2 over Pd supported on rare earths promoted zirconia. *Catalysis Today*.

[33] Biasi, P., García-Serna, J., Bittante, A., & Salmi, T. (2013). Direct synthesis of hydrogen peroxide in water in a continuous trickle bed reactor optimized to maximize productivity. *Green Chemistry*, *15*(9).

[34] Ranade, Vivek V., Chaudhari, R. V. & Gunjal, Prashant R. (2011). *Trickle Bed Reactors: Reactor Engineering & Applications*, 1st ed., Elsevier.

[35] Inoue, T., Ohtaki, K., Murakami, S., Matsumoto, S. (2013). Direct synthesis of hydrogen peroxide based on microreactor technology. *Fuel process technology*, 108, 8–11.

[36] Choudhary, V. R., Gaikwad, A. G., Sansare, S. D. (2001). Nonhazardous Direct Oxidation of Hydrogen to Hydrogen Peroxide Using a Novel Membrane Catalyst. *Angewandte Chemie.*, Int. Ed., 40, 1776–1779.

[37] Melada, S., Pinna, F., Strukul, G., Perathoner, S., & Centi, G. (2006). Direct synthesis of H_2O_2 on monometallic and bimetallic catalytic membranes using methanol as reaction medium. *Journal of Catalysis*, *237*(2), 213–219.

[38] Zhou, B., Lee, L.-K. (2001). Catalyst and process for direct catalystic production of hydrogen peroxide. US 6168775, Hydrocarbon Technologies, Inc.

[39] Samanta, C., & Choudhary, V. R. (2007). Direct synthesis of H_2O_2 from H_2 and O_2 over Pd/H-beta catalyst in an aqueous acidic medium: Influence of halide ions present in the catalyst or reaction medium on H_2O_2 formation. *Catalysis Communications*, *8*(1), 73–79.

[40] Chinta, S., & Lunsford, J. H. (2004). A mechanistic study of H_2O_2 and H_2O formation from H_2 and O2 catalyzed by palladium in an aqueous medium. *Journal of Catalysis*, *225*(1), 249–255.

[41] Liu, Q., Gath, K., Bauer, J., Schaak, R., Lunsford, J., The Active Phase in the Direct Synthesis of H_2O_2 from H_2 and O_2 over Pd/SiO_2 Catalyst in a H_2SO_4/Ethanol System, *Catalysis Letters*. 132 (2009) 342-348.

[42] Landon, Philip, Collier, Paul J., Papworth, Adam J., Kiely, Christopher J., Hutchings, Graham J., 2002. Direct formation of hydrogen peroxide from H_2/O_2 using a gold catalyst. *Chem. Commun.*, 18, 2058–2059.

[43] Menegazzo, F., Signoretto, M., Frison, G., Pinna, F., Strukul, G., Manzoli, M., & Boccuzzi, F. (2012). When high metal dispersion has a detrimental effect: Hydrogen peroxide direct synthesis under very mild and nonexplosive conditions catalyzed by Pd supported on silica.

[44] Edwards, J. K., Thomas, A., Solsona, B. E., Landon, P., Carley, A. F., & Hutchings, G. J. (2007). Comparison of supports for the direct synthesis of hydrogen peroxide from H2 and O_2 using Au-Pd catalysts. *Catalysis Today*, *122*(3-4), 397–402.

[45] Ishihara, T., Ohura, Y., Yoshida, S., Hata, Y., Nishiguchi, H., & Takita, Y. (2005). Synthesis of hydrogen peroxide by direct oxidation of H_2 with O_2 on Au/SiO_2 catalyst. *Applied Catalysis A: General*, *291*(1-2), 215–221.

[46] Abate, S., Perathoner, S., & Centi, G. (2012). Deactivation mechanism of Pd supported on ordered and non-ordered mesoporous silica in the direct H_2O_2 synthesis using CO_2-expanded methanol. *Catalysis Today*, *179*(1), 170–177.

[47] Fu, F., Chuang, K.T., Fiedorow, R. (1992) Selective Oxidation of Hydrogen to Hydrogen Peroxide. *Studies in Surface Science and Catalysis*, 72, 33-41.

[48] Samanta, C., & Choudhary, V. R. (2007). Direct oxidation of H_2 to H_2O_2 over Pd/Ga_2O_3 catalyst under ambient conditions: Influence of halide ions added to the catalyst or reaction medium. *Applied Catalysis A: General*, *326*(1), 28–36.

[49] Burato, C., Centomo, P., Rizzoli, M., Biffis, A., Campestrini, S., Corain, B. (2006). Functional Resins as Hydrophilic Supports for Nanoclustered Pd(0) and Pd(0)-Au(0) Catalysts Designed for the Direct Synthesis of Hydrogen Peroxide. *Advaced Synthesis Catalalyst*, 348, 255 – 259.

[50] Choudhary, V. R., & Samanta, C. (2006). Role of chloride or bromide anions and protons for promoting the selective oxidation of H_2 by O_2 to H_2O_2 over supported Pd catalysts in an aqueous medium. *Journal of Catalysis*, *238*(1), 28–38.

[51] Moreno, T., García-Serna, J., & Cocero, M. J. (2011). Decomposition reaction of H_2O_2 over Pd/C catalyst in an aqueous medium at high pressure: Detailed kinetic study and modelling. *Journal of Supercritical Fluids*, *57*(3), 227–235.

[52] Abate, S., Centi, G., Melada, S., Perathoner, S., Pinna, F., & Strukul, G. (2005). Preparation, performances and reaction mechanism for the synthesis of H_2O_2 from H_2 and O_2 based on palladium membranes. *Catalysis Today*, *104*(2-4), 323–328.

[53] Krishnan, V., Dokoutchaev, A. & Thompson, M., 2000. Direct production of hydrogen peroxide with palladium supported on phosphate viologen phosphonate catalysts. *Journal of Catalysis*, 196(2), 366 – 374.

[54] Liu, Q., & Lunsford, J. H. (2006). Controlling factors in the direct formation of H_2O_2 from H_2 and O_2 over a Pd/SiO_2 catalyst in ethanol. *Applied Catalysis A: General*, *314*(1), 94–100.

[55] Abate, S., Arrigo, R., Perathoner, S., & Centi, G. (2014). Role of Feed Composition on the Performances of Pd-Based Catalysts for the Direct Synthesis of H2O2. *Topics in Catalysis*, *57*(14-16).

[56] Rueda, T. M., Serna, J. G., & Alonso, M. J. C. (2011). Direct production of H_2O_2 from H_2 and O_2 in a biphasic H2O/scCO2 system over a Pd/C catalyst: Optimization of reaction conditions. *The Journal of Supercritical Fluids*, *61*, 119–125.

[57] Moreno, T., García-Serna, J., Plucinski, P., Sánchez-Montero, M. J., & Cocero, M. J. (2010). Direct synthesis of H2O2 in methanol at low pressures over Pd/C catalyst: Semi-continuous process. *Applied Catalysis A: General*, *386*(1-2), 28–33.

[58] Biasi, P., Gemo, N., Eranen, K., Carucci, J.R., Canu, P., Pinna, F., Wärna, J., & Salmi, T. O. (2012). Kinetics and mechanism of H_2O_2 direct synthesis over a Pd/C catalyst in a Batch reactor. *Industrial and engineering chamical research*, 51, 8903-8912.

[59] Choudhary, V. R., Samanta, C., Jana, P. (2007). Hydrogenation of Hydrogen Peroxide over Palladium/Carbon in Aqueous Acidic Medium Containing Different Halide Anions under Static/Flowing Hydrogen. *Industrial & Engineering Chemical Research*, 46, 3237-3242.

[60] Huerta, I., García-Serna, J., & Cocero, M. J. (2013). Hydrogenation and decomposition kinetic study of H_2O_2 over Pd/C catalyst in an aqueous medium at high CO_2 pressure. *Journal of Supercritical Fluids*, *74*, 80–88.

[61] Biasi, P. (2013). Combination of catalyst development and chemical reaction engineering: a key aspect to improve the hydrogen peroxide direct synthesis. *PhD Thesis, Department of Chemical Engineering*, Abo Akademi.

[62] Pudukudy, M., & Yaakob, Z. (2014). Catalytic aspects of ceria-zirconia solid solution : Part-I An update in the synthesis , properties and chemical reactions of ceria zirconia solid solution Manoj Pudukudy and Zahira Yaakob, *6*(1), 188–216.

[63] Burato, C., Campestrini, S., Han, Y. F., Canton, P., Centomo, P., Canu, P., & Corain, B. (2009). Chemoselective and re-usable heterogeneous catalysts for the direct synthesis of hydrogen peroxide in the liquid phase under non-explosive conditions and in the absence of chemoselectivity enhancers. *Applied Catalysis A: General*, *358*(2), 224–231.

[64] Damyanova, S., Pawelec, B., Arishtirova, K., Huerta, M. V. M., & Fierro, J. L. G. (2008). Study of the surface and redox properties of ceria-zirconia oxides. *Applied Catalysis A: General*, *337*(1), 86–96.

[65] Descorme, C. (2000). Infrared Study of Oxygen Adsorption and Activation on Cerium–Zirconium Mixed Oxides. *Journal of Catalysis*, *196*(1), 167–173.

[66] Madier, Y., Descorme, C., Le Govic, a M., & Duprez, D. (1999). Oxygen mobility in CeO_2 and $Ce_xZr_{(1-x)}O_2$ compounds: Study by CO transient oxidation and $^{18}O/^{16}O$ isotopic exchange. *Journal of Physical Chemistry B*, *103*(50), 10999–11006.

[67] Nagai, Y., Yamamoto, T., Tanaka, T., Yoshida, S., Nonaka, T., Okamoto, T., Sugiura, M. (2002). X-ray absorption fine structure analysis of local structure of CeO_2–ZrO_2 mixed oxides with the same composition ratio (Ce/Zr=1). *Catalysis Today*, *74*(3-4), 225–234.

[68] McGuire, N. E., Kondamudi, N., Petkovic, L. M., & Ginosar, D. M. (2012). Effect of lanthanide promoters on zirconia-based isosynthesis catalysts prepared by surfactant-assisted coprecipitation. *Applied Catalysis A: General*, *429-430*, 59–66.

[69] Park, S., Lee, J., Song, J. H., Kim, T. J., Chung, Y. M., Oh, S. H., & Song, I. K. (2012). Direct synthesis of hydrogen peroxide from hydrogen and oxygen over Pd/HZSM-5 catalysts: Effect of Brönsted acidity. *Journal of Molecular Catalysis A: Chemical*, *363-364*, 230–236.

[70] Toebes, M. L., Van Dillen, J. a., & De Jong, K. P. (2001). Synthesis of supported palladium catalysts. *Journal of Molecular Catalysis A: Chemical*, *173*(1-2), 75–98.

[71] Sing, K. (2001). The use of nitrogen adsorption for the characterisation of porous materials. *Colloids and Surfaces A: Physicochemical and Engineering Aspects*, *187-188*, 3–9.

[72] Halsey, GD (1948). Physical Adsorption on Non-Uniform Surfaces. *Journal of Chemical Physics*, 16, 931.

[73] Deutsch, M., Hölzer, G., Härtwig, J., Wolf, J., Fritsch, M., & Förster, E. (1995). K alpha and K beta x-ray emission spectra of copper. *Physical Review A*, *51*(1), 283.

[74] Fadoni, M., & Lucarelli, L. (1999). Temperature programmed desorption, reduction, oxidation and flow chemisorption for the characterisation of heterogeneous catalysts. Theoretical aspects , instrumentation and applications. *Studies in Surface Science and Catalysis*, *120*, 177–225.

[75] Robison, J.W., Atomic Absorption Spectroscopy (1960). *Analytical Chemistry*, 32 (8), 17A–29A.

[76] Pérez-Hernández, R., Gutiérrez-Martínez, a., Palacios, J., Vega-Hernández, M., & Rodríguez-Lugo, V. (2011). Hydrogen production by oxidative steam reforming of methanol over Ni/CeO2-ZrO2 catalysts. *International Journal of Hydrogen Energy*, *36*(11), 6601–6608.

[77] Jewell, L. L., & Davis, B. H. (2006). Review of absorption and adsorption in the hydrogen-palladium system. *Applied Catalysis A: General*, *310*(1-2), 1–15.

[78] Abate, S., Lanzafame, P., Perathoner, S., & Centi, G. (2011). SBA-15 as a support for palladium in the direct synthesis of H_2O_2 from H_2 and O_2. *Catalysis Today*, *169*(1), 167–174.

[79] Forrester, S. E., Rielly, C. D., & Carpenter, K. J. (1998). Gas-inducing impeller design and performance characteristics. *Chemical Engineering Science*, *53*(4), 603–615.

[80] Deshmukh, N., Patil, S., & Joshi, J. (2006). Gas induction characteristics of hollow self-inducing impeller. *Chemical Engineering Research and Design*, *84*(February), 124–132.

[81] Martin, G.O. (1972). Gas-inducing agitator. *Industrial Engineering Chemical Process Design Device, 11,* 397-404.

[82] Evans, G. M., Rielly, C. D., Davidson, J. F. & Carpenter, K. J. (1990). Modelling and design of gas-inductiong reactor. *A.I.Ch.E. Spring National Meeting, Houston, TX, Paper 33e.*

[83] Chen, J. J., & Ruckenstein, E. (1981). Sintering of palladium on alumina model catalyst in a hydrogen atmosphere. *Journal of Catalysis*, *69*(2), 254–273.

Acknowledgements

I would like to express my immense gratitude to Professor Paolo Canu for supporting and providing me the means to experience the Thesis project abroad. A special mention goes to Academic Professor Tapio Salmi for giving me the possibility to work at the laboratory. Thanks to Laboratory manager Docent Kari Eranen for the aid efforts in ensuring the best continuation of laboratory activity.

My warmest thankfulness goes to Dr. Pierdomenico Biasi and Dr. Nicola Gemo for their priceless help during the whole scientific project, from the lab applications to the Thesis writing. In particular, I would like to thank Pierdomenico for his constant supervision and guidance. Nicola was a reference figure in my stay in Turku, not only sharing without hesitation his scientific knowledge, but also in facing everyday issues. Their working and life experiences are inspiring for my future choices.
A hearty appreciation goes to all friends in Finland for the precious and happy occasions we had together. I would like to mention Alice and Stefano for their invaluable help in first period and during the whole permanence in Turku.

A special thought goes to my Italian friends, near or far, that accompanied me in this academic pathway. Thanks to everyone who in his way, as confidant friend or just for a coffee break, spent with me moments of his life.

I am forever in debt with my family for their unconditional care and support throughout these years. The strength of my parents in believing in my success is reason of great motivation and gratification.

Finally Letizia, the person who shares all the aspects of my life and is able to bring out the best things from me. Thank you for supporting me in any my choice.